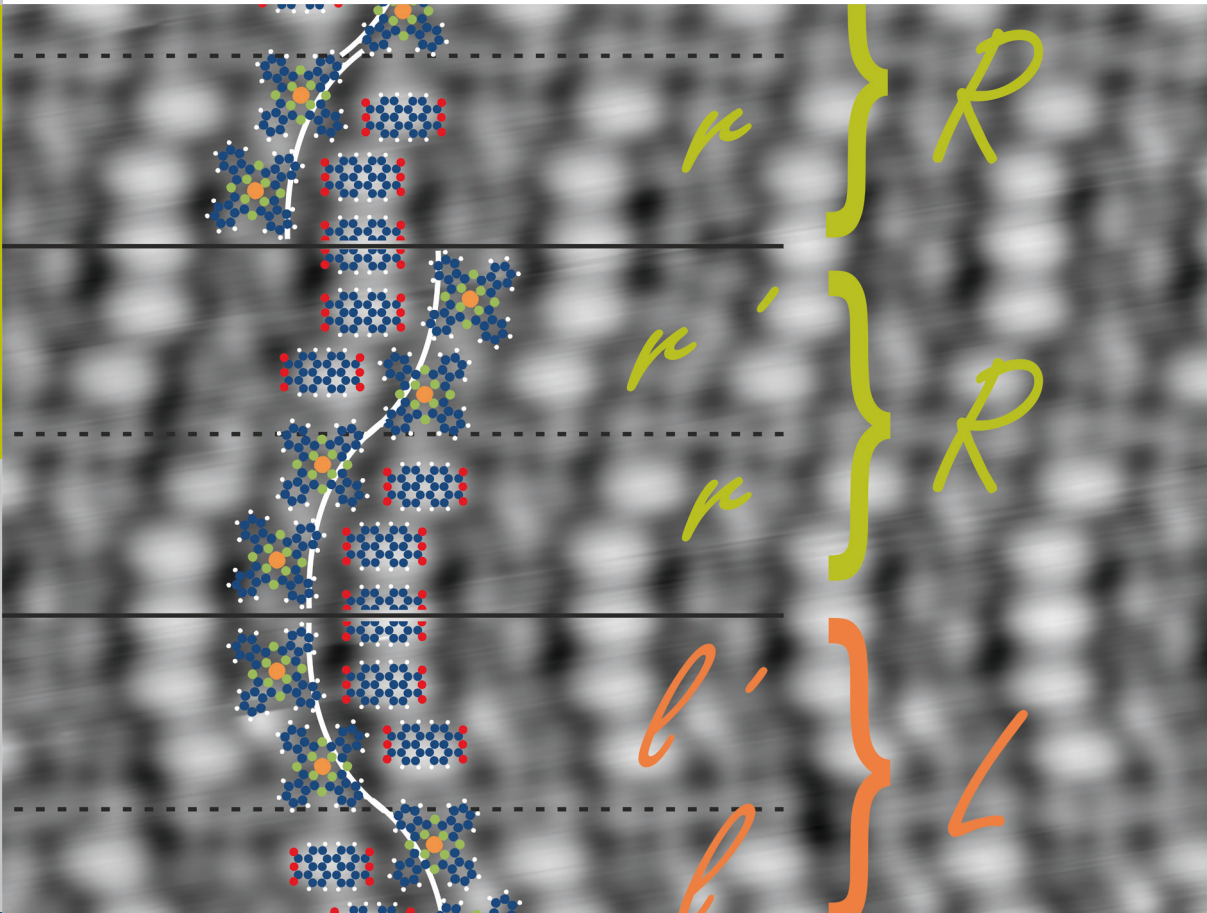


Structural and electronic investigations on homo- and hetero-organic layers involving CuPc on silver single crystal surfaces

Kathrin Maria Schönauer



Forschungszentrum Jülich GmbH
Peter Grünberg Institut (PGI)
Functional Nanostructures at Surfaces (PGI-3)

Structural and electronic investigations on homo- and hetero-organic layers involving CuPc on silver single crystal surfaces

Kathrin Maria Schönauer

Schriften des Forschungszentrums Jülich
Reihe Schlüsseltechnologien / Key Technologies

Band / Volume 116

ISSN 1866-1807

ISBN 978-3-95806-112-5

Bibliographic information published by the Deutsche Nationalbibliothek.
The Deutsche Nationalbibliothek lists this publication in the Deutsche
Nationalbibliografie; detailed bibliographic data are available in the
Internet at <http://dnb.d-nb.de>.

Publisher and Distributor:	Forschungszentrum Jülich GmbH Zentralbibliothek 52425 Jülich Tel: +49 2461 61-5368 Fax: +49 2461 61-6103 Email: zb-publikation@fz-juelich.de www.fz-juelich.de/zb
Cover Design:	Grafische Medien, Forschungszentrum Jülich GmbH
Printer:	Grafische Medien, Forschungszentrum Jülich GmbH
Copyright:	Forschungszentrum Jülich 2015

Schriften des Forschungszentrums Jülich
Reihe Schlüsseltechnologien / Key Technologies, Band / Volume 116

D 82 (Diss. RWTH Aachen University, 2015)

ISSN 1866-1807

ISBN 978-3-95806-112-5

The complete volume is freely available on the Internet on the Jülicher Open Access Server (JuSER)
at www.fz-juelich.de/zb/openaccess.

Neither this book nor any part of it may be reproduced or transmitted in any form or by any
means, electronic or mechanical, including photocopying, microfilming, and recording, or by any
information storage and retrieval system, without permission in writing from the publisher.

Zusammenfassung

Im Rahmen dieser Arbeit zur Grundlagenforschung der organischen Elektronik werden die strukturellen und elektronischen Eigenschaften von Metall-Organik-Grenzflächen untersucht. Drei Variationen des Ausgangssystems, eine homo-molekulare Lage CuPc auf der Ag(111)-Oberfläche, werden mittels STM und LEED auf ihre laterale Struktur und mittels STM-basierter STS und winkelaufgelöster PES auf ihre elektronische Struktur hin vermessen.

Für eine zweite Lage CuPc auf der ersten Lage CuPc auf Ag(111) beobachten wir eine schwächere Wechselwirkung zwischen den beiden Moleküllagen als zwischen dem Substrat und der ersten Lage. Dadurch können die Moleküle der zweiten Lage eine geneigte Konfiguration annehmen, im Gegensatz zu flach liegenden Molekülen in der ersten Lage. Das HOMO von CuPc verschiebt sich mit steigender molekularer Bedeckung zu stärkeren Bindungsenergien. Das (frühere) LUMO, welches in der ersten Lage durch Ladungstransport vom Substrat in die Moleküle zum Teil besetzt ist, ist in der zweiten Lage aufgrund der schwächeren Wechselwirkung mit dem darunterliegenden Material unbesetzt.

Bei der Untersuchung einer dichten, geschlossenen Lage von CuPc auf Ag(110) ist der stärkere Einfluss dieses Substrats auf die Bildung der Moleküllage der offeneren Oberfläche mit geringerer Symmetrie zuzuschreiben. Die Metalloberfläche dominiert die molekulare Anordnung, welche an einigen Stellen, an denen die intermolekulare Wechselwirkung durchdringt, von Versetzungslinien durchzogen ist. Die eigentlich 4-zählige Symmetrie der Moleküle wird aufgrund einer Kombination von geometrischen und elektronischen Effekten auf 2-zählig reduziert. Der Teil eines Moleküls, welcher fast parallel zur Ag[001]-Richtung orientiert ist, wird leicht nach unten gebogen, wechselwirkt stärker mit dem Substrat und erhält Ladung vom Silber. Durch diese Asymmetrie wird die ursprüngliche Entartung der beiden Teile des LUMOs aufgehoben.

Die Bildung lateral gemischter, geordneter hetero-organischer Schichten aus CuPc und PTCDA auf Ag(110) wird ebenfalls stark vom Substrat beeinflusst. Die Tendenz zur Bildung komplexer, großer Strukturen zeigt sich in den zwei verschiedenen von uns beobachteten Phasen mit 5 bzw. 9 Molekülen pro Einheitszelle. Messungen der lokalen elektronischen Eigenschaften zeigen, dass das PTCDA LUMO hier mindestens so stark besetzt ist wie in homo-molekularen PTCDA-Phasen. Das LUMO von CuPc hingegen scheint unbesetzt zu sein, wodurch eine intermolekulare Wechselwirkung mit ungleicher Ladungsverteilung angedeutet wird.

Abstract

In this work we investigate variations of a homo-molecular layer of CuPc adsorbed on the Ag(111) surface, which is a well known example in research on organic electronics where the structural and electronic properties at the metal-organic interface are of interest. Three modifications of the mentioned system are realized by addition of a second layer, exchange of the substrate, and addition of a second type of organic molecules. Measurements on the lateral structure are performed by STM and LEED. For experiments on the electronic structure, STM-based differential conductance spectroscopy and angle-resolved PES are applied.

For a second layer of CuPc on top of the first layer of CuPc on Ag(111) we observe a weaker interaction between the two molecular layers than between the substrate and the first molecular layer. This allows molecules in the second layer to adsorb in an inclined configuration in contrast to the flat lying geometry of molecules in the first layer. The HOMO of CuPc shifts towards larger binding energies with increasing coverage. The (former) LUMO, which in the first layer is weakly occupied by charge donation from the silver substrate, is unoccupied in the second layer because of a significantly weaker interaction with the underlying material.

Experiments on a dense, closed layer of CuPc molecules on the Ag(110) surface reveal a stronger effect of this substrate on the layer formation than the Ag(111) surface. The stronger interacting substrate of lower symmetry dominates the formation of the lateral molecular arrangement interspersed by dislocation lines where the intermolecular interaction breaks through. The initially 4-fold symmetry of the molecules is reduced to 2-fold due to a combination of geometric and electronic effects. The part of the molecule that is aligned with a more acute angle to the Ag[001] direction is slightly bent down, interacting stronger with the substrate and receiving charge donated by the silver. By this asymmetry the original degeneracy of the two parts of the LUMO is lifted.

Laterally mixed hetero-organic layers of CuPc and PTCDA on Ag(110) show the stronger influence of the substrate on the formation of ordered structures compared to mixed ordered layers on Ag(111). A tendency to form complex packing motifs is observed and we investigate two different structures that are described by large unit cells comprising 5 and 9 molecules, respectively. Measurements on the local electronic structure are dominated by signals from PTCDA molecules and we observe that the PTCDA LUMO is occupied to at least the same degree as it is in a homo-molecular PTCDA layer. The CuPc LUMO is unoccupied indicating a molecule-molecule interaction with an unequal charge distribution for the two types of molecules.

List of acronyms

ARPES	angle-resolved photoelectron emission spectroscopy
BW	brickwall
CuPc	copper phthalocyanine
DOS	density of states
HB	herringbone
HOMO	highest occupied molecular orbital
LEED	low-energy electron diffraction
LT	low temperature
LUMO	lowest unoccupied molecular orbital
ML	monolayer
NEXAFS	near-edge x-ray adsorption fine structure spectroscopy
NTCDA	naphthalene tetracarboxylic dianhydride
PEEM	photoelectron emission microscopy
PES	photoelectron emission spectroscopy
p.o.l	point-on-line
PTCDA	perylene tetracarboxylic dianhydride
RT	room temperature
SOMO	singly occupied molecular orbital
SPA-LEED	spot profile analysis LEED
STM	scanning tunneling microscopy
STS	scanning tunneling spectroscopy (= differential conductance spectroscopy)
XSW	x-ray standing waves

Contents

1. Introduction	1
2. Experimental background	5
2.1. Sample system components	5
2.1.1. Silver single crystals	5
2.1.2. Copper phthalocyanine (CuPc)	6
2.1.3. Perylene tetracarboxylic dianhydride (PTCDA)	8
2.1.4. Adsorption of organic molecules on metal surfaces	9
2.2. Determination of geometric structures	10
2.2.1. Scanning tunneling microscopy	11
A. Theoretical foundation	11
B. Experimental realization	17
2.2.2. Low-energy electron diffraction	19
2.3. Determination of electronic properties	23
2.3.1. Differential conductance measurements	23
2.3.2. Photoelectron emission spectroscopy	25
2.4. Experimental procedures	28
2.4.1. Measurement conditions	28
2.4.2. Sample preparation	29
3. Multilayer adsorption of CuPc on Ag(111)	31
3.1. Structural properties: Inclination of molecules	33
3.2. Electronic properties: Orbital depopulation	38
3.3. Summary and Conclusion	42
4. Monolayer formation of CuPc on Ag(110)	47
4.1. Structural properties: Interplay of forces	48
4.2. Electronic properties: Reduction of symmetry	58
4.3. Summary and Conclusion	66

5. Hetero-organic layers of CuPc and PTCDA on Ag(110)	71
5.1. Hetero-organic systems involving CuPc and PTCDA	71
5.1.1. PTCDA as additional component	71
5.1.2. Sample preparation	73
5.2. Mixed phases of CuPc and PTCDA on Ag(110)	74
5.3. Windmill structure (ratio 1:4)	76
5.3.1. Structural properties: Chiral structure formation	76
5.3.2. Electronic properties	83
5.4. Stripe structure (ratio 4:5)	88
5.4.1. Structural properties: Combination of chiral building elements . .	88
5.4.2. Electronic properties	96
5.5. Summary and Conclusion	101
6. Summary, Conclusion, and Outlook	105
List of Figures	109
List of Tables	121
Bibliography	121

1. Introduction

Materials with semiconducting properties are an essential part of today's life due to their crucial role in electronic devices. Organic materials with similar properties as hitherto provided by inorganic semiconductors have become interesting for research some decades ago [Tan86, ATG91, GG10, WWKB12] due to reasons explained in the following. Organic materials offer a variety of interesting properties and advantages that are not achievable with materials traditionally used. For example, electronic components and devices consisting of organic materials are mechanically flexible and of light weight. Numerous reports about successful constructions of applications can be found, for example on organic field effect transistors [Hee98], organic light emitting diodes (OLEDs) [ATG91, Hee98, WMPL07, KKL⁺11], or organic photovoltaic cells (OPVCs) [Tan86, PF01, SH06, WMPL07]. In addition, organic materials require lower temperatures for processing than the corresponding classic inorganic materials, and large areas of organic films can easily be prepared by, e.g., classical printing techniques or vapor deposition making the production much less expensive. Nevertheless, research and industry are still facing major challenges and many aspects about organic electronics require further developments. The remarkably lower charge carrier mobility of organic materials compared to the inorganic counterparts is responsible for the limited speed of certain charge transfer processes and the lower efficiency. Also, the long-term stability of power and, e.g. especially for OLEDs, the color of the emitted light do not yet match the expected values for a device's lifetime.

In modern electronics, not only the choice of materials is a central question but also the size of components. Devices are to be built even smaller, which increases the importance of surfaces and interfaces, leading towards molecular electronics and controlling single charge carriers. In combination with organic materials, this requirement evokes a whole field of research on the various properties and effects occurring at metal-organic interfaces representing the contact between conducting and semiconducting material [WW04, BCK05, Tau07, GG10, WWKB12]. But also organic-organic interfaces

1. Introduction

are investigated as the transition between two semiconductors [HMSK00, CQH⁺11]. The interface dominates the overall structural and electronic properties of these sample systems.

In order to improve the functionality of sustainable electronic devices, which are to be built smaller and smaller, we investigate the properties of the very first molecular layer of organic semiconducting material on metal substrates. Taking previous studies and results into account, the involved components of known sample systems will be varied and the behavior and properties of the new systems will be explored in this thesis.

Prototype materials for samples with one metallic component and one to two semiconducting organic components are silver as the conducting substrate and copper phthalocyanine (CuPc) and perylene tetracarboxylic dianhydride (PTCDA) as organic materials, which have been used for experimental and theoretical studies for a long time. The properties of a molecular layer adsorbed onto a metal surface do not only depend on the inherent features of the molecules themselves but also on the substrate features. Moreover, the choice of a certain metal and also the orientation of the substrate surface affect the interaction strength between the involved components [GSS⁺98, STS⁺00, TES⁺02, GSS⁺07, RLZ⁺12, WLS⁺15]. Thus, different forms of layer growth can be observed, comprising island formation or a gas phase-like distribution for sub-monolayer up to monolayer coverage [LWM⁺89, BBS97, CGD⁺07, WH01, LH02, SHK⁺09, WGM⁺09, LUR⁺14]. Regarding the electronic structure, both types of molecules show n-type semiconducting behavior when in contact with silver by receiving electrons, which act as the conducting charge carriers, from the metal [ZKS⁺06, KSS⁺10].

For the work that will be presented in this thesis, the adsorption of one monolayer (ML) copper phthalocyanine molecules on the silver (Ag) crystal surface with (111) orientation is the starting point. Comprehensive studies have been performed on the growth, the layer formation, and the electronic level alignment by various methods [GKH⁺96, MEP⁺07, KSS⁺10, SKRK11]. For example, tunneling microscopy and electron diffraction experiments revealed that the intermolecular interaction in the first layer is repulsive, causing a dilute distribution of molecules as long as the coverage on the substrate surface is low enough [GKH⁺96, KSS⁺10]. Adsorption height measurements by the x-ray standing wave method yielded the distance of the molecules above the silver substrate and proved a planar adsorption geometry [KSS⁺10]. Charge transfer from the

silver substrate into the molecules as a result of a chemisorptive bonding mechanism has been observed in photoelectron emission spectroscopy [KSS⁺10].

We performed experiments on several variations of this system by exchanging or adding components, i.e. using different metallic substrates and up to two organic materials in the adsorbate layer. In Ch. 2 the properties of the involved components, the preparation of the samples, and the applied techniques for characterization will be explained. In the following parts (Chs. 3, 4, and 5), experimental data, results, and discussions about the properties of the various sample systems will be presented.

The first variation of the known system of 1 ML CuPc on Ag(111) is realized by changing the amount of adsorbed layers, i.e. to prepare a second layer of CuPc on top of the first layer CuPc on Ag(111). Some studies about higher adsorbed layers of iron phthalocyanine molecules on the (111) surface of noble metals [CGD⁺07, SCK⁺08, GG10, GBK⁺11] and one report on the second layer of CuPc on Ag(111) [HHP⁺09] can be found in literature. They all observe similar effects regarding the adsorption geometry. In contrast to the flat lying molecules in the first layer, the second layer consists of inclined molecules. Our experiments will contribute further data about multilayers of CuPc on Ag(111) and compare the obtained results to the mentioned reports.

In the second variation, the Ag(111) substrate is exchanged by a Ag(110) substrate. As mentioned before, the metal surface structure strongly affects the properties of the organic layer [TES⁺02], as the reactivity of the surface changes with the packing density of atoms. Here, we focus on the lateral ordering of molecules in the first layer and the rearrangement of electronic states. With the stronger interacting substrate we expect to observe a stronger influence on the formation of the lateral molecular structure and also a new alignment of orbital energies due to chemisorption.

Finally, we modify the molecular layer of CuPc on the Ag(110) substrate by adding PTCDA as a second type of organic semiconducting material. These hetero-organic systems have become interesting for research some years ago [HMSK00, VGFK05, CQH⁺11], since here not only the metal-organic contact but also the organic-organic contact is of importance. A lot of studies, experimental as well as theoretical, have been performed on vertically stacked hetero-organic samples systems involving PTCDA as one prototype molecule and phthalocyanines as the second component, e.g., for a layer

1. Introduction

of PTCDA on a layer of CuPc on the copper(110) surface [SA94] and for a layer of CuPc on a layer of PTCDA on salt substrates [LBF07], on graphene [CHC⁺08], or on silver(111) [SSK⁺12, ERS⁺13]. Tin phthalocyanine has also been used in combination with PTCDA on Ag(111) [HGS⁺10, HGW⁺10]. Stacked layers offer the possibility to investigate large areas of organic-organic interfaces forming the transition from one semi-conducting material to the adjacent as it is important for completely organic electronic devices, such as OLEDs, involving organic p-n-junctions. We will focus on laterally mixed hetero-organic systems involving CuPc and PTCDA. Lateral mixing has not yet been addressed very often [BWBM03, CSS⁺12, SLW⁺14, SHS⁺15]. It provides the opportunity to tailor the properties of the first molecular layer and, thus, the properties of the following layers adsorbed on top by different mixing ratios and mixing components affecting the lateral order, the intermolecular interaction, and the electronic level alignment. The most challenging task in the project about the hetero-organic layers will be the sample preparation. For the vertically stacked layers it has been found that certain combinations of molecules do not yield stable configurations [Sta13, SGP⁺14] and the structure of laterally mixed layers can be affected by many variables during the preparation process such as the substrate temperature during deposition of molecules, the deposition rate, and subsequent annealing [Hen15, MEP⁺07]. We will present results on two different laterally mixed structures investigated by microscopy, diffraction, and spectroscopic methods.

The last chapter will summarize the results obtained on the different presented sample systems, compare them to each other, and conclude what has been found out about interactions at the metal-organic interfaces and between molecules within an adsorbed layer.

2. Experimental background

In this chapter the fundamentals for understanding and interpreting the experiments and results presented in the following chapters will be introduced. First, the properties of the materials used as probed samples will be elucidated, describing the geometric and electronic properties of the metal substrates and the organic molecules forming ultra thin films on the substrate surface. Next, working principles and setups of the experimental methods, separately for structural and electronic investigations, will be explained. Last, the preparation of the samples and measurement conditions will be listed.

2.1. Sample system components

The two components of the sample systems are the metallic, conducting substrate and the organic, semiconducting material. The following sections treat the important properties and prerequisites establishing the selection of these materials.

2.1.1. Silver single crystals

Silver as a noble metal is in the same group as copper and gold in the periodic table of elements. An important property of this element is that it is rather inert to chemical reactions, e.g. oxidation happens only slowly since the reaction requires further components besides oxygen. The melting temperature of silver is 961 °C although the vapor pressure strongly increases from 700 °C on, which has to be considered when treating silver in vacuum.

As depicted in Fig. 2.1a, the metallic bound crystal has a face-centered cubic (fcc) lattice with densely packed atoms and a lattice constant of 4.09 Å. The pure low-index surfaces (111), (100) and (110) do not reconstruct. Hence, the (111) surface (Fig. 2.1b) exhibits a 2-dimensional hexagonal lattice defined by the unit cell vectors $|\vec{a}_{1(111)}| = 2.89 \text{ \AA}$ along the $[\bar{1}10]$ direction and $|\vec{a}_{2(111)}| = 2.89 \text{ \AA}$ along the $[0\bar{1}1]$ direction with an angle of

2. Experimental background

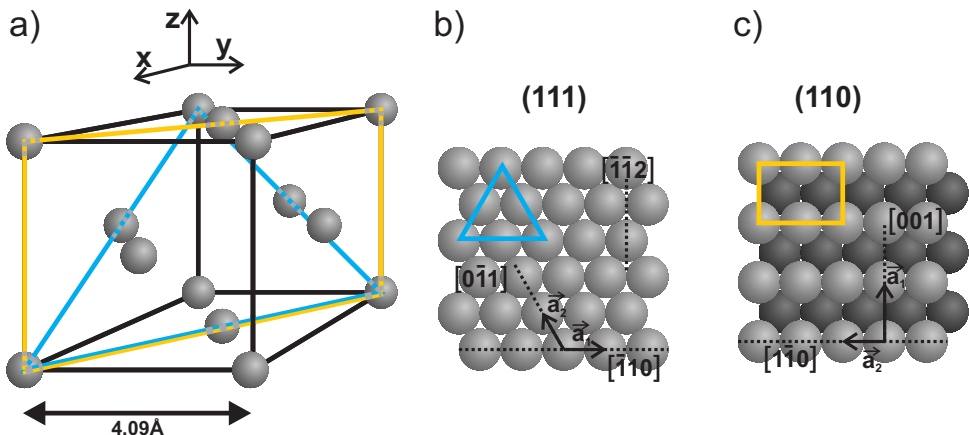


Figure 2.1.: (a) Model of a silver crystal showing a face centered cubic (fcc) lattice with a lattice constant of 4.09 Å. The blue and yellow lines mark the (111) and (110) plane. (b) The Ag(111) surface is 3-fold rotational symmetric and the atoms form a hexagonal surface lattice (c) The Ag(110) surface is 2-fold rotational symmetric with a rectangular surface lattice. The uppermost layer of molecules is given in bright gray and the next underlying layer in dark gray.

120° between them. This surface is smooth with little corrugation and is the least reactive of the three mentioned low-index surfaces of silver. In comparison, the (110) surface (Fig. 2.1c) is a rather open and reactive surface due to less saturated bonds in this less densely packed structure. Its unit cell vectors are $|\vec{a}_{1(110)}| = 4.09 \text{ Å}$ along the [001] direction and $|\vec{a}_{2(110)}| = 2.89 \text{ Å}$ along the $[1\bar{1}0]$ direction with an angle of 90° between them.

Not only due to its relatively inert property but also regarding the electronic structure, silver is an appropriate substrate for the study of ultra thin layers adsorbed on it, since its density of states (DOS) for electrons close (few electron volts) to the Fermi energy is flat [HWST72, Chr72, CWH⁺84, FTB⁺90]. Hence, silver does not cause strong resonances in spectroscopic measurements of adsorbed molecules in the energy range we are going to examine.

2.1.2. Copper phthalocyanine (CuPc)

Phthalocyanine molecules (Pc) with their variety of interesting properties have been a subject of research for almost a century [DL34, Rob35, BDL36]. They are macrocyclic organic molecules (Fig. 2.2a,b) with four identical wings, each consisting of a benzene ring attached to a pyrrol ring. The pyrrol rings are connected to each other via nitrogen

atoms and, where applicable, to the center of the molecule. This center can be filled by, e.g., two hydrogen atoms, one metal atom (e.g. copper, cobalt, tin, zinc, iron, lead), or a larger complex (e.g. TiO, VO) [BDL36]. This way, their magnetic, optical, and electrical properties can be tuned and adjusted for certain applications by exchanging the central metal atom. Thus, for instance, there exist planar and non-planar phthalocyanines or spin neutral as well as spin active ones [CKB⁺08, MHSK08, IRH⁺08, MRK⁺12].

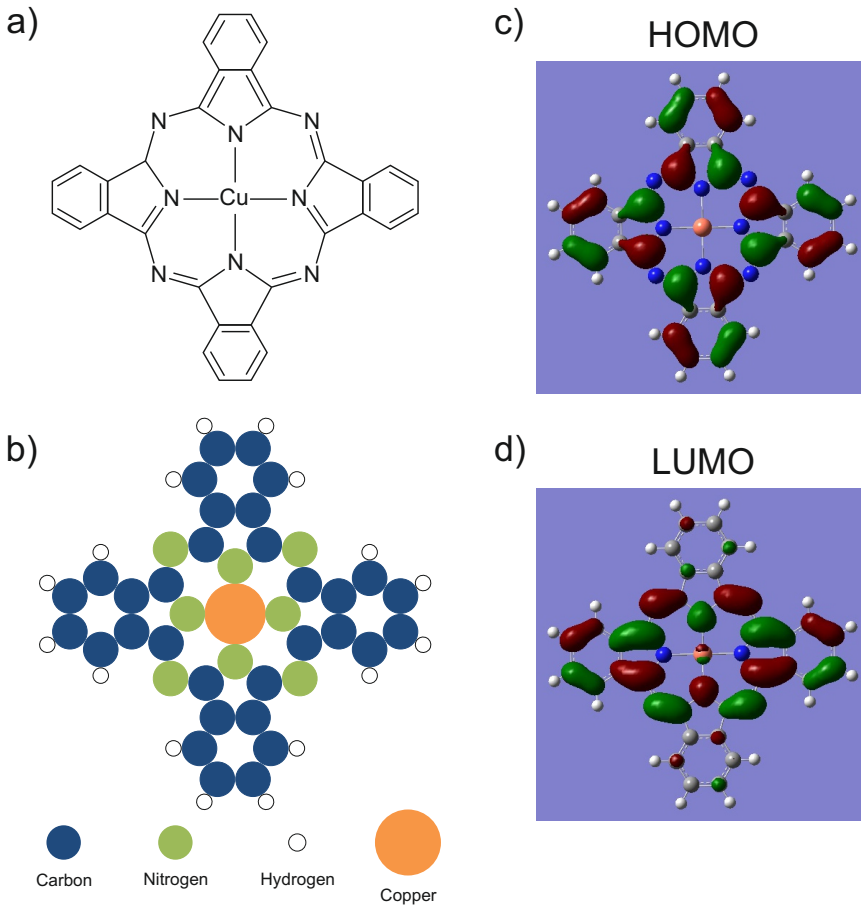


Figure 2.2.: (a,b) CuPc is a geometrically 4-fold symmetric macrocyclic molecule. The distributions of the electron wave functions of the (c) HOMO and (d) LUMO across a CuPc molecule were calculated by Gaussian [FTS⁺04].

2. Experimental background

The experiments presented here involve copper(II) phthalocyanine (CuPc). CuPc is a planar molecule since the copper atom is small enough to fit completely into the central position. Its geometry is 4-fold symmetric and the chemical formula is $C_{32}H_{16}N_8Cu$. It offers a high thermal stability and is often used as a dye [Rob35, Pio57]. Due to an odd number of electrons leaving one state singly occupied, CuPc is spin polarized [RB92, MHSK08, MRK⁺12]. The conjugated π -electron system extending over the central carbon and nitrogen atoms and the semiconducting properties of CuPc are of great interest for the adsorption studies on silver [BCN56, HH63, HA64]. Especially interesting are the molecular orbitals close to the Fermi energy, namely, the highest occupied molecular orbital (HOMO) and the lowest unoccupied molecular orbital (LUMO) whose electron wave functions are shown in Fig. 2.2c,d. The HOMO is equally distributed over the entire molecule while the LUMO extends mainly across two opposite benzene rings. In fact, the LUMO comprises two orbital parts (LUMO_A and LUMO_B) that are degenerate regarding the energy of these states in an isolated molecule. They have the same shape of electron wave function and only differ in their spatial distribution across the molecule being rotated by 90° to each other, thus, together covering all four benzene rings.

Concerning the names of the two lowest unoccupied states of phthalocyanines, two different ways of naming can be found in literature. The first is to call them the two degenerate parts of the one LUMO and the second is to call them LUMO and LUMO+1. We will use the first way of naming in this work because the second way, despite the degeneracy, implies a certain order regarding the energy of the states.

2.1.3. Perylene tetracarboxylic dianhydride (PTCDA)

The second type of molecule this work will later deal with in Ch. 5 is the aromatic molecule perylene-3,4,9,10-tetracarboxylic dianhydride (PTCDA) with the chemical formula $C_{24}H_8O_6$, cf. Fig. 2.3. Its geometry is 2-fold symmetric with an elongated perylene core and an anhydride group at each end. The extended carbon backbone equips the molecule with a π -electron system and the anhydride groups cause negative partial charges at the ends of the molecule, whereas the hydrogen atoms at the long sides have positive partial charges. This uneven distribution of charge strongly affects the structure of PTCDA layers assembling from deposited molecules. The adsorption of PTCDA on different low index single crystal metal surfaces such as silver, gold, and copper is very well studied and often used for prototype sample sys-

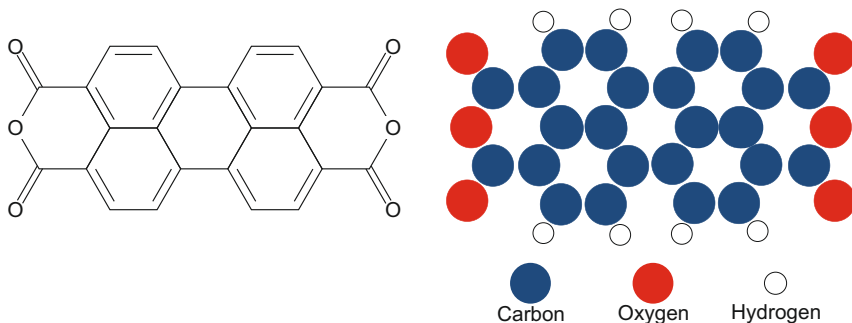


Figure 2.3.: PTCDA is a geometrically 2-fold symmetric aromatic molecule with negative partial charge located at the oxygen atoms and positive partial charge at the hydrogen atoms. The delocalized π -electron system is distributed over the carbon backbone (perylene core).

tems [FLSY89, Umb90, JBS⁺93, SA94, TVD⁺95, USF96, SHFS⁺97, SAL⁺97, GSS⁺98, UGS98, SHFS⁺99, TES⁺02, Tau07, WSS⁺13, Sta13]. Therefore, we will also use PTCDA together with CuPc to form new sample systems by combination of previously well studied systems.

2.1.4. Adsorption of organic molecules on metal surfaces

In experiments with layers of organic materials adsorbed on a metal substrate, the basis for all layers is built right at the interface. The first organic layer in contact with the conducting substrate determines, for instance, geometric arrangements of further layers and the charge transfer between adjacent materials. Especially the charge injection from one component to the other and the charge transport inside the layers play crucial roles for the application of organic materials in electronic devices such as solar cells where charges are separated under light irradiation and conducted to the corresponding electrodes.

The molecules are thermally evaporated and adsorb onto the single crystal metal surface, which provides a periodic template for adsorbate layer growth. The strength of the formed bond varies depending on the structure of the substrate surface and the molecular reactivity. The most general descriptions are physisorption, for interaction where mainly attractive van der Waals forces keep the molecule attached to the surface, and chemisorption, for interaction where a chemical bond is formed between molecule and

2. Experimental background

substrate. CuPc and PTCDA are known to chemisorb on silver and form a bond to the substrate with their π -electron system. In this process, charge is transferred between the involved components and hybridization of molecular orbitals with substrate states takes place. The molecule-substrate interaction also affects the lateral positioning of molecules and so does the molecule-molecule interaction. The intermolecular interaction drives the molecules to arrange such that adjacent molecules tend to be located in potential minima determined by pair potential forces. Adsorbed on the substrate surface, restrictions to the intermolecular arrangement appear and – in the cases presented here – will force the molecules into a flat lying adsorption geometry in the first layer. Depending on the reactivity of the surface, the substrate may cause the molecules to adsorb only at certain substrate lattice sites, forming a commensurate molecular structure, or it offers the freedom for a variety of different lateral positions resulting in an incommensurate structure at the other extreme. Thus, the adsorption process and the layer formation are driven by an interplay of several forces.

The molecular lattice structure can be described by the pair of vectors (\vec{b}_1, \vec{b}_2) , which relate to the substrate vectors (\vec{a}_1, \vec{a}_2) (cf. Fig. 2.1) by a matrix M via the expression

$$\begin{pmatrix} \vec{b}_1 \\ \vec{b}_2 \end{pmatrix} = \begin{pmatrix} m_{11} & m_{12} \\ m_{21} & m_{22} \end{pmatrix} \begin{pmatrix} \vec{a}_1 \\ \vec{a}_2 \end{pmatrix}. \quad (2.1)$$

A commensurate molecular structure is described by a matrix with only integer elements. The coverage of the sample surface is usually expressed as a portion of a monolayer (ML) where 1 ML corresponds to the complete surface covered with the densest possible molecular structure.

2.2. Determination of geometric structures

A great variety of methods offers possibilities to investigate the arrangement of adsorbed molecular layers on single crystal metal surfaces. Here we apply scanning tunneling microscopy as a real space method and low-energy electron diffraction yielding reciprocal space images. These two are expected to complement each other for the construction of a comprehensive picture.

2.2.1. Scanning tunneling microscopy

By the development of an effective isolation against vibrations and a positioning control system based on several piezo actuators for tunneling experiments, Binnig et al. invented the scanning tunneling microscopy (STM) in 1982 [BRGW82b, BR82]. This new technique offered the possibility to non-destructively map the surface of conducting and semiconducting samples in real space at the atomic scale [BRGW82a, BR83a, BR83b, BBR83, HT87].

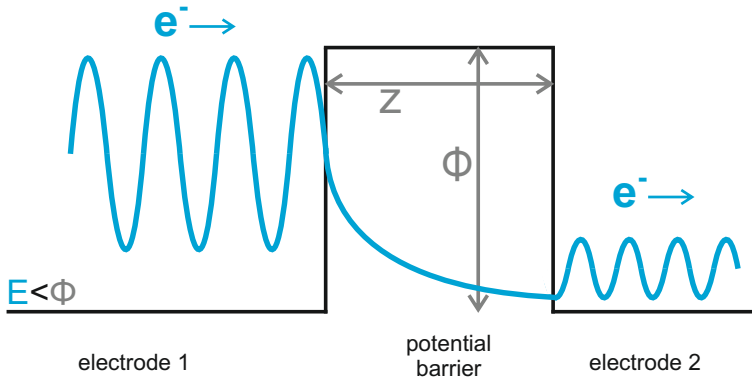


Figure 2.4.: In quantum mechanics, a particle, e.g. an electron, with an energy E that is smaller than the height ϕ of a potential barrier of width z between two electrodes can tunnel from one electrode through this barrier into a state of equal energy in the other electrode. Inside the barrier, the particle wave function is exponentially damped.

A. Theoretical foundation

The basic working principle is the quantum mechanical tunnel effect. In classical mechanics, a particle, e.g. an electron, with an energy E cannot get over a potential barrier with a height ϕ if $E < \phi$. In a quantum mechanical treatment, considering that each particle is described by a corresponding wave function, there is a finite probability for the particle to ‘tunnel’ through this barrier, as demonstrated in Fig. 2.4. The particle wave function ψ oscillating on one side outside the barrier (plane wave state), decays exponentially inside the potential barrier, but propagates further on the other side if the barrier width is finite. In a tunneling experiment, the allowed areas for wave propagation are represented by the electrodes, i.e. an atomically sharp probing tip and the sample to be investigated. The tip is placed above the sample surface with a distance $z \sim 1\text{-}10 \text{ \AA}$

2. Experimental background

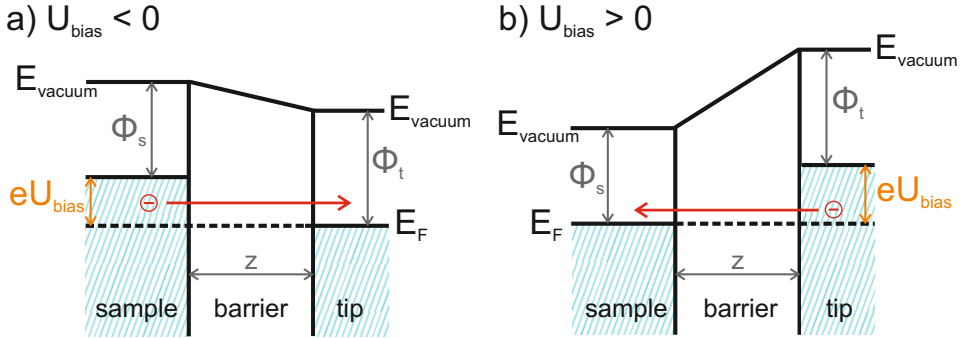


Figure 2.5.: For STM, a voltage U_{bias} is applied to the sample to be investigated shifting the level of occupied states relatively to the level of the Fermi energy E_F . (a) A negative bias voltage raises the sample Fermi level and electrons can tunnel from occupied sample states through the vacuum barrier into the tip. (b) A positive bias voltage lowers the Fermi level in the sample and electrons from the tip can tunnel into unoccupied sample states.

and the vacuum between tip and surface is the gap to be tunneled through by electrons. In order to obtain a directed and measurable tunneling current, a bias voltage U_{bias} is applied to the sample while the tip is grounded (or vice versa), shifting the level up to which electronic states are occupied in one electrode, allowing the electrons to tunnel elastically from occupied states on one side into unoccupied states of the same energy on the other side of the vacuum barrier. Thus, by U_{bias} the window of states participating in the tunneling process is selected. The diagram in Fig. 2.5 illustrates tunneling for negative (a) and positive (b) bias voltages between the metallic sample and the metallic tip with a vacuum barrier. If, in addition, there are semiconducting organic molecules on top of the metal sample surface, these can be involved in the tunneling process. The molecular electronic structure consists of discrete states, which are occupied up to the Fermi energy E_F , with the HOMO right below E_F , and unoccupied states starting with the LUMO right above E_F . If the absolute value of the applied bias voltage is large enough to comprise one or more molecular orbitals, tunneling can occur mediated via molecular states.

In order to obtain a 2-dimensional image, the tunneling current I_{tunnel} is measured while the tip is scanned over the sample surface. As the setup in Fig. 2.6 shows, the scanning movement is controlled by several piezo elements, in the classic version of Binnig et al. [BRGW82b, BRGW82a] by one for each direction in space, where x and y

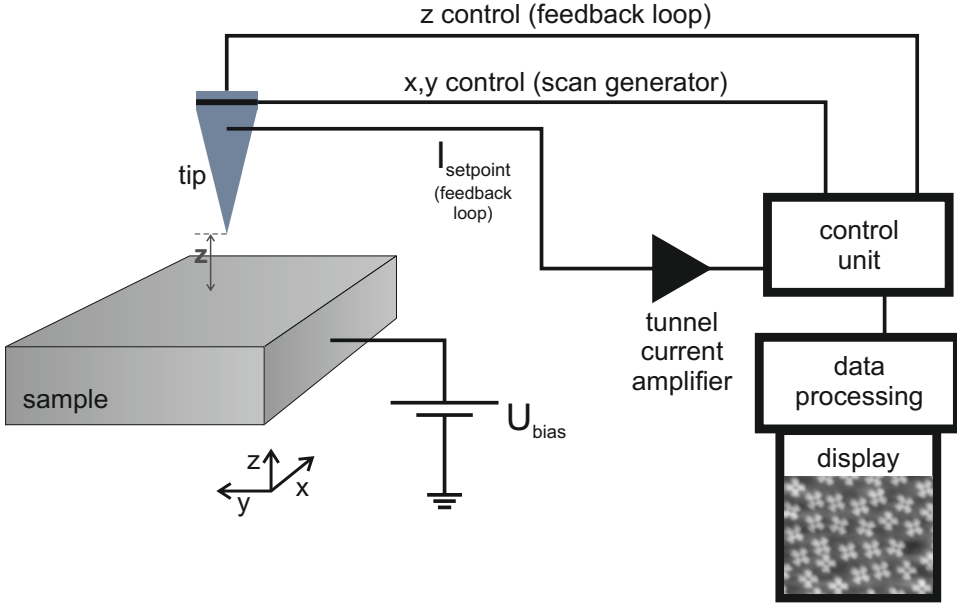


Figure 2.6.: In STM measurements a sharp metallic tip is scanned laterally over the (semi)conducting sample surface controlled by piezo elements for the x - and y -direction. The tunneling current is set to be constant. Thus, the distance z between tip and sample is permanently controlled and corrected by a feedback loop and a piezo element adjusting the tip height. The height signal is recorded and processed yielding an image of the sample surface.

stand for the plane parallel to the sample surface and z is the direction perpendicular to the surface. In the ‘constant current mode’, I_{tunnel} is kept constant for every lateral position. This means that the z -position of the tip is permanently adjusted by a feedback loop. By recording the z -position, for a constant barrier height, a topographic image of the sample surface is obtained.

In most experimental cases, the barrier height ϕ is not constant over the whole surface, since it represents the work that has to be done to remove an electron from the material. This means, the tip does actually not follow the topographic height of the sample, but a contour of constant wave function overlap between tip and sample is mapped, which is the electron local density of states (LDOS) of the sample [BBR83, BR83c], cf. Fig. 2.7, which is the number of states that can be occupied in an energy interval. A spatial selection of the electron DOS just outside the sample is realized by changing the desired

2. Experimental background

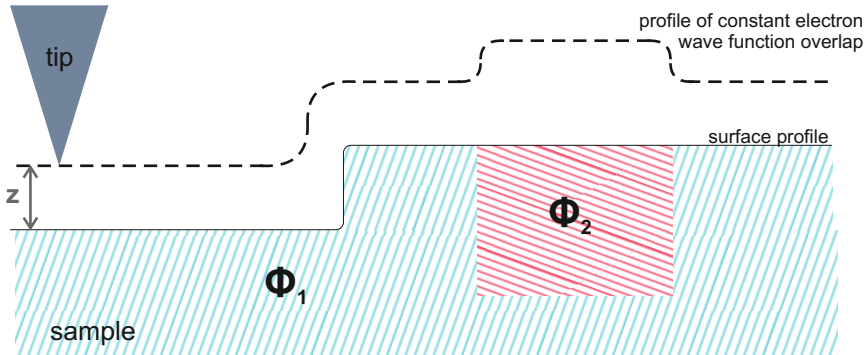


Figure 2.7.: Constant current mode in STM: The distance z between tip and sample is constant for one material work function ϕ_1 , also across a step of the surface. z changes with changing ϕ adjusting the tip height so that the current between tip and sample is constant. An image of a constant electron LDOS right above the sample surface is obtained by this method.

value for the tunneling current, which we will now call the setpoint: $I_{\text{tunnel}} = I_{\text{setpoint}}$. This variable adjusts the height of the tip above the sample. A change of the applied voltage U_{bias} means an adjustment of the image regarding the energy of the sample states by selecting the energy up to which electrons are allowed to participate in the tunneling process.

Already in the first years of STM, the resolution perpendicular to the surface reached down to 0.1 \AA limited by the stability of the instrument. The lateral resolution can reach atomic resolution depending on several influences as the tip curvature, the tip-sample distance, the barrier height ϕ and the spatial extension of the surface state wave function [BR82, BR83b, BR83c].

The tunneling current I_{setpoint} is a function of the tip-sample distance, the LDOS of the sample, and the applied voltage U_{bias} , among other variables. It is the product of the electron current in one electrode (e.g. the sample) impinging onto the barrier (the vacuum) and the transmission coefficient for tunneling of electrons through this barrier. The transmission coefficient is the ratio of the transmitted wave function behind the barrier and the wave function in front of the barrier and is given by

$$T = e^{\frac{-2z}{\hbar} \sqrt{2m_e \phi}} = e^{-2z\kappa} \quad (2.2)$$

with the distance z between sample and tip, the electron mass m_e and the barrier height ϕ . The exponential decay of the current with increasing tip-sample distance has already been observed in the first STM experiments [BRGW82b]. Further dependencies of the tunneling current can, for example, be derived from Bardeen's theory of tunneling, starting with the evaluation of Schrödinger's equation with a time-dependent approach and the transfer Hamiltonian \widehat{H}_T [Bar61, Che08, Wie94]. The shapes of sample (s, summation index σ) and tip (t, summation index τ) play a role as they determine the participating states (ψ_σ, ψ_τ) and the corresponding possible tunneling processes between these two electrodes. The tunneling current in this model is given by Eq. 2.3 with the Fermi distribution function $f(E)$.

$$\begin{aligned}
 I_{\text{setpoint}} \propto \sum_{\sigma, \tau} \{ & \underbrace{f(E_\tau)[1 - f(E_\sigma + eU_{\text{bias}})]}_{\text{tunneling from tip to sample}} - \underbrace{f(E_\sigma + eU_{\text{bias}})[1 - f(E_\tau)]}_{\text{tunneling from sample to tip}} \} \\
 & \times \delta(E_\sigma - E_\tau) \times \underbrace{\left| \langle \psi_\tau | \widehat{H}_T | \psi_\sigma \rangle \right|^2}_{\text{tunneling matrix element}}
 \end{aligned} \tag{2.3}$$

The tunneling matrix element $M_{t,s}$ describes the interaction energy due to the overlap of the tip wave function and the sample wave function [Che08]. $M_{t,s}$ is calculated as a surface integral over a surface in the vacuum (barrier) separating tip and sample. The integrand is formed by the wave functions of tip and sample containing the exponential decay of the wave functions into vacuum. So, $M_{t,s}$ contains the formerly mentioned transmission coefficient.

Since especially the shape of the tip is not known in experiment and these calculations are rather complicated, a simplified model has been introduced by Tersoff and Hamann, assuming a spherical tip with only s-wave function states contributing to the tunneling process [TH83, TH85, Che08, Wie94]. The tip has a radius R and its center is located at \vec{r}_t as depicted in Fig. 2.8. Applying this simplification, $M_{t,s}$ is expressed by the product of the tip density of states ρ_t and the wave function at distance R from the tip center. Including further the approximations of small temperature and small bias voltage, i.e. only states from the tip (t) and the sample (s) close to the Fermi energy E_F participate, the expression for the tunneling current becomes

$$\begin{aligned}
 I_{\text{setpoint}} \propto U_{\text{bias}} \rho_t(E_F) e^{2R\kappa} \underbrace{\sum_{\sigma} |\psi_\sigma(\vec{r}_t)|^2 \delta(E_\sigma - E_F)}_{= \rho_s(E_F, \vec{r}_t) = \rho_s(E_F) e^{-2\kappa(z+R)}}
 \end{aligned} \tag{2.4}$$

2. Experimental background

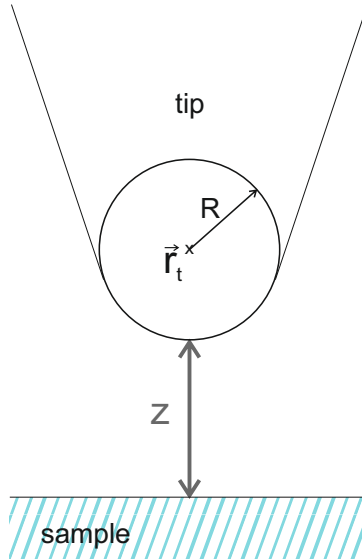


Figure 2.8.: In the Tersoff-Hamann model the tip is assumed to be spherical and represented by an s-wave function. The center of the tip is located at \vec{r}_t^x and its radius is R . The distance between the tip and the sample is z .

This way one can see the dependency of the tunneling current on the sample LDOS ρ_s at the Fermi energy E_F , the applied bias voltage U_{bias} , the tip sample distance z , and the effective barrier height (ϕ is contained in κ), which is the average of tip work function and sample work function [TH83, TH85, Che08, Wie94]:

$$I_{\text{setpoint}} \propto U_{\text{bias}} \rho_t(E_F) \rho_s(E_F) e^{-2z\kappa} . \quad (2.5)$$

The exponential term comprising the tip-sample separation z is responsible for the high vertical resolution of this technique, because if the height of the tip above the sample surface changes by about 1 \AA , I_{setpoint} changes by about one order of magnitude.

For a finite bias voltage applied, Eq. 2.5 has to be integrated over energy in the window between E_F and eU_{bias} :

$$I_{\text{setpoint}} \propto U_{\text{bias}} \int_{E_F}^{eU_{\text{bias}}} \rho_t(E - eU_{\text{bias}}) \rho_s(E) e^{-2z\kappa_{\text{bias}}} dE \quad (2.6)$$

with

$$\kappa_{\text{bias}}(E, U_{\text{bias}}) = \frac{1}{\hbar} \sqrt{2m_e \phi_{\text{bias}}(E, U_{\text{bias}})} \quad (2.7)$$

and the effective barrier height

$$\phi_{\text{bias}}(E, U_{\text{bias}}) = \frac{\phi_t + \phi_s + eU_{\text{bias}}}{2} + (E - E_F) \quad (2.8)$$

for electrons at the energy E participating in the tunneling process. The dependencies of the tunneling current on the applied bias voltage and on the sample LDOS ρ_s will play an important role for differential conductance measurements described in Sec. 2.3.1.

B. Experimental realization

The microscope used for experiments described in this thesis is a Besocke type STM developed in 1987 [Bes87]. The setup of this STM unit is more compact, more stable, and more simple than the previous one developed by Binnig and Rohrer, since it comprises remarkably less elements, namely, only a base plate, piezo elements, and the sample. Four identical hollow piezo tubes are mounted onto the base plate such that three of them form a triangle and the fourth is in the center. The three outer piezo tubes carry the sample on small sapphire balls mounted on top of the tubes. All piezo tubes have four segments at their outside, opposite located elements are contacted with opposite polarity, one contact at the bottom and one at the top, and the inner contact is grounded. By applying an appropriate voltage to the contacts at the outside, the tubes can bend in any direction allowing all movements in the x - y -plane. A voltage applied between the top and bottom contact causes contraction and extension, respectively, of the tube for movements in the z -direction perpendicular to the sample surface. The piezo tube in the center holds the probing tip and is contacted similar to the other piezo tubes such that the tip can be approached to or retracted from the sample surface as well as scanned laterally across the surface. In this highly stable setup thermal drift is mostly self-compensated. Coarse lateral movement of the sample with respect to the tip is realized by a simultaneous slip-stick motion of the three outer piezo tubes.

The setup of our STM unit, depicted in Fig. 2.9, is quite similar to the original Besocke type, except for the fact that the tip is not mounted on the base plate, scanning the sample face down. Our sample is placed on the base plate, on which there are

2. Experimental background

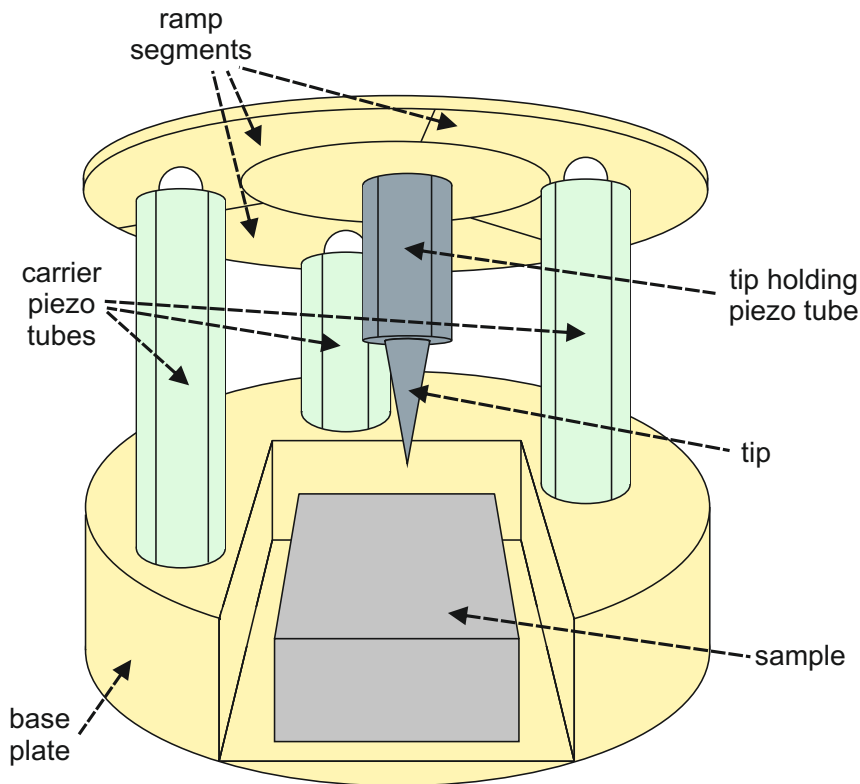


Figure 2.9.: Setup of a very compact, rigid, easily operable, and thermally stable STM unit: The sample is placed in the middle of three piezo tubes that carry the ramp plate on small insulating spheres. A fourth piezo tube with the probing tip is attached to the center of the ramp plate. Each piezo tube has four contacted segments at its outside for any movements in the x - y -plane parallel to the sample surface. Contacts at the top and at the bottom allow motion along the z -direction.

mounted three piezo tubes in a triangular arrangement holding an annular ramp plate with one inclined segment for each piezo tube allowing for coarse movements in the z -direction. The fourth piezo tube holding the tip is attached to the ramp plate such that the tip approaches the sample from above. This modification is more practical for low temperature STM [GGR⁺92, SR94] where the whole STM unit is attached to the bottom of a cryostat containing liquid helium. The connection between cryostat and STM unit is realized by copper blocks of good thermal conduction for cooling of the sample before the performance of experiments. The helium cryostat is surrounded by another cryostat

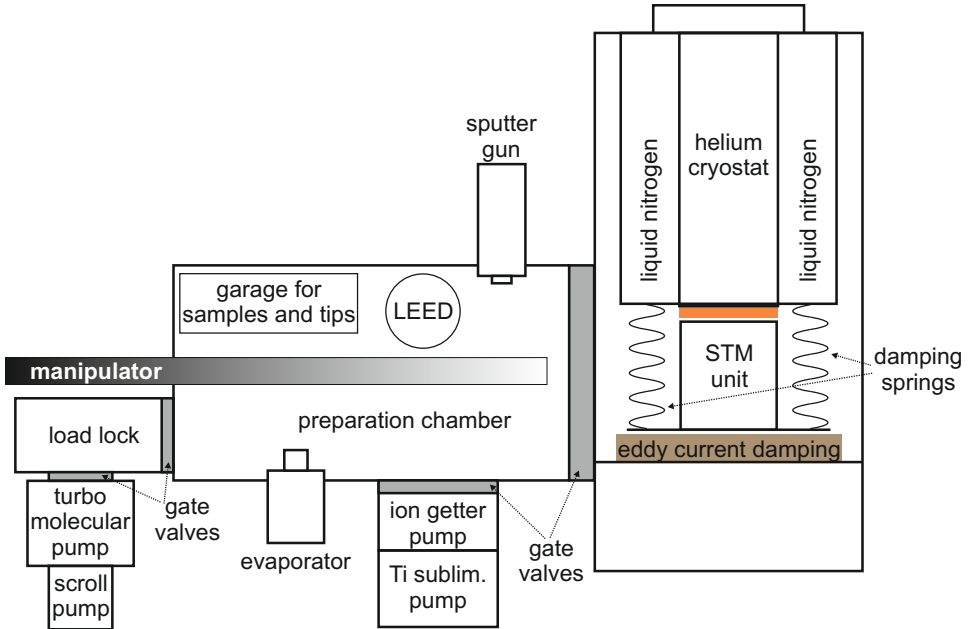


Figure 2.10.: The complete experimental setup comprises the STM unit in a separate vacuum chamber attached to a cryostat system and the preparation chamber with additional elements for sample preparation and investigation. Springs and an eddy current damping system isolate the STM unit from mechanical vibrations. For further explanations on the preparation chamber see Sec. 2.4.

filled with liquid nitrogen. During experiments, the STM unit is decoupled from the cryostat and the other parts of the vacuum chamber needed for experiments (cf. Sec. 2.4) by vibration damping springs. The whole experimental setup with STM unit, cryostat, vacuum chamber, and additional elements is illustrated in Fig. 2.10.

2.2.2. Low-energy electron diffraction

The diffraction of electrons at periodic structures has been known for decades and a surface sensitive tool has been developed based on this effect [EK85, HWC86]. In low-energy electron diffraction (LEED) the kinetic energy of electrons with mass m_e hitting the sample surface lies between 10 eV and 1 keV so that their corresponding de Broglie wave length

$$\lambda_{dB} = \frac{h}{\sqrt{2m_e E_{kin}}} \quad (2.9)$$

2. Experimental background

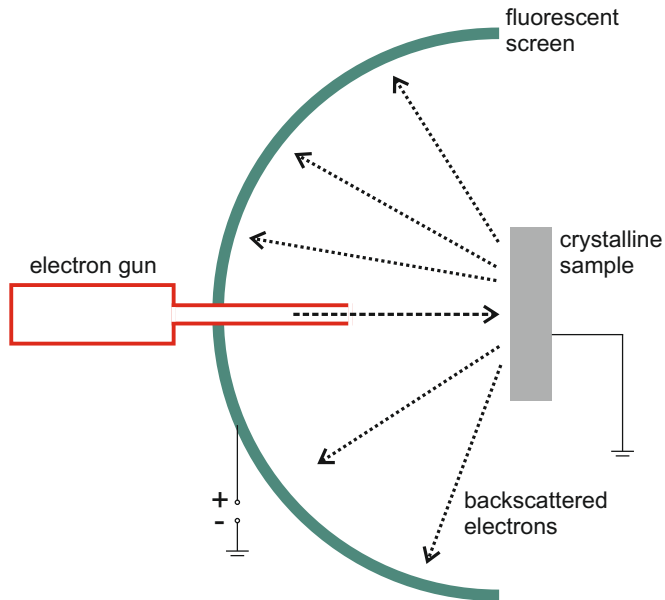


Figure 2.11.: In a conventional low-energy electron diffraction experimental setup, electrons hit the crystalline sample surface at normal incidence. The interference pattern of the scattered electrons is detected with angular resolution on a fluorescent screen.

is in the order of magnitude of 1 \AA . This value approximately matches the lattice constant of metallic and semiconducting crystals, and with a kinetic energy in the mentioned range the penetration depth amounts up to 10 \AA probing the first layers of the crystal. The backscattered electrons interfere with each other and the diffraction pattern, which is the Fourier transformation of the crystalline structure of the sample surface, is detected, for example, on a fluorescent screen, cf. Fig. 2.11. Since here we are only interested in a description of the position of the diffraction spots for the purpose of a simple geometric analysis of the surface structure, inelastic and multiple scattering effects are neglected in the following explanation of the method. The creation of the electron diffraction pattern can easily be explained in reciprocal space where a wave with a vector

$$|\vec{k}_0| = \frac{1}{\hbar} \sqrt{2m_e E_{\text{kin}}} \quad (2.10)$$

is assigned to an incident electron of energy E_{kin} . The scattered electron has the wave vector \vec{k}' . The reciprocal lattice of a three-dimensional crystal is also a lattice with dis-

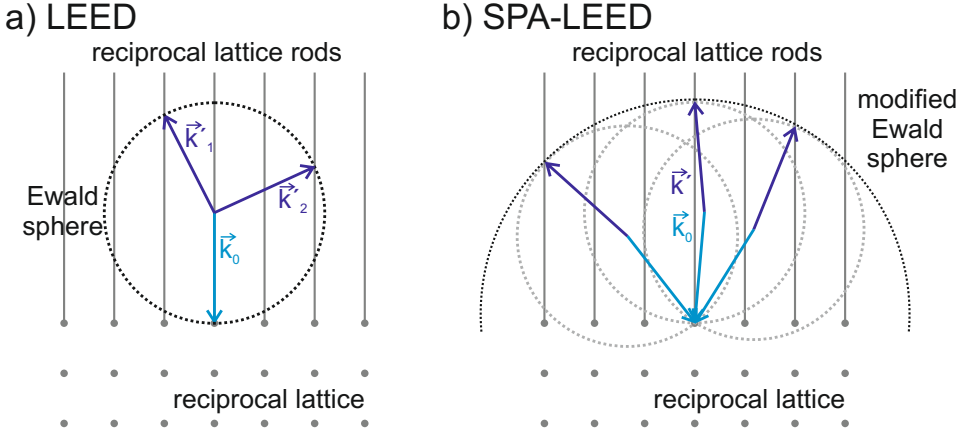


Figure 2.12.: The Ewald construction illustrates the creation of an electron diffraction pattern. (a) In a conventional LEED setup the incoming electrons with a wave vector \vec{k}_0 hit the sample at normal incidence and are scattered into the direction of \vec{k}' . Diffraction spots can be observed where the Ewald sphere intersects the reciprocal lattice rods. (b) In a SPA-LEED setup the angle between incident and scattered electrons is fixed and does not change, but the angle of incidence, i.e. the direction of \vec{k}_0 is rotated for a complete scan of the reciprocal space, together with the direction of \vec{k}' .

crete lattice points. At the surface, the symmetry is broken and in real space the distance to the next atoms becomes infinite. In reciprocal space, these diffraction spots therefore have an infinitely small distance to each other, forming lattice rods. In a conventional LEED setup, the electrons, coming from an electron gun, hit the sample surface at normal incidence, are scattered back at the crystalline surface structure, and interfere constructively with each other according to the Laue-condition

$$\vec{k}' - \vec{k}_0 = \vec{G} \quad , \text{ which for only 2 dimensions becomes } \vec{k}'_{\parallel} - \vec{k}_{0,\parallel} = \vec{G}_{\parallel} \quad , \quad (2.11)$$

where \vec{G} is the reciprocal lattice vector. Figure 2.12a illustrates the creation of the interference pattern during the diffraction process by an Ewald construction. The Ewald sphere has its center at the beginning of \vec{k}_0 and the vector's magnitude is the radius. Diffraction spots are observable where the Ewald sphere intersects with reciprocal lattice rods. When the wave vector of the diffracted electron \vec{k}' , starting also at the center of the sphere, ends at one of these intersection points, the Laue condition is fulfilled.

2. Experimental background

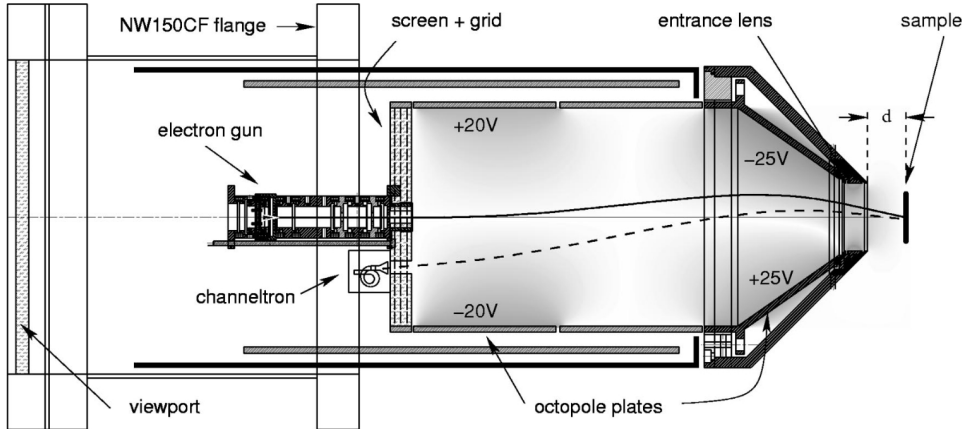


Figure 2.13.: In a SPA-LEED the electron detector is mounted at a certain position with a fixed angle relative to the electron gun. The octopole plates control and vary the path of incident and scattered electrons, thus, scanning the reciprocal space to obtain a 2-dimensional diffraction image. Figure taken from [ZH02].

A variation of the conventional LEED setup is called spot profile analysis LEED (SPA-LEED). Instead of a fluorescent screen it contains one channeltron as electron detector mounted at a certain position with a fixed angle relative to the electron gun as shown in Fig. 2.13. This way it is not possible to obtain a LEED image at one shot, but the reciprocal space is scanned for an image, since the channeltron only detects electrons from a small area. The path of the electrons from the gun to the sample (solid line in Fig. 2.13) is determined by the octopole plates, which deflect the electrons for a variation of the angle of incidence at the sample. The path of the backscattered electrons (dashed line in Fig. 2.13) towards the channeltron detector is close to the path from the gun to the sample surface, again regulated by the octopole plates. Thus, the angle between incident and diffracted electrons is constant, i.e. the angle between \vec{k}_0 and \vec{k}' is fixed and for certain angles of incidence the channeltron detects corresponding diffraction spots. To obtain a complete reciprocal space image, \vec{k}_0 and \vec{k}' are rotated together enlarging the detected area of the reciprocal space as demonstrated in Fig. 2.12b.

The SPA-LEED has been invented in 1986 [SMH86] and improved over the last decades [Hoe99, ZH02]. Compared to LEED it offers several advantages. Images without the shadow of the electron gun and with a higher k -space resolution are obtained. The latter feature is achieved by an improved ratio of the detector aperture (which is smaller

in a SPA-LEED than in a conventional LEED) to the sample-detector distance (which is larger in a SPA-LEED than in a conventional LEED). Further, the profile of diffraction spots can be analyzed (which gave the instrument its name) and a study of the spot intensity depending on the electron energy is possible. Especially important for the investigation of organic molecular layers is that a much lower electron flux than required for conventional LEED is applicable due to the highly sensitive detector, decreasing the sample damage remarkably and allowing higher electron energies for patterns of larger reciprocal space areas.

2.3. Determination of electronic properties

There exist many different spectroscopic methods for the detection of the electronic properties of adsorbed layers. We will mainly apply STM-based differential conductance spectroscopy, often referred to as scanning tunneling spectroscopy, giving information about the local electronic structure within an area of few \AA^2 . A very popular method for experiments on the global electronic structure over the whole sample surface is photoemission spectroscopy.

2.3.1. Differential conductance measurements

Scanning tunneling spectroscopy (STS) is based on the tunnel effect similar as described in Sec. 2.2.1 for scanning tunneling microscopy and depicted in Fig. 2.14a. The tunneling current between the metallic tip and the (semi)conducting substrate for a finite voltage U_{bias} applied to the sample is given by Eq. 2.6. Due to its dependency on the sample density of states $\rho_s(E)$, the current increases when the biased energy window eU_{bias} above E_F is large enough to comprise sample states, i.e. resonances. The increasing slope of I_{tunnel} is observed as a peak in the derivative $dI_{\text{tunnel}}/dU_{\text{bias}}$, cf. Fig. 2.14b. Thus, by measuring the derivative of I_{setpoint} with respect to U_{bias} one has direct access to the sample LDOS as a function of energy, assuming that the tip DOS is flat around the Fermi energy:

$$\frac{dI_{\text{setpoint}}}{dU_{\text{bias}}}(U_{\text{bias}}) \propto \rho_t(E_F) \rho_s(E_F + eU_{\text{bias}}) e^{-2z\kappa_{\text{bias}}(eU_{\text{bias}}, U_{\text{bias}})} \quad (2.12)$$

The exponential term describing the transmission function causes the background to increase with U_{bias} superimposed by a pattern of resonances that is proportional to the sample LDOS. Hence, STS yields information about the structure of electronic states.

2. Experimental background

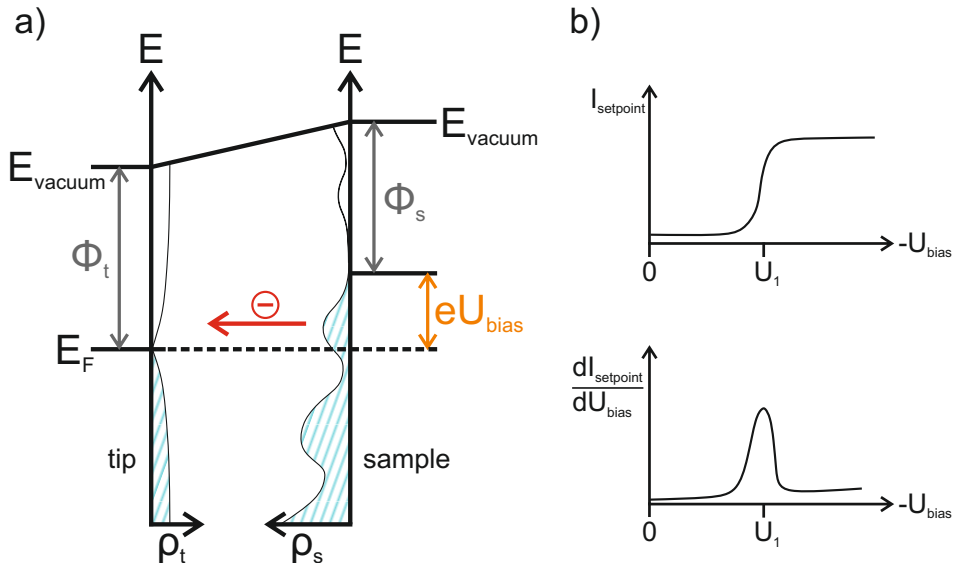


Figure 2.14.: (a) In an STS measurement the bias voltage is ramped, e.g. from 0 V towards negative U_{bias} . (b) The tunneling current I_{setpoint} increases when going through a resonance. The increase of the current is observable as a peak in the differential conductance $dI_{\text{setpoint}}/dU_{\text{bias}}$, which is directly proportional to the sample LDOS.

For spectroscopy, the tip is placed above the point of interest of the sample surface and the feedback loop controlling and correcting the tip height is switched off. The voltage applied between tip and sample is ramped from e.g. -1 V to 1 V (and back) while the tip is held at one height. Measuring the tunnel current and its derivative during this process yields the local density of states of the sample at the investigated spot. Occupied sample states appear as resonance peaks on the side of negative bias and unoccupied sample states appear on the side of positive bias in these differential conductance spectra.

Our experiments are carried out with the lock-in amplifier technique filtering the desired signal. The derivative of I_{setpoint} with respect to U_{bias} is recorded while the voltage is ramped up from negative to positive values and for the ramping vice versa. During the data evaluation process, these two spectra are averaged and noise is filtered out in the program Origin by application of a fast Fourier transformation and suppression of perturbing frequencies.

2.3.2. Photoelectron emission spectroscopy

When Hertz [Her87] and Hallwachs [Hal88] discovered the effect of light irradiation on metal plates, explained as the photoelectric effect by Einstein some years later [Ein05], the fundamentals for a new method were there [Hö3]. Photoelectron emission spectroscopy (PES) uses the photoeffect to investigate the electronic properties of surfaces. In experiment, photons of a certain energy $E_\gamma = \hbar\omega$ are irradiated onto the sample and transfer their energy to electrons. If the energy of an excited electron is great enough, it can leave the sample and continue in the vacuum outside as a free electron with a certain kinetic energy. The photon energy can be selected such that the kinetic energy of the emitted electrons is less than 100 eV. In this case, only electrons from the first layers are able to leave the sample as their mean free path is in the order of magnitude of 10 Å. Hence, PES can be used as a surface sensitive technique. The emitted electrons are detected and the intensity is measured as a function of the electron energy. For a known photon energy $\hbar\omega$ and analyzer work function ϕ_a , which is to be smaller than the sample work function ϕ_s , the binding energy E_B of the state where an electron is emitted from can be calculated according to energy conservation (cf. Fig. 2.15):

$$\hbar\omega = E_{\text{kin}} + E_B + \phi_a . \quad (2.13)$$

The sample work function can also be calculated from the photon energy and the width of the analyzed spectrum:

$$\hbar\omega = \phi_s + (E_{\text{kin,max}} - E_{\text{kin,min}}) . \quad (2.14)$$

In this simple picture neglecting final state effects we assume an immediate relaxation of the remaining sample system missing one electron and exclude interaction between the escaping electron and the created positively charged hole. The spectrum of detected electrons corresponds to the sample DOS (at the surface), as demonstrated in Fig. 2.15 for discrete sample states, which is the case for organic molecules that will be in the focus of experiments presented in this thesis. The finite width of the measured peaks appears naturally due to, e.g., thermal broadening.

A further developed variation of PES is angle-resolved photoelectron spectroscopy (ARPES), which here is performed with ultraviolet light because these wavelengths cor-

2. Experimental background

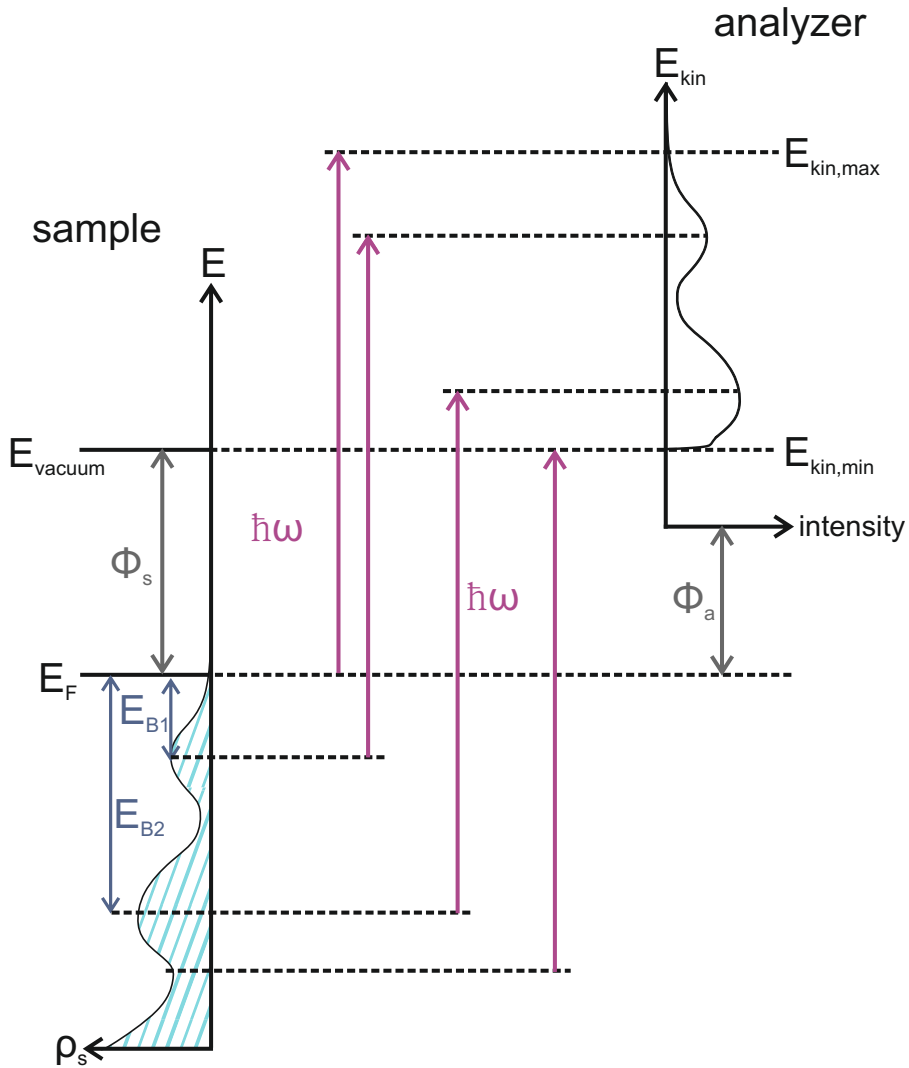


Figure 2.15.: Photoelectron spectroscopy is based on the photo effect where photons release electrons from a sample. The kinetic energy of the emitted electrons is measured and the binding energy of the state they come from can be calculated as the difference between the photon energy $\hbar\omega$, the work function ϕ_a of the analyzer, and the kinetic energy E_{kin} of the electrons.

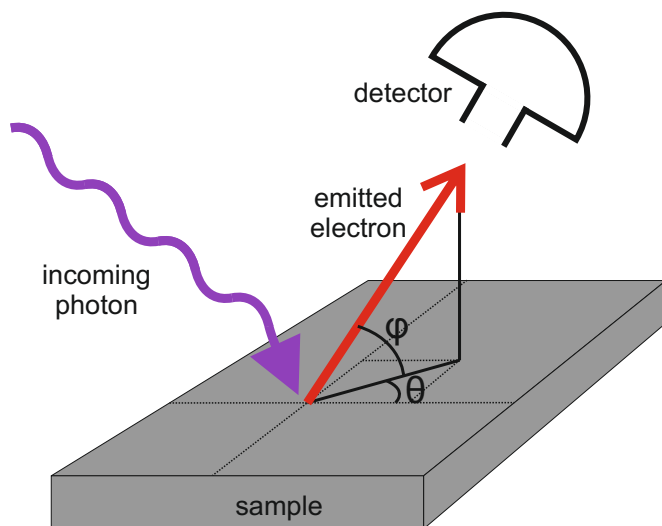


Figure 2.16.: In angle-resolved photoelectron spectroscopy not only the energy but also the emission angle φ is detected. By a rotation of the sample around the azimuthal angle θ , the full hemisphere above the sample can be imaged.

respond to the binding energies of the valence states we are interested in. The schematics in Fig. 2.16 illustrates the experiment: The electron leaving the sample after excitation by a photon has a certain momentum \vec{k} inside the sample. When penetrating through the sample surface, the momentum components k_x and k_y parallel to the surface are conserved while the component perpendicular to the surface changes with the surrounding medium similar to Snell's law of refraction. The parallel components are detected as emission angles φ measured with respect to the surface normal and θ as azimuthal angle in the surface plane. The detection can be carried out separately for all angles φ , θ . The data are transformed from polar and azimuthal coordinates into reciprocal space coordinates k_x and k_y so that a momentum space image for the full hemisphere above the sample surface is obtained. For a certain kinetic energy corresponding to the binding energy of a molecular orbital, the 2-dimensional momentum space image gives a fingerprint of the orbital in reciprocal space according to the Fourier transformation of the wave function distribution of the orbital in real space. This technique allows a direct identification and assignment of observed spectroscopic resonances.

2. Experimental background

Two different setups are used for the experiments performed for the work presented here. At the synchrotron BESSY II at the Helmholtz Zentrum Berlin, a toroidal analyzer detects the emitted electrons in a wide emission angle range of $\varphi = \pm 85^\circ$ for a certain energy [LR85, Lec87, TRH⁺10]. The sample is rotated around the surface normal in steps of 1° yielding data for every azimuthal angle θ . The second setup used at the Elettra synchrotron in Trieste yields the whole 2-dimensional image at once by a photoelectron emission microscope (PEEM) where the electrons of all emission angles reach the detector screen via several electron lenses [SWP⁺12, FGN⁺14].

2.4. Experimental procedures

This section contains short descriptions of the conditions under which the measurements were performed with the techniques explained above. Also, the sample preparation procedure is elucidated. Although the experiments took place in three different laboratories, all steps of preparation and measurement were carried out in ultra-high vacuum chambers. In this environment the contamination of the sample surface by residual gas particles is low enough to keep the surface clean over the time span necessary for measurements.

2.4.1. Measurement conditions

The pressure for LEED and PES experiments was $\sim 10^{-9}$ mbar and these were carried out at room temperature. For STM and STS, values of the pressure of $\sim 10^{-10}$ mbar to $\sim 10^{-11}$ mbar could be reached and these measurements took place at low temperature. At the STM unit, which for cooling is attached to the bottom of the helium cryostat and released for experiments in thermal equilibrium, a temperature of ≈ 5 K could be measured and the temperature at the sample is assumed to be about 10 K. The cold environment is required to suppress thermal drift, for good spectroscopic resolution with low noise and peak broadening, and to minimize diffusion of molecules on the metal surface and enable stable imaging in STM. In order to avoid mechanical disturbance by vibrations from the building, the whole vacuum chamber as depicted in Fig. 2.10 can be lifted by air-filled laminar flow isolator feet by Newport Corporation. Electric cables not used for the ongoing measurement are detached from the chamber system to avoid electric noise.

The STM used in this work has been build by CreaTec Fischer & CO. GmbH and is operated with an etched platinum-iridium tip (Pt_{0.8} Ir_{0.2}; 0.25 mm diameter). The SPA-LEED has been made by Omicron NanoTechnology GmbH and the micro channel plate (MCP-)LEED by OCI Vacuum Microengineering Inc. PES experiments were partly carried out at the NIM/SGM beamline with a toroidal analyzer at BESSY II in Berlin (photon energy 30 eV) and with the photoelectron emission microscope (PEEM) ‘NanoESCA’ by Omicron NanoTechnology GmbH at the Elettra synchrotron in Trieste (photon energies 35 eV and 40 eV).

The performance and results of STS as carried out in this work strongly depends on the tip DOS, the molecular states and the substrate DOS. In order to facilitate the interpretation of obtained spectra it is desirable to have a tip with a flat DOS around the Fermi energy. Therefore, the tip has to be prepared, which can be done by application of a short voltage pulse to the tip to release dirt or parts of molecules and also by carefully dipping the tip into the surface in an uncovered (clean) area to pick up silver substrate atoms as outermost part of the tip, which offers the desired flat tip DOS. In all cases discussed here, the preparation of an adequate tip is difficult as we usually work with dense, complete molecular layers leaving no uncovered silver surface areas. Thus, after preparing the tip by voltage pulses and careful dipping we do not know which atoms or clusters form the tip and what its DOS is like. This makes the interpretation of the measured spectra more difficult and will affect the results through the entire data analysis.

In addition, CuPc as a molecule usually yields less intensity in spectroscopic methods (e.g. differential conductance spectroscopy, photoelectron spectroscopy) than, for instance, the also well-known PTCDA molecule, probably due to a lower interaction cross-section, which could not yet be explained.

2.4.2. Sample preparation

Before the preparation of molecular layers on the substrate, the single crystal metal surface is cleaned by repeated cycles of argon sputtering ($\pm 50^\circ$ and $\pm 65^\circ$ incidence angle towards the surface normal) and annealing up to $\approx 600^\circ\text{C}$. For the deposition of organic molecules the sample was held at room temperature. The powder of organic material is filled into a crucible and, in a home-made evaporator, heated by electric current providing temperatures high enough for the molecules to sublime, i.e. about 500°C for CuPc and about 220°C for PTCDA are measured near the crucibles.

3. Multilayer adsorption of CuPc on Ag(111)

The properties of the first monolayer of CuPc molecules adsorbed onto the Ag(111) surface are very well studied [GKH⁺96, MEP⁺07, KSS⁺10]. The molecule-substrate interaction is weak enough to allow a non-commensurate molecular arrangement and the intermolecular interaction determines the lateral structure described by the matrix

$$M_{111} = \begin{pmatrix} 2.52 & 5.50 \\ 4.66 & -0.34 \end{pmatrix}. \quad (3.1)$$

Corresponding LEED and STM images are shown in Fig. 3.1. The molecular structure vectors \vec{b}_1 and \vec{b}_2 are marked in both images. \vec{b}_1 has a length of 13.7 Å, \vec{b}_2 has a length of 13.9 Å, and the angle between them is 96°. According to the 3-fold symmetric Ag(111) substrate, there are 6 domains (including mirror domains) of which all are observable by LEED.

For a coverage of 0.9 ML, photoelectron spectroscopy data yielded several occupied states for binding energies up to 1.5 eV, namely, the HOMO located at 1.25 eV, the LUMO at 0.15 eV, and a residual at 0.007 eV [KSS⁺10]. The position of the HOMO depending on the coverage has also been measured and a shift from 1.25 eV at 0.9 ML to 1.51 eV at 2 ML and to 1.7 eV at 3 ML is observed [KSS⁺10].

Another study by Huang et al. presents STM data on a coverage of 1.3 ML CuPc on Ag(111) [HHP⁺09]. Here it is found that the molecules in the first layer lie flat on the substrate surface but molecules in the second layer islands are inclined according to the difference in their shape and contrast compared to molecules in the first layer. The unit cell of the second layer with tilted molecules seems to be the same as the unit cell of the first layer regarding length and orientation of the molecular structure vectors.

3. Multilayer adsorption of CuPc on Ag(111)

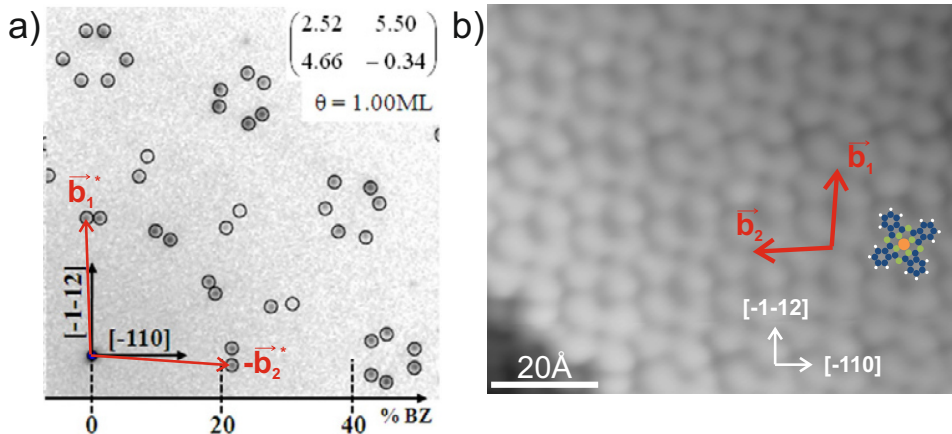


Figure 3.1.: (a) The SPA-LEED image of one monolayer CuPc on Ag(111) shows the experimentally obtained pattern superimposed by a pattern simulated according to the matrix describing the superstructure. The vectors \vec{b}_1^* and \vec{b}_2^* mark the unit cell in reciprocal space. The image is adapted from [KSS⁺10], the abscissa is given in percentage of the Ag(111) Brillouin zone, the matrix relates to the substrate vectors \vec{a}_1 (parallel to $[\bar{1}10]$) and \vec{a}_2 (parallel to $[0\bar{1}1]$) with an angle of 120° between them. (b) STM image of the first layer CuPc on Ag(111) with the unit cell vectors \vec{b}_1 and \vec{b}_2 marked, $U_{\text{bias}} = -1.250 \text{ V}$, $I_{\text{setpoint}} = 23 \text{ pA}$.

A similar inclination of molecules has been observed for iron phthalocyanine (FePc) on Cu(111) [SCK⁺08], on Ag(111) [GBK⁺11], and on Au(111) [CGD⁺07, GG10] as well as for CuPc on Au(110) in density functional theory calculation [LMH⁺14].

Besides the two presented studies on higher layers of CuPc on Ag(111) by PES and STM, there are not much data about this system in literature. Thus, we will try to fill in information on a coverage of 1.3 ML CuPc on Ag(111). The lateral structure will be investigated by STM as well as by LEED, confirming the similarity of the first and second layer structure not only in real but also in reciprocal space. STS is expected to reveal the energetic positions of the HOMO and LUMO of the first and second layer, which will be compared to the known data mentioned above.

The sample was prepared according to the procedure described in Sec. 2.4.2 and after deposition of 1.3 ML the sample was annealed up to 270°C to enable diffusion and improve the lateral ordering. Measurement conditions are as described in Sec. 2.4.1.

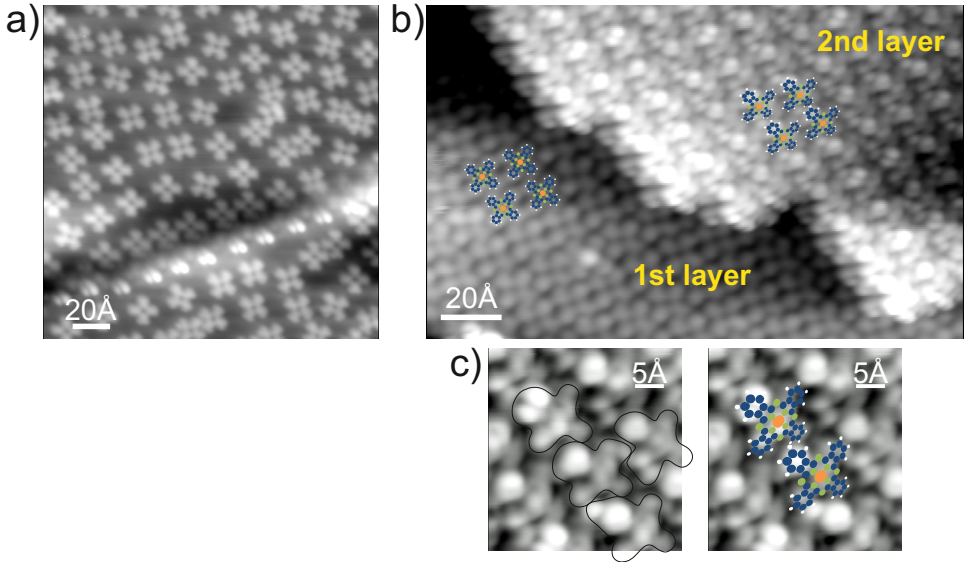


Figure 3.2.: (a) As long as the coverage is in the submonolayer regime, CuPc molecules distribute in a dilute phase all over the surface, $U_{\text{bias}}=-0.200$ V, $I_{\text{setpoint}}=26$ pA. (b) Flat lying molecules are ordered in the densest possible structure in the first layer. Molecules in the second layer are tilted and form islands even if the second layer is not completed, $U_{\text{bias}}=-1.250$ V, $I_{\text{setpoint}}=59$ pA. (c) In the zoom image of few molecules in the second layer one can estimate the direction of inclination, $U_{\text{bias}}=-1.250$ V, $I_{\text{setpoint}}=59$ pA.

3.1. Structural properties: Inclination of molecules

At a coverage of 1.3ML the sample surface is completely covered with molecules and no clean silver patches are visible. The first layer is closed and exhibits the densest possible structure. The second layer is not completed and the molecular arrangement will be determined by the lateral interaction between molecules in the second layer and by interaction with the underlying molecular layer on the metal substrate. The examination of the molecular structures will be carried out in real space by STM and in reciprocal space by LEED.

The image in Fig. 3.2b shows the first and second layer of CuPc molecules on Ag(111). In contrast to a coverage of less than one monolayer where the molecules are distributed in a dilute phase all over the surface (cf. Fig. 3.2a), the molecules in the second layer form islands with sharp edges even if the layer is not completely filled. The intermolecular

3. Multilayer adsorption of CuPc on Ag(111)

repulsion observed for the sub-monolayer coverage seems to be eliminated. We assume that during the growth of the first layer it occurs due to Coulomb forces as a result of the molecule-substrate interaction and the charge transfer at the metal-organic interface. The second layer does not feel the influence of the metal, molecules do not get charged, and hence these tend to cluster and form ordered islands. As expected and described by Huang et al. [HHP⁺09], molecules in the second layer do not show the typical 4-fold symmetric structure but, in contrast to flat lying molecules in the first layer, seem to be tilted. Taking a closer look as shown in Fig. 3.2c, one can estimate the direction of inclination and see that the tilt angle probably amounts to only few degrees and the molecules do not overlap. The molecules do not all appear with the same contrast but small differences can be observed, e.g. the brightest and uppermost benzene ring can consist of one or two sphere-like features. This effect hints towards a registry with a unit cell comprising more than one molecule, similar as reported for a layer of CuPc on top of a closed layer of PTCDA on Ag(111) [SSK⁺12]. In this hetero-organic system the CuPc unit cell contains six equally oriented molecules. The difference in contrast is purely electronic and originates from three different adsorption sites of the CuPc molecules with respect to the underlying PTCDA lattice. Compared to the case of CuPc on CuPc on Ag(111) discussed here, the second layer molecules may also adsorb at different sites of the first layer lattice yielding a different electronic contrast for adjacent molecules.

Figures 3.3 and 3.4 show several line profiles across STM images (height is not calibrated) obtained in WSXM [HFGR⁺07]. One can clearly see that the surface roughness of the second layer (Fig. 3.3c,d) differs from that of the first layer (Fig. 3.3a,b). The increase of the layer roughness confirms the inclination of molecules and so does the periodic asymmetric double peak shape in Fig. 3.3d. In the profile Fig. 3.4c,d, the step size between the first and the second layer on the same silver terrace is depicted. The step in image Fig. 3.4a,b goes from the second layer of a lower terrace to the first layer of the upper terrace across upright standing molecules right at the step edge. The total thickness of the second layer matches the step height of Ag(111), since the height difference is equalized between the two areas in Fig. 3.4a,b.

A comparison of the first and second layer unit cell, as depicted in Fig. 3.5a, suggests that these two pairs of vectors are equal, i.e. the second layer adsorbs commensurate on top of the first layer. The grid in Fig. 3.5b coincides with the first layer structure such that the grid nodes are on top of the molecular centers. Extending this grid across the

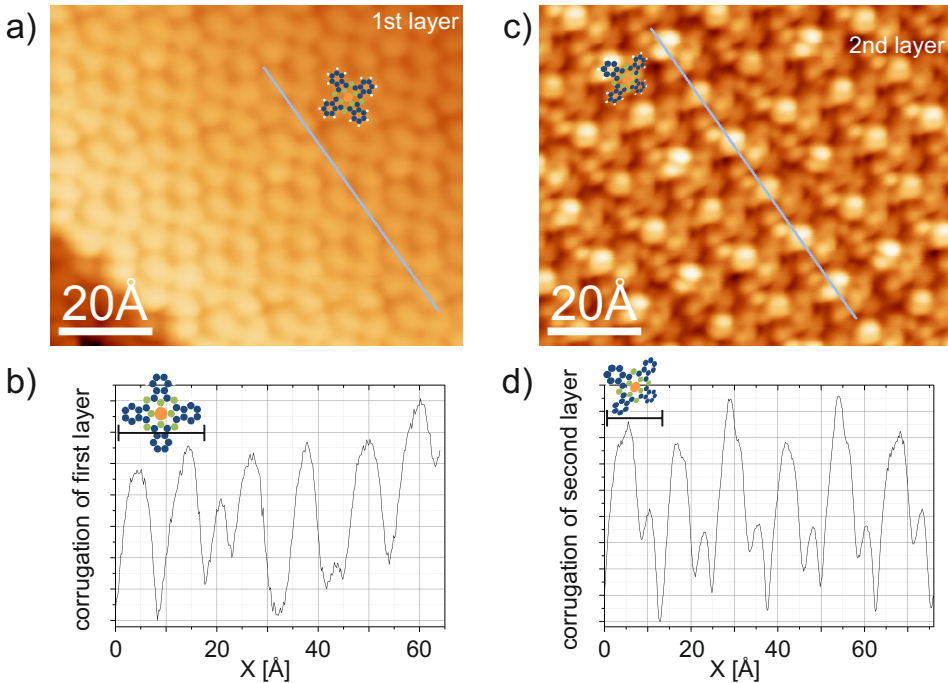


Figure 3.3.: Line profiles of STM images (obtained in WSXM [HFGR⁺07]): A sample area with a line is given in the upper row, the corresponding profile is depicted below (from the left end to the right end of the line in the image above). The height (ordinate of profile graph) is not calibrated. (a,b) The roughness of the first layer is that of flat lying molecules, $U_{\text{bias}} = -1.250$ V, $I_{\text{setpoint}} = 23$ pA. (c,d) The roughness of the second layer shows the inclination of the molecules, $U_{\text{bias}} = -1.250$ V, $I_{\text{setpoint}} = 59$ pA.

second layer structure, we find that the molecules in the second layer adsorb with their most elevated benzene ring right above the center of the underlying molecule. This fact, however, gives rise to a different possible interpretation of the observed contrast of the second molecular layer. According to the position of one benzene ring of a second layer molecule right above a Cu atom of a molecule of the underlying CuPc layer, the other benzene rings are above underlying benzene rings and above empty space between the underlying molecules, respectively. Since the benzene rings of the second layer molecules are distributed over different sites of the underlying molecules, the contrast in STM may also be a purely electronic effect instead of showing inclined molecules. It is hard to decide on the origin of the observed contrast effect since STM always shows topography

3. Multilayer adsorption of CuPc on Ag(111)

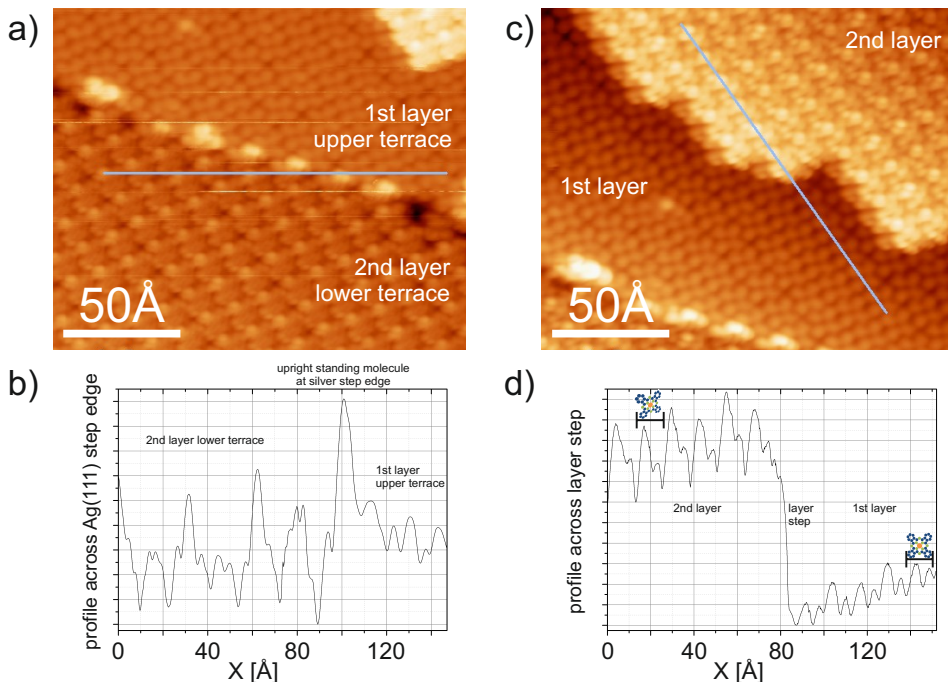


Figure 3.4.: Line profiles of STM images (obtained in WSXM [HFGR+07]): A sample area with a line is given in the upper row, the corresponding profile is depicted below (from the left end to right end of the line in the image above). The height (ordinate of profile graph) is not calibrated. (a,b) A height profile across a Ag(111) step is shown, i.e. from the second layer with inclined molecules on the lower terrace to the first layer with flat lying molecules on the upper terrace across upright standing molecules at the step edge, $U_{\text{bias}} = -1.250$ V, $I_{\text{setpoint}} = 240$ pA. (c,d) A height profile across a step from the second layer with inclined molecules to the first layer with flat lying molecules on the same terrace is depicted, $U_{\text{bias}} = -1.250$ V, $I_{\text{setpoint}} = 59$ pA.

convoluted with electron density. Standing x-ray wave experiments are also difficult to interpret for two layers of molecules of the same type. For the investigation of molecular orientations near edge x-ray absorption fine structure (NEXAFS) measurements might be helpful giving information about the orientation of molecular orbitals and, thus, about the molecular geometry.

Concerning the interpretation of our data, we assume that the asymmetric contrast of molecules in the second layer is not a purely electronic effect but the molecules adsorbed

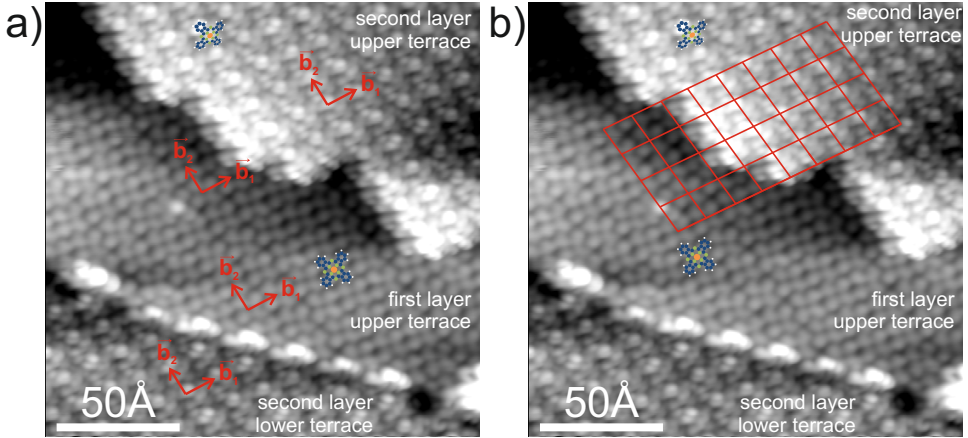


Figure 3.5.: STM images of the flat lying molecules in the first and inclined molecules in the second layer on two adjacent terraces, $U_{\text{bias}} = -1.250$ V, $I_{\text{setpoint}} = 59$ pA. (a) The unit cells are the same for the first and the second layer. The pair of vectors (\vec{b}_1 , \vec{b}_2) can be shifted laterally and does describe both appearing structures. (b) The adsorption site of the second layer on top of the first layer can be determined by an additional grid. The nodes coincide with the centers of the molecules in the first layer and with the uppermost benzene ring of the molecules in the second layer.

in a inclined configuration. This assumption is supported by calculations on the adsorption of CuPc molecules on the Au(110) surface, which interacts weaker with adsorbates than silver, where the molecules are inclined [LMH⁺14].

LEED patterns as given in Fig. 3.6 were recorded with a conventional LEED and an MCP-LEED. The pattern displays a triangular structure, which we fit in the program Spot-Plotter [Bay08] with the pattern simulated with the first layer unit cell vectors. The simulation completely reconstructs the experimental pattern, and since we cannot distinguish two patterns in the experimental images (one for the first and one for the second layer), this fit confirms that the pattern of the second layer has exactly the same structure as the pattern of the first layer. Thus, the results of the LEED measurements are in good agreement with the STM findings.

The reduction of symmetry of the pattern from expected 6-fold to observed 3-fold is probably due to an asymmetric distribution of domains in the examined area.

3. Multilayer adsorption of CuPc on Ag(111)

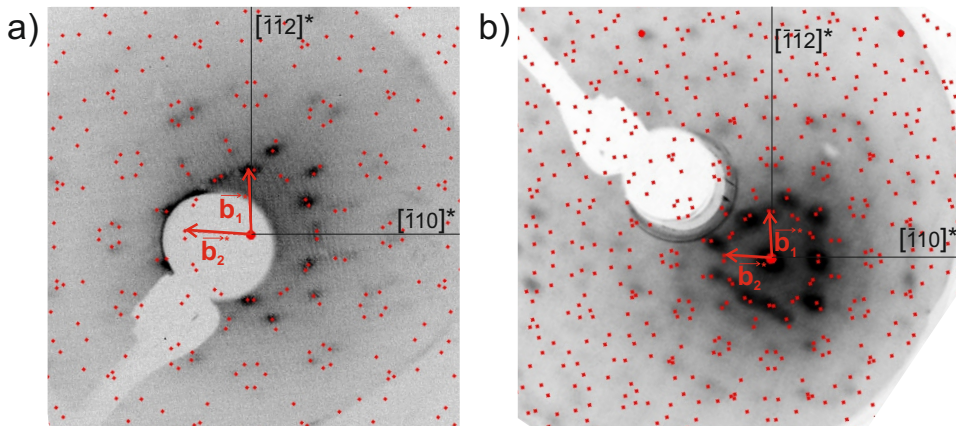


Figure 3.6.: LEED images of 1.3 ML CuPc on Ag(110), i.e. the first and the second layer, show 3-fold symmetric diffraction patterns. The experimentally obtained patterns are superimposed with the pattern simulated by Spot-Plotter [Bay08] according to the values describing the molecular lattice of the first layer of adsorbed molecules. (a) Image recorded with a conventional LEED, 12.4 eV. (b) Image recorded with an MCP-LEED, 45 eV. Obviously, the second layer structure can be described by the same values as the first layer structure.

3.2. Electronic properties: Orbital depopulation

In the work presented by Kröger et al. [KSS⁺10], some orbital binding energies have been determined, but the binding energies of the two frontier orbitals HOMO and LUMO are not given for 1 ML coverage. We investigate the local density of states of the first and second layer CuPc on Ag(111) by STS for a range of ± 2 eV around the Fermi energy. As mentioned above, the surface is completely covered with molecules and, thus, it is difficult to prepare the tip. So we have to consider the possible occurrence of tip states in the analysis of the spectra.

First, STS data from flat lying molecules in the first layer are collected, cf. Fig. 3.7a. Spectra are measured above the center and the four benzene rings of the molecule (Fig. 3.7b). Since the spectra recorded above the benzene rings do not differ from each other, these four are averaged. All first layer spectra feature a strong resonance at approximately -0.5 V and a weaker resonance at approximately -1.4 V. Compared to the data from [KSS⁺10], depicted in Fig. 3.7d, the feature at -1.4 V can probably be assigned to the HOMO. The LUMO, expected as a weakly occupied state at -0.15 V, is

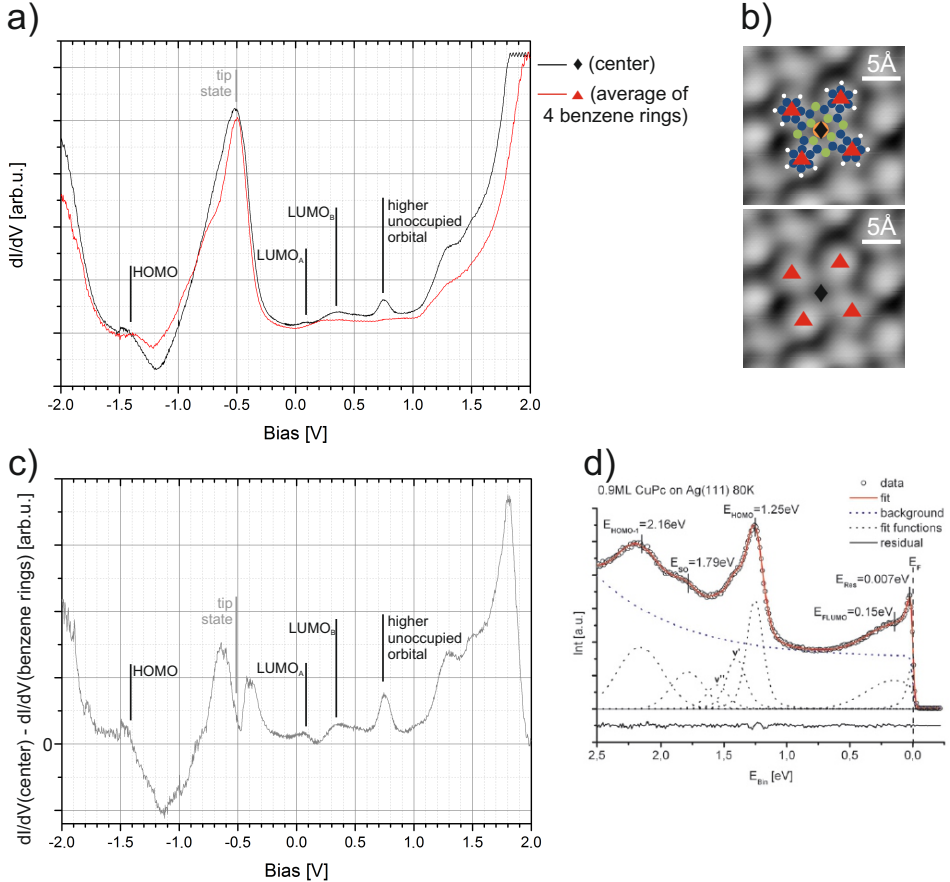


Figure 3.7.: (a) Differential conductance spectra of flat lying CuPc molecules in the first layer on Ag(111) feature many resonances, of which several might occur due to tip states. The HOMO can be observed at -1.4 V . The LUMO is expected at approximately -0.15 V and probably disappears in the strong resonance at -0.5 V ; $I_{\text{setpoint}} = 550 \text{ pA}$ (b) In an STM image of one CuPc molecule the positions are marked where spectra are recorded, $U_{\text{bias}} = -1.250 \text{ V}$, $I_{\text{setpoint}} = 59 \text{ pA}$. (c) In the difference of the spectrum taken above the molecular center and the spectra taken above the benzene rings the individual contributions can be discriminated more easily. (d) The UPS data of 0.9 ML CuPc on Ag(111) are depicted for comparison with the STS data, figure taken from [KSS⁺10].

3. Multilayer adsorption of CuPc on Ag(111)

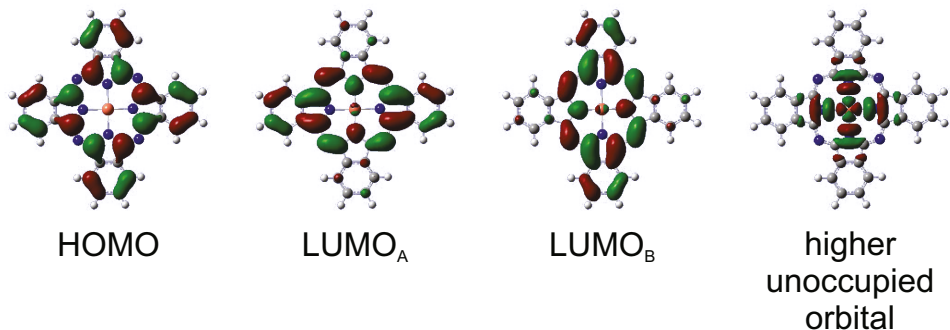


Figure 3.8.: Real space distributions of the frontier CuPc orbitals which yield resonances in the differential conductance spectra.

not observable at this position in our data. The striking feature at -0.5 V may either originate from the former LUMO, which in this case would be occupied to a substantially higher degree than assumed according to PES data in [KSS⁺10], or it is due to a tip state and the weakly occupied LUMO disappears in it. Since such a strong occupation of the LUMO does not seem realistic compared to previous data, we suppose that a tip state causes the resonance at -0.5 V. For positive bias, all spectra show several resonances, which may also appear due to tip states since no certain unoccupied orbital is expected to lie so close to the Fermi energy.

There are only tiny differences between spectra recorded above the benzene rings and above the center of the molecules. Therefore, the spectra of the benzene rings are subtracted from the spectrum of the molecular center (Fig. 3.7c) to increase the visibility of deviations. The spectrum of the center yields stronger intensity for most parts of the spectra, except for the range between -0.8 V and -1.4 V. In this region, the spectra of the benzene rings feature a shoulder to the peak at -0.5 V, but we cannot name an involved distinct sample state. A similar feature can be observed at about 0.75 V where mainly the center of the molecule causes a resonance, which may stem from a higher unoccupied orbital mainly distributed across the inner part of the molecules, cf. Fig. 3.8. The two originally degenerate parts LUMO_A and LUMO_B may cause the two close peaks at 0.1 V and 0.3 V, of which LUMO_A, reaching over the Fermi edge, has formerly been interpreted as the partly filled LUMO at 0.15 eV binding energy.

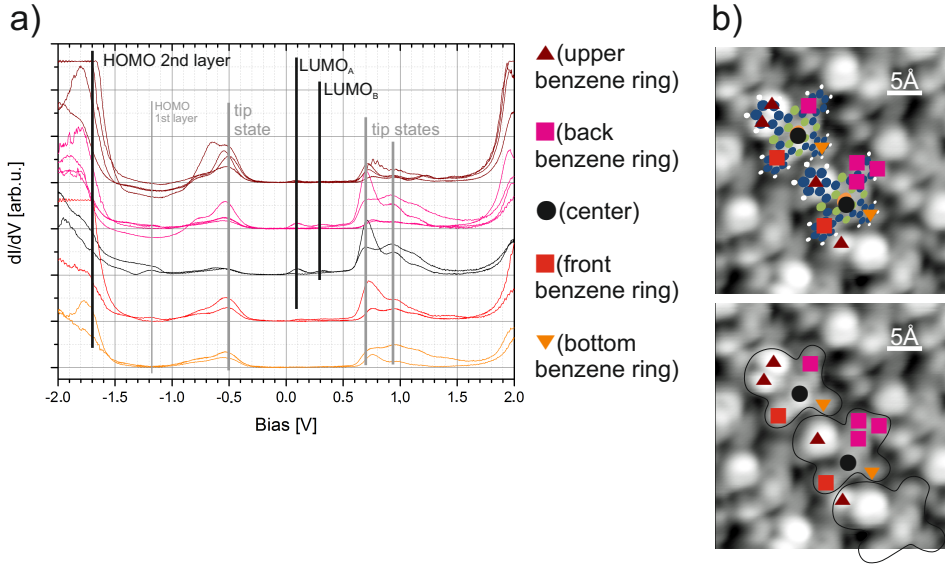


Figure 3.9.: (a) Differential conductance spectra of inclined CuPc molecules in the second layer on Ag(111) exhibit many features that partly occur due to tip states, $I_{\text{setpoint}}=59$ pA. The HOMO at -1.7 V is shifted to a larger binding energy compared to spectra of first layer molecules (Fig. 3.7). The LUMO is probably not occupied and may cause the resonances at 0.1 V and 0.3 V taking the degeneracy of LUMO_A and LUMO_B of an isolated molecule into account. (b) The positions where spectra are recorded are marked in STM images, $U_{\text{bias}}=-1.250$ V, $I_{\text{setpoint}}=59$ pA.

Next, differential conductance spectra of second layer molecules are taken, cf. Fig. 3.9a, above several positions marked in Fig. 3.9b. On the side of negative bias, all spectra feature a strong resonance at -0.5 V and increasing intensity from -1.6 V towards -2 V. The latter can by comparison with previous data be assigned to the HOMO whose binding energy shifts with increasing coverage from 1.25 eV at 0.9 ML to 1.7 eV at 3 ML [KSS⁺10]. In addition to these two features, the spectra of the molecular center feature a double resonance between -1.5 V and -1.2 V, of which one may be a remnant of the HOMO of the underlying first layer molecules. Such a coverage-dependent energetic shift of the HOMO is, for example, also reported for the adsorption of zincphthalocyanine (ZnPc) on Ag(110) and is attributed to the screening of electrons in the first layer molecules by the substrate (electrons) [GAA⁺10]. The second layer molecular electrons are significantly less affected by the screening and for higher layers the metal

3. Multilayer adsorption of CuPc on Ag(111)

does not affect the molecular level ordering so that the orbitals are aligned similar as in an isolated molecule. On the other hand, the spectra recorded above the benzene rings feature a resonance at -0.7V , which cannot be assigned to any orbital. The feature at -0.5V , which was also observable in the spectra of the first layer molecules (cf. Fig. 3.7a), appears again in the spectra of the second layer molecules. Hence, our conclusion is that this is the same tip state as assumed before. For positive bias, all second layer spectra feature two resonances at 0.7V and 0.9V , which have not been observed in the first layer spectra and might be due to the unoccupied LUMO. On the other hand, the band gap of a bulk crystal CuPc is 1.98eV [HH63, Ham67] and with the HOMO at -1.8V the LUMO would be expected at about 0.2V . Close to this value only the spectra taken above the molecular center feature weak resonances at 0.1V and 0.3V , which may originate from the two parts of the degenerate LUMO. Thus, we assign tip states to the features at 0.7V and 0.9V . Two resonances at 1.2V and 1.5V are only observable in some spectra of the benzene rings and may stem from the interaction with the underlying material. Further resonances at positive bias probably also appear due to tip states.

3.3. Summary and Conclusion

With our investigations presented here we contribute to the information about the second layer CuPc on Ag(111), i.e. CuPc on CuPc on Ag(111). It is confirmed that the unit cell of the second layer is the same as for the first layer, but molecules in the second layer do not lie flat on the surface. They appear with a contrast suggesting an inclination by some degrees with one benzene ring as the top-most point of the molecule. Alternatively, the asymmetric contrast could be purely electronic due to the underlying molecular layer, similar as reported for a layer of CuPc on a layer of PTCDA on Ag(111) where adjacent CuPc molecules appear with different electronic contrast due to different adsorption sites on the underlying layer [SSK⁺12]. We assume an inclination of molecules, which has also been reported for CuPc molecules on a substrate interacting weaker with adsorbates than silver [LMH⁺14]. The CuPc molecules in the first layer on Ag(111) are forced to lie flat by molecule-substrate interaction. The π -electron system of a molecule forms a bond to the substrate and charge is transferred via this bond from the silver into the CuPc. The charging of the molecules causes intermolecular repulsion and the formation of a dilute phase when the coverage is substantially less than 1 ML. When the first monolayer is completed, the molecules come so close to each other that they have to

form an ordered structure for a further minimization of the adsorption energy. The molecule-substrate interaction between CuPc and the Ag(111) surface is weak enough to allow a non-commensurate registry and a lateral molecular arrangement determined mainly by intermolecular forces. When the second layer of CuPc starts to adsorb on top of the first layer, these uppermost molecules are not affected by the silver crystal in their arrangement, but they have a weakly interacting, only slightly charged CuPc layer as substrate. The second layer molecules do not receive any charge from the silver or the first CuPc layer so that the formerly mentioned repulsive interaction occurring during the growth of the first layer is not observed for the growth of the second layer. Here, the lateral intermolecular interaction is attractive. It causes the molecules to cluster and form islands, even for a low percentage of the second layer covered with molecules, and it allows an inclination of the molecules. This is to avoid overlap of the benzene rings, but the inclination is not large enough for π - π interaction between neighboring molecules in the second layer. The attractive lateral interaction between molecules in the second layer has also been observed for a layer of CuPc on PTCDA on Ag(111). In contrast, for the hetero-organic system the influence of the first molecular layer of PTCDA molecules is strong enough to force the CuPc molecules to lie flat and to chemisorb on top of the PTCDA layer [SSK⁺12].

The obtained differential conductance spectra show a rich electronic structure that can partly be attributed to tip states. Although we cannot certainly assign resonances to the LUMO, which usually yields a weaker signal than the already quite weak HOMO resonance, in either spectra, we can suggest which features might stem from the LUMO_A and the LUMO_B. We can also confirm the shift of the HOMO to larger binding energies for increasing coverage such as reported in [KSS⁺10]. The diagram in Fig. 3.10 depicts a comparison of the energetic orbital alignment as found out in [KSS⁺10] and in this work. The data for a coverage of 0.9 ML and 1.0 ML deviate slightly as the HOMO in our data is located at a larger binding energy and we do not observe the strongest intensity of the LUMO on the side of positive binding energy. The feature at 0.5 eV discussed earlier in this section is assigned to a tip state. It is clear that charge is transferred from the metal into the molecule, but it is not clear to which degree the LUMO is occupied. Hence, the resonance observed by PES in [KSS⁺10] might be a tail of the LUMO_A peak reaching across the Fermi edge with its maximum still on the side of unoccupied states but almost at the Fermi energy. Data about further unoccupied orbitals have not been reported, so we suggest an allocation of the LUMO_B and another unoccupied orbital,

3. Multilayer adsorption of CuPc on Ag(111)

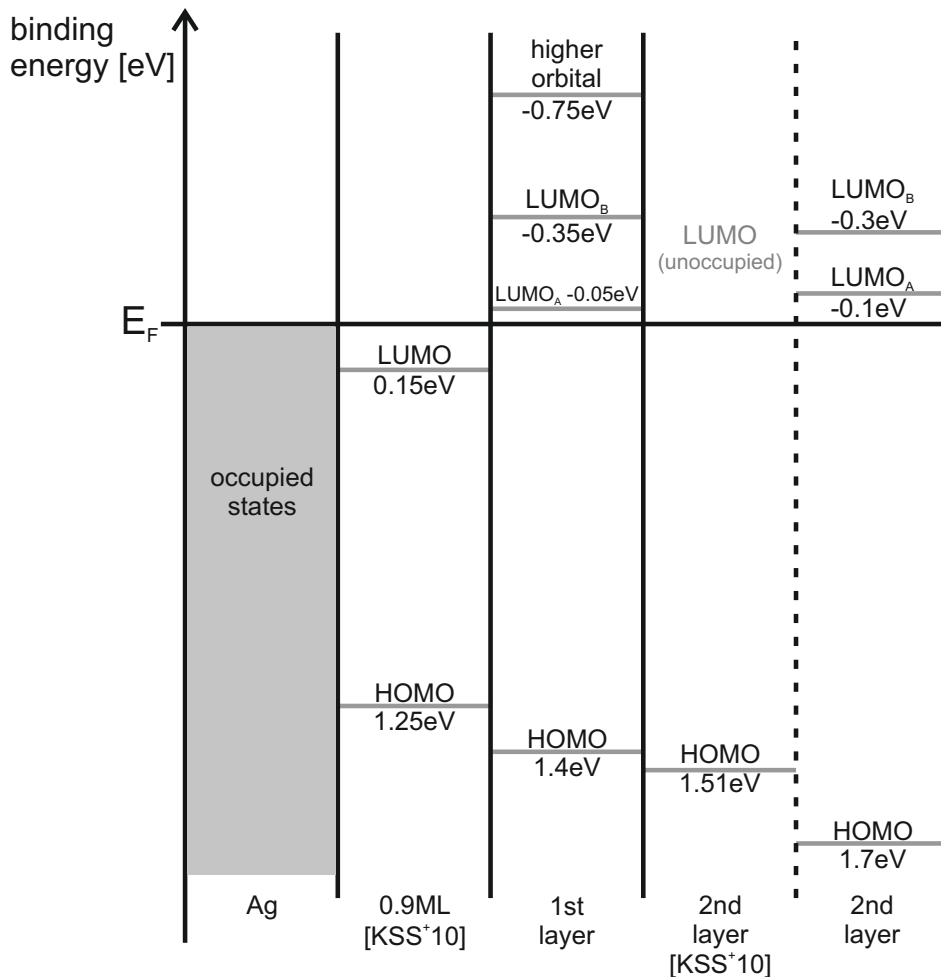


Figure 3.10.: The energy level rearrangement for the first and second layer of CuPc on Ag(111) found in this work is compared to literature [KSS+10].

which is mainly distributed over the central part of the molecule, to the resonances on the side of unoccupied states observed at 1 ML coverage by STS. The molecules in the second layer at a coverage of 1.3 ML are less affected by the substrate, i.e. the screening effect is weaker so that the HOMO lies at a larger binding energy and no charge is donated to the molecules so that the LUMO is expected to be depopulated. The shift of the HOMO is confirmed by PES in [KSS+10] as well as by STS data presented here

albeit we observe the HOMO at an even larger binding energy. Since PES does not yield any information about unoccupied sample states, we provide the only data and carefully propose an assignment to unoccupied orbitals.

STM and STS alone do not provide a comprehensive image about the structural and electronic properties of the second layer CuPc on Ag(111). So we suggest further investigations, for instance, by XSW and NEXAFS for the geometric arrangement, by ARPES for an identification of the occupied sample states, and maybe inverse PES (IPES) or 2-photon photoemission (2PPE) spectroscopy for more information about unoccupied sample states.

4. Monolayer formation of CuPc on Ag(110)

In the previous chapter, we extended the investigations from a monolayer CuPc on the highly symmetric Ag(111) substrate to the second layer of molecules, i.e. CuPc on CuPc on Ag(111). Next we will exchange the Ag(111) surface by the only 2-fold rotational symmetric, more open, and thus more reactive Ag(110) surface, which affects, for example, the adsorption height as shown for PTCDA on different silver surfaces [BMW⁺12]. In addition, the reduced number of symmetry domains on the (110) surface compared to the (111) surface simplifies the analysis of angle-resolved photoemission spectroscopy data. This will help to clarify the origin of the reduction of the 4-fold molecular symmetry to 2-fold that has been observed in scanning tunneling microscopy data for CuPc layers adsorbed on highly symmetric (111) surfaces [CKB⁺08, KLS⁺09].

The adsorption of a monolayer CuPc on Ag(110) has so far been rarely addressed. For instance, Schäfer et al. proposed a model for the lateral arrangement of a closed monolayer CuPc on Ag(110) based solely on electron diffraction data [SSF01]. Unfortunately, the suggested model cannot fully describe the structure observed by the authors (and as well by us, cf. Sec. 4.1), because the experimentally obtained electron diffraction pattern comprises more spots than the model can produce. The electronic properties have been investigated by Song et al. using photoelectron emission spectroscopy to probe the electronic structure for binding energies up to 15 eV [SHD⁺07]. Still, a detailed analysis of the states close to the Fermi energy is missing as the quality of the achieved data does not allow an unambiguous analysis of the valence band and understanding of electronic processes at the interface. Therefore, this chapter will complete the information about the structural and electronic properties of a monolayer CuPc on the Ag(110) surface. We have applied several methods including STM, LEED, STS, and ARPES to investigate the geometry of the adsorbed molecular layer and the energetic ordering of molecular orbitals close to the Fermi energy. The first part of the data presentation will deal with

4. Monolayer formation of CuPc on Ag(110)

unraveling the lateral molecular arrangement by a thorough analysis of STM images and a comparison to experimental and simulated LEED patterns. In the second part, STS and ARUPS data will reveal the nature of the frontier occupied molecular states.

The sample cleaning and the deposition of molecules were carried out according to the preparation steps described in Sect. 2.4.2. In order to obtain the densest possible structure in a monolayer, we deposited more molecules than fit into one monolayer and subsequently annealed the sample up to 340 °C for 10 min to desorb molecules from higher layers. Measurement conditions are as summarized in Sect. 2.4.1.

4.1. Structural properties: Interplay of forces

The STM images in Fig. 4.1 show that CuPc molecules on Ag(110) form a laterally extended ordered structure only at complete monolayer coverage. For the low coverage regime, repulsive forces dominate the intermolecular interaction and cause the CuPc molecules to distribute in a dilute phase all over the surface. When the coverage is high enough for the molecules to sense each other they start to form short chains and

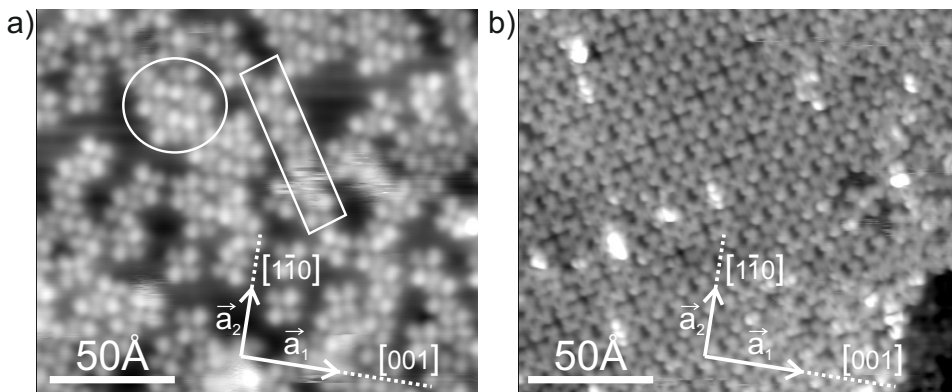


Figure 4.1.: STM images of CuPc on Ag(110) at different coverage. (a) At a low coverage of less than one monolayer the molecules distribute in a dilute phase all over the surface. When the coverage is high enough for the molecules to touch, they start to form chains and clusters as marked in the image by a box and an ellipse, $U_{\text{bias}}=0.4\text{ V}$, $I_{\text{setpoint}}=0.75\text{ nA}$. (b) At one monolayer coverage the molecules form an extended ordered structure covering the whole surface, $U_{\text{bias}}=0.6\text{ V}$, $I_{\text{setpoint}}=1.1\text{ nA}$. No clean substrate is visible.

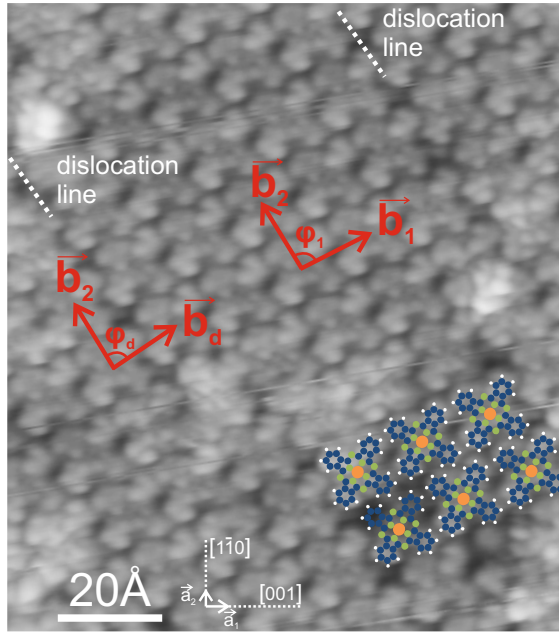


Figure 4.2.: STM image showing the densest structure of one monolayer CuPc on Ag(110), $U_{\text{bias}} = -0.2$ V, $I_{\text{setpoint}} = 30$ pA. Dislocation lines of the molecular lattice are marked with dashed lines. The unit cell, consisting of \vec{b}_1 and \vec{b}_2 , and the second pair of vectors describing structure with dislocation lines, consisting of \vec{b}_d and \vec{b}_2 , are marked by arrows.

partly ordered clusters as depicted in Fig. 4.1a. Similar observations have been reported for CuPc on Ag(111), Au(111) and Cu(111) [KSS⁺10, SKRK11]. A laterally extended ordered structure is only formed when the coverage is close to a complete monolayer (Fig. 4.1b).

The unit cell of the molecular structure, cf. Fig. 4.2, contains one CuPc molecule. There are two different mirror domains of this structure, i.e. two different rotational orientations of the molecules on the surface, originating from the 2-fold symmetric substrate and the orientation of molecules with respect to the substrate high symmetry directions. The rotation of the long molecular axis on the surface is $\pm(28^\circ \pm 1^\circ)$ with respect to the $[001]$ direction of the silver crystal. From STM images the approximate size of the unit cell can be extracted as the following: The unit cell vectors \vec{b}_1 and \vec{b}_2 have each a length of about $13.5 \text{ \AA} \pm 0.3 \text{ \AA}$. The angle φ_1 between them is $\approx 101^\circ \pm 1^\circ$ and

4. Monolayer formation of CuPc on Ag(110)

\vec{b}_1 is rotated by $\approx 25^\circ \pm 1^\circ$ with respect to the Ag[001] direction. This molecular lattice extends over large distances along the translation direction of \vec{b}_2 , but it is regularly interspersed in the perpendicular direction by dislocation-like defects. These dislocation lines, marked by dashed lines in Fig. 4.2, may stem from the lattice mismatch between the substrate lattice and the molecular lattice described by the unit cell (\vec{b}_1, \vec{b}_2) . Similar lattice imperfections, reducing strain in the molecular structure, have been observed for CuPc on PTCDA on HOPG [CHC⁺08] and for ZnPcCl₈ on Ag(111) [KAM⁺06]. The dislocations repeat in approximately equal distances of 3 to 5 (mostly 4) molecular rows, thus occupying a significant portion of the entire surface. One dislocation line separates two domains of the same structure and the translation between neighboring domains can be described by the dislocation vector \vec{b}_d , which has a length of approximately $13.5 \text{ \AA} \pm 0.3 \text{ \AA}$. The angle between \vec{b}_d and the Ag[001] direction is $\approx 36^\circ \pm 2^\circ$ and the angle φ_d between \vec{b}_d and \vec{b}_2 is $\approx 89^\circ \pm 1^\circ$. As we will see in a later section, taking into account the unit cell associated with the two vectors (\vec{b}_d, \vec{b}_2) is necessary to accurately describe the diffraction pattern of CuPc on Ag(110) samples.

The model for the geometric structure of the adsorbed monolayer CuPc on Ag(110) obtained from STM data is not precise due to possible uncontrolled distortions in the images. Therefore, we simulate a LEED pattern according to the STM-based model and compare it to experimental LEED patterns. The simulation is optimized by fitting it to the experimental diffraction patterns. The optimized simulation gives exact values for the magnitudes of all vectors and the relevant angles.

The simulated LEED pattern according to the vectors \vec{b}_1 and \vec{b}_2 (in reciprocal space correspondingly called \vec{b}_1^* and \vec{b}_2^*), given in Fig. 4.3 by small white spots, is in good agreement with the experimental image for the first order spots and also matches some but not all spots of the second order. When a second LEED pattern with the dislocation vector \vec{b}_d and vector \vec{b}_2 is simulated and fitted, given in Fig. 4.3 by large white circles and the corresponding reciprocal space vectors \vec{b}_d^* and \vec{b}_2^* , it also agrees well with the first order spots and with some second order spots that cannot be fitted by the previous pair (\vec{b}_1, \vec{b}_2) . Only when both simulated LEED patterns are superimposed onto the experimental image, all spots can be accounted for. Since the same LEED pattern has been observed in several experiments, we conclude that a monolayer of CuPc on Ag(110) always consists of large areas of the molecular structure described by (\vec{b}_1, \vec{b}_2) , interspersed by a large number of dislocation lines, which yield such a strong signal in

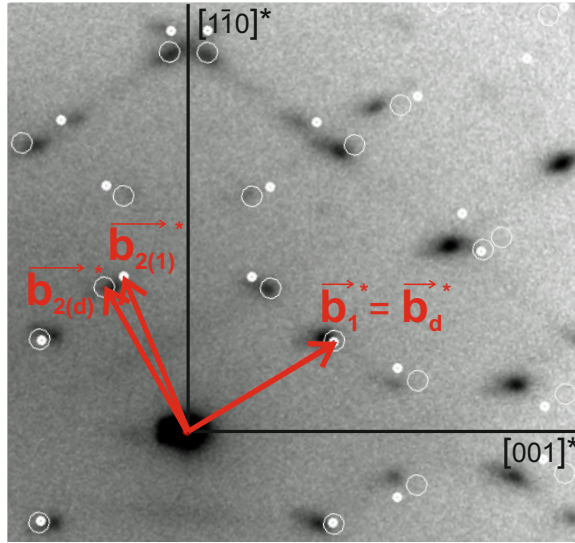


Figure 4.3.: Experimental SPA-LEED image, $E_{\text{kin}}=30$ eV, with simulated LEED patterns for both sets of vectors (\vec{b}_1 , \vec{b}_2 as small spots and \vec{b}_d , \vec{b}_2 as large rings) showing complete reconstruction.

electron diffraction that the overall LEED pattern actually is a superposition of two patterns originating from (\vec{b}_1, \vec{b}_2) and (\vec{b}_d, \vec{b}_2) . A monolayer of CuPc on Ag(110) thus tends to have structural dislocations representing an interesting example of a strain induced mechanical relaxation at the molecule-metal interface.

The optimized values for vectors and angles are listed in Tab. 4.1 and result in two superstructure matrices, M_1 for the extended ordered domains and M_d describing the molecular arrangement across dislocation lines:

$$M_1 = \begin{pmatrix} 3.00 \pm 0.05 & 1.72 \pm 0.08 \\ -1.77 \pm 0.05 & 4.00 \pm 0.06 \end{pmatrix} \quad \text{and} \quad M_d = \begin{pmatrix} 2.76 \pm 0.04 & 2.26 \pm 0.07 \\ -1.77 \pm 0.05 & 4.00 \pm 0.06 \end{pmatrix} \quad (4.1)$$

According to the classification by Hooks et al., these matrices with only rational elements are of the type ‘coincidence-II’ [HFW01].

As mentioned above, CuPc molecules repel each other and form a gas phase if the coverage is less than one monolayer. As a consequence, when the ordered structure ap-

4. Monolayer formation of CuPc on Ag(110)

	length	angle to [001]	angle to \vec{b}_2
\vec{b}_1	$13.2 \text{ \AA} \pm 0.2 \text{ \AA}$	$22^\circ \pm 1^\circ$	$100^\circ \pm 1^\circ$
\vec{b}_2	$13.6 \text{ \AA} \pm 0.2 \text{ \AA}$	$122^\circ \pm 1^\circ$	–
\vec{b}_d	$13.0 \text{ \AA} \pm 0.2 \text{ \AA}$	$30^\circ \pm 1^\circ$	$92^\circ \pm 1^\circ$

Table 4.1.: Values describing the molecular structure of a closed monolayer CuPc on Ag(110)

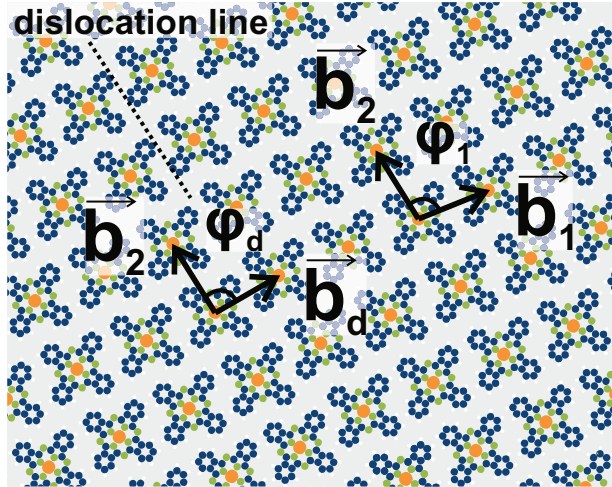


Figure 4.4.: Model of the unit cell of extended ordered domains of CuPc on Ag(110) described by (\vec{b}_1, \vec{b}_2) and the second pair of vectors (\vec{b}_d, \vec{b}_2) describing the molecular arrangement at a dislocation line.

pears at coverages around one monolayer it does so on the whole surface. Hence, no free patches of silver are available and, thus, it is not possible to image the substrate and we cannot find out the adsorption sites of the molecules. So the structural model depicted in Fig. 4.4, while correct as far as unit cell size and shape are concerned, may be translated laterally over the surface.

Origin and role of the dislocation lines in a monolayer of CuPc on Ag(110) can be understood by comparing to the structure of a monolayer CuPc on the Ag(111) surface. As described by Kröger et al. [KSS⁺10], in the low coverage regime CuPc molecules distribute in a dilute phase over the entire Ag(111) surface due to intermolecular repulsion. When the coverage reaches 89%, a long-range ordered structure is formed. With

increasing coverage between 89% and a full monolayer, the molecular structure changes continuously and the unit cell constantly becomes smaller as more molecules are forced into the layer so that they come closer to each other. At every stage, the long-range molecular ordering on Ag(111) can be described by one unit cell and no defects are observed with electron diffraction. The densest structure is reached at a coverage of 1.0 ML. All different structures found are of ‘point-on-line’ character. This shows that the molecule-substrate interaction on Ag(111) is weak enough to allow the molecules to deviate from a commensurate registry, which usually is the preferred one for molecular adsorption on chemically active surfaces.

Ag(110) is a more reactive surface compared to Ag(111) and the interaction with the adsorbed molecules is expected to be stronger. The molecule-substrate interaction is strong enough to force the molecules to arrange in a coincident structure over large areas, which is reflected by the rational elements of matrix M_1 . Within the uncertainties of the matrix elements, M_1 describes a structure that is commensurate in higher order, since one ends up with integer elements when multiplying M_1 by the factor 4. The intermolecular interaction is weaker than the molecule-substrate interaction and – in contrast to the layer formation on the less reactive substrate Ag(111) – for the most part cannot overcome the molecule-substrate interaction. But this structure is energetically not favorable regarding the molecule-molecule interaction and, thus, from time to time, the intermolecular interaction dominates the molecule-substrate interaction and shifts a row of molecules slightly to an energetically preferable position.

These positions favored by the molecule-molecule interaction can be found by pair potential calculations as has been done by Kröger et al. [KSW⁺11, Kro10]. The calculations performed for CuPc on the Au(111) surface can be regarded as calculations for isolated molecules, since the interaction with Au(111) is weak enough to be neglected in this case. The pair potential map for two CuPc molecules yields several minima where the interaction is weakly attractive if the center of the next molecule is located in this area. For CuPc on Ag(111), the lateral arrangement at 0.89 ML is a compromise between the interfacial energy of adsorption and the intermolecular interaction. The unit cell vectors end at pair potential minima and are aligned with the high symmetry directions of the substrate. At 1.0 ML, the structure is slightly shifted and the vectors end at new positions that actually lie in the regime of strong repulsion although they are close to the previous positions. The structure is stabilized by the energetic gain from adsorption

4. Monolayer formation of CuPc on Ag(110)

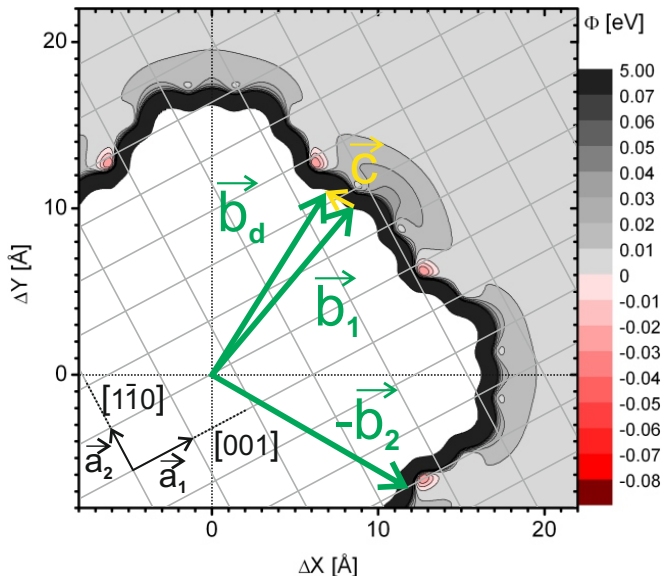


Figure 4.5.: Pair potential calculation for CuPc molecules, modified from [KSW⁺11]. The green arrows labeled \vec{b}_1 , \vec{b}_2 , and \vec{b}_d mark the positions of the neighboring molecules in the CuPc monolayer on Ag(110). \vec{b}_2 and \vec{b}_d clearly point towards favorable positions close to energy minima whereas \vec{b}_1 points towards an unfavorable position that the molecules are forced to take by interaction with the substrate.

energy due to higher coverage prevailing over intermolecular repulsion. The transformation between the first and the final ordered structure goes smoothly by sliding of the unit cell vertices along a high symmetry direction of the (111) substrate allowing an experimentally observed continuous train of alike ordered structures [Kro10, KSS⁺10].

Figure 4.5 shows a pair potential map taken from [KSW⁺11] and the directions from one CuPc molecule to its neighbors in the monolayer structure of CuPc on Ag(110) by green arrows labeled \vec{b}_1 , \vec{b}_2 , and \vec{b}_d . As can clearly be seen, \vec{b}_2 almost points towards a potential minimum as position for the center of the next molecule, and therefore combines well intermolecular and molecule-substrate interaction forces. The vector for the coincident structure \vec{b}_1 , describing the lateral arrangement in the extended ordered domains, points to a position with increased interaction potential, which the molecules are forced to adsorb at by the molecule-substrate interaction. The vector \vec{b}_d is slightly

rotated away from this unfavorable position and also almost points towards a potential minimum. The tendency towards these favorable sites is observable although all three vectors of this very dense structure end in the repulsive regime. We conclude that the dominating interface interaction, induced by the enhanced chemical reactivity of Ag(110), forces the molecules to be located at the positions of better registry with the substrate. The corresponding lateral arrangement, described by matrix M_1 , would lead to commensurism in 4th order (Fig. 4.6 upper part). However, commensurism is not established as the internal repulsive strain provokes periodic defects, the dislocation lines, to appear at approximately every fourth row for a relaxation of the structure, cf. Fig. 4.6 lower part. The direction of the strain relaxing shift given by vector \vec{c} in Figs. 4.5 and 4.7 is directed towards the nearest minimum of the pair potential and goes along the translation vector \vec{b}_2 . Still, vector \vec{b}_d describing the molecular arrangement at a dislocation line ends in the regime of intermolecular repulsion, thus, the overall layer remains highly strained.

Taking into account the pair potential calculations, it becomes clear that the lateral order at a dislocation line is the rather preferred order originating from molecule-molecule interaction while the extended ordered domains are formed due to molecule-substrate interaction. The displacement of molecules at a dislocation line is shown in Fig. 4.7. The black molecules are at the positions calculated for a coincident structure (commensurate in 4th order) determined by interaction with the Ag surface and described by matrix M_1 , whereas the colored molecules beneath are at the positions favored by molecule-molecule interaction and described by M_d . The yellow vector \vec{c} marks the displacement as the difference between \vec{b}_1 and \vec{b}_d .

$$\vec{c} = \vec{b}_d - \vec{b}_1 = \begin{pmatrix} 2.76 \\ 2.25 \end{pmatrix} - \begin{pmatrix} 3.00 \\ 1.72 \end{pmatrix} = \begin{pmatrix} -0.24 \\ 0.46 \end{pmatrix} \quad (4.2)$$

Hence, the monolayer structure with dislocation lines shows the interplay between two interactions affecting the formation of the final ordered structure.

4. Monolayer formation of CuPc on Ag(110)

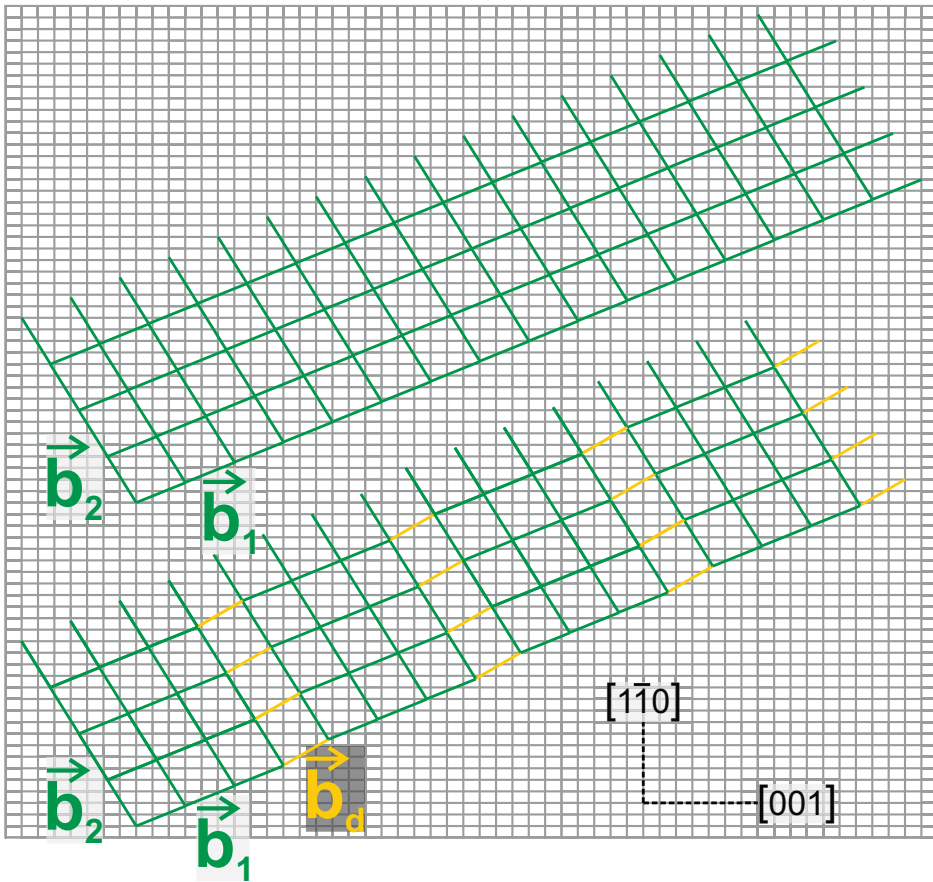


Figure 4.6.: Ag(110) surface lattice (gray) and CuPc lattice (green) with dislocation lines (yellow) depicting how the dislocation lines interrupt the coincident lattice so that commensurism in 4th order is not established.

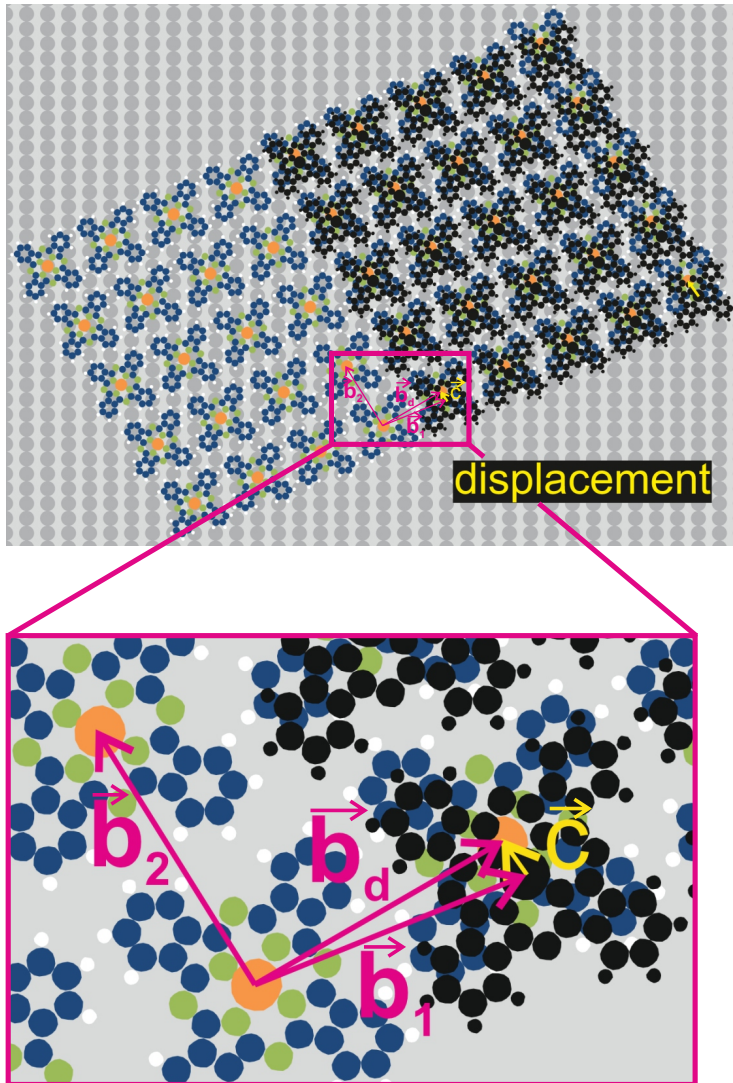


Figure 4.7.: top: model of the monolayer CuPc on Ag(110) without (black) and with (colored) dislocation lines; bottom: zoom of shift between the structure forced by the molecule-substrate interaction and the structure favored by molecule-molecule interaction

4.2. Electronic properties: Reduction of symmetry

When taking a closer look at the STM images in Figs. 4.1 and 4.2, one notices that the four benzene rings of CuPc do not appear with the same brightness. The pair of opposite rings with the more acute angle (28°) to the Ag[$1\bar{1}0$] direction appears brighter than the pair of rings with the more acute angle to the Ag[001] direction. Thus, the symmetry of the originally 4-fold symmetric molecules is reduced to a 2-fold symmetric contrast in STM. This effect is strongest when imaging is performed at positive bias, i.e. depicting unoccupied molecular states. Images recorded in constant height mode as depicted in Fig. 4.8 exhibit an even enhanced difference in contrast between bright and dark molecular wings. A similar reduction of symmetry has been observed in STM studies and DFT calculations for several metal phthalocyanine molecules on certain metal surfaces [CKB⁺08, MRK⁺12, WGM⁺09, KLS⁺09, CCW⁺10, TGAHH10, TGSH10, USR13, BL13]. Explanations that have been put forward include geometrical and electronic effects, in particular the filling of unoccupied molecular states when the molecule adsorbs onto a metal surface. According to theory, the lowest unoccupied states of an isolated phthalocyanine molecule ($LUMO_A$ and $LUMO_B$) are degenerate [MHSK08, RB92, ECS⁺07]. Each of the two states is distributed over two opposite benzene rings of the molecule, such that they are rotated by 90° with respect to each other. Upon adsorption onto a metal substrate, charge may be transferred into the molecule, filling unoccupied states with electrons. This trend has been observed for many metal phthalocyanine molecules on different single crystal metal surfaces [KSS⁺10, REG⁺08, PAN⁺08, AGTA09, GAA⁺10, KRMG13, FGN⁺14]. Here the question arises if the $LUMO_A$ and the $LUMO_B$ become equally occupied or if one state becomes stronger occupied than the other and the degeneracy is lifted. The latter effect would lead to a reduced 2-fold symmetry of the originally 4-fold symmetric molecule, since the two involved states are spread over different areas of the molecule as mentioned above, and it would explain the experimentally observed contrast.

STM data presented here show a difference between the two pairs of opposite benzene rings, which appear brighter and darker, respectively. Hence, assuming that the two pairs of rings belong to differently filled $LUMO_A$ and $LUMO_B$ states, there are two possible cases of different occupation:

i) If the peaks of $LUMO_A$ and $LUMO_B$ are on opposite sides of the Fermi edge, i.e. the $LUMO_A$ is (mostly) occupied and the $LUMO_B$ (mostly) unoccupied, we expect a switch-

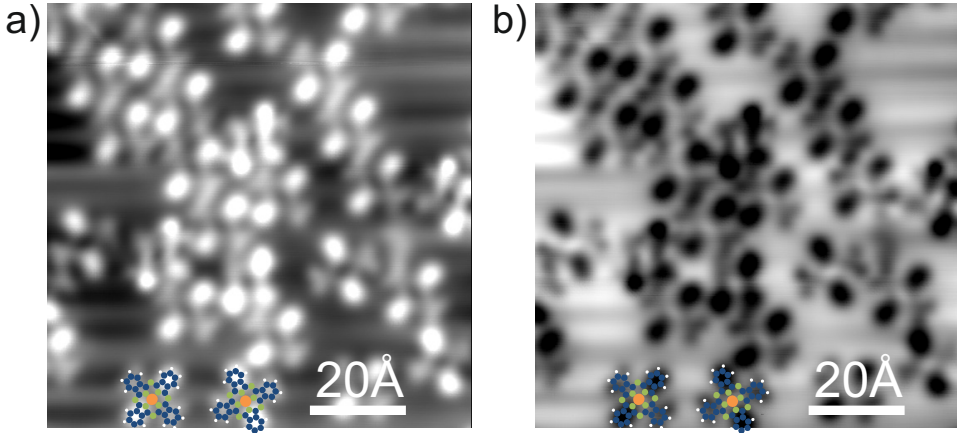


Figure 4.8.: STM images of CuPc on Ag(110) recorded in constant height mode. (a) $U_{\text{bias}}=0.05$ V, $I_{\text{setpoint}}=0.75$ nA, (b) $U_{\text{bias}}=-0.05$ V, $I_{\text{setpoint}}=0.75$ nA.

ing of the contrast when turning from (finite) positive sampling bias, imaging unoccupied molecular states, to (finite) negative sampling bias, imaging occupied molecular states, and equally bright contrast when imaging with bias values between the two peaks.

ii) If both peaks are on the same side of the Fermi edge, e.g. LUMO_A and LUMO_B are both partly occupied but to different degrees, we expect approximately equally dark molecular wings when imaging unoccupied states with positive bias. Upon imaging occupied states, we expect one pair of benzene rings to be always brighter than the other for small negative sampling bias and again equally bright wings when the negative sampling bias is strong enough for tunneling from both orbital parts into the tip. The imaging contrast for the case of both peaks on the side of unoccupied states is obtained by analogous considerations.

In experiment, however, a switching of the contrast does not appear (Fig. 4.9). The same pair of molecular wings is brighter in all images, but for negative bias the difference in the contrast between bright and dark wings slightly decreases. Additionally, the darker wings become v-shaped, pointing towards the center of the molecule, which is also observed in the constant height images in Fig. 4.8. The same contrast change has already been reported for CoPc on Cu(111) and SnPc on Ag(111) and assigned to an asymmetric filling of the LUMO [WGM⁺09]. Considering the enhanced intensity difference observed in constant height images, another interpretation of these observations

4. Monolayer formation of CuPc on Ag(110)

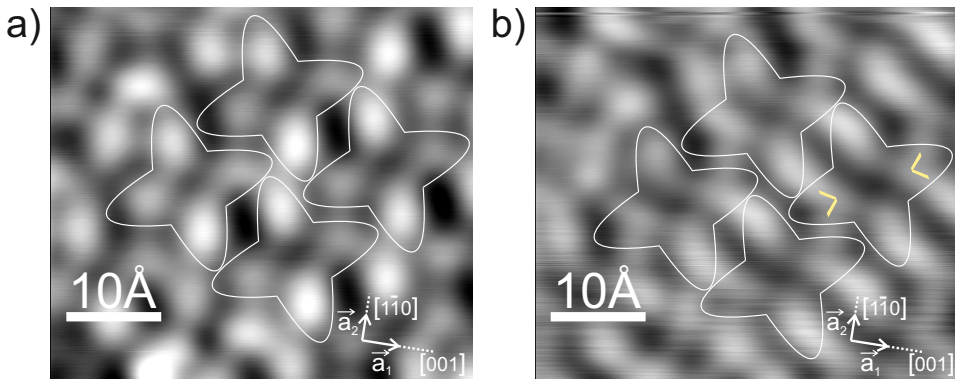


Figure 4.9.: STM images of CuPc on Ag(110) recorded at different bias voltages: (a) $U_{\text{bias}}=0.342$ V, $I_{\text{setpoint}}=0.5$ nA, (b) $U_{\text{bias}}=-0.300$ V, $I_{\text{setpoint}}=0.5$ nA. A strong contrast difference between the pairs of opposite benzene rings can be observed for positive bias (a). For negative bias (b), the contrast difference is less and v-shaped split wings can be observed.

can be suggested. A geometric distortion of the molecules may occur, with the pair of benzene rings with the more acute angle to the Ag[001] direction bent down towards the substrate. In general, this does not necessarily imply a difference in the charge transfer between the metal substrate and the initially degenerate molecular states. However, based exclusively on STM images, we cannot distinguish between contrast features due to electron density and due to topography and, hence, cannot conclude which of the two reasons plays a decisive role.

In order to complement the information gained by microscopy, we investigate the local electronic structure of the compact monolayer of CuPc on Ag(110) by tunneling spectroscopy. Expecting to find features at different energetic positions, matching one stronger occupied and one less occupied or even unoccupied state of the formerly degenerate LUMO_A and LUMO_B, we compare differential conductance spectra recorded above dark and bright molecular wings. The positions where spectra are recorded are marked in Fig. 4.10c and the corresponding data (recorded on different days with unknown, deviating tip condition) are presented in Fig. 4.10a,b.

Surprisingly, regardless of the position where a certain spectrum was taken, all curves in Fig. 4.10a reveal only one strong resonance at about -0.33 V corresponding to an oc-

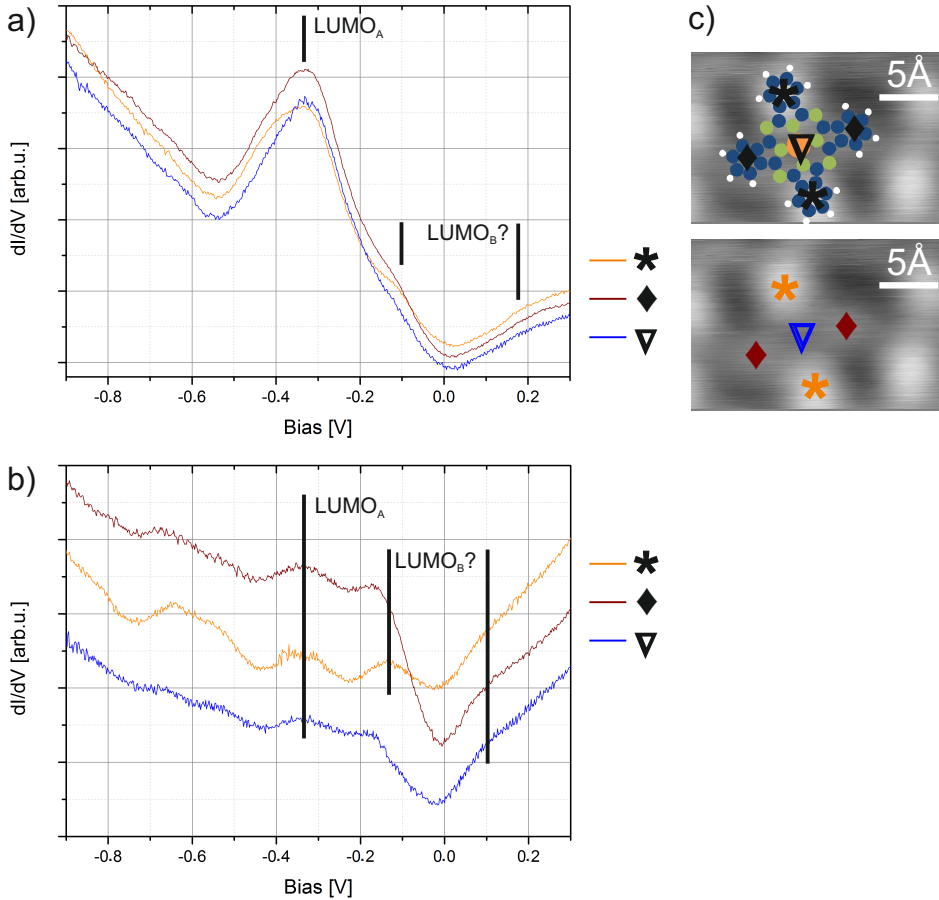


Figure 4.10.: Scanning tunneling spectra, (a) $I_{\text{setpoint}}=1.2\text{ nA}$, (b) $I_{\text{setpoint}}=1.0\text{ nA}$; the resonance at -0.33 V corresponds to an occupied state, namely, of the former LUMO the part $LUMO_A$, which is filled and shifted to a binding energy of 0.33 eV ; (c) STM image ($U_{\text{bias}}=1.407\text{ V}$, $I_{\text{setpoint}}=1.2\text{ nA}$) and model of a CuPc molecule with positions marked where corresponding spectra are recorded: ♦ at dark molecular wings, * at bright wings, ∇ at the center of the molecule.

4. Monolayer formation of CuPc on Ag(110)

cupied state with a binding energy of 0.33 eV. The intensity of the resonance is the same over the entire molecule, even in the center where the intensities of LUMO_A and LUMO_B are assumed to be weakest. The small differences ranging between -0.1 eV and -0.2 eV are weak and do not demonstrate significant deviations. The spectra in Fig. 4.10b also exhibit an occupied sample state at about 0.33 eV binding energy in accordance with the previous spectra, but there are additional resonances between -0.1 eV and -0.2 eV as well as around -0.65 eV. For the peaks close to the Fermi energy, small differences between dark wings, bright wings, and the center of the molecule can be observed similar as for the previous spectra, maybe pointing towards small differences in the occupation of the different orbital parts over the dark and bright benzene rings, respectively. Regarding all spectra, it seems that STS happens to be rather insensitive to slight differences of the spatial distribution of the local DOS of an object, i.e. to sensing the tails of molecular wave functions extending far into vacuum. Nevertheless, the resonance at -0.33 V, which appears in all spectra, may stem from the LUMO_A contribution. The LUMO_B – if also weakly occupied – might cause one of the resonances between -0.1 V and -0.2 V or – if it is unoccupied – the feature between $+0.1$ V and $+0.2$ V. One has to keep in mind that the condition of the tip is not known and tip states have to be considered, which may cause the resonances, e.g. at -0.65 V, that cannot be assigned to molecular orbitals. The HOMO is not assigned to any feature in the spectra presented in Fig. 4.10 as from previous experiments on Ag(111) we expect it to have a binding energy larger than 1 eV.

Considering solely the differential conductance spectra, it is not possible to assign the observed resonance to a molecular orbital and, in particular, distinguish between LUMO_A and LUMO_B. But as we show now, ARUPS data and momentum space imaging help to reveal the orbital ordering. The ARUPS data in Fig. 4.11 are in very good agreement with the previously presented STS data, showing a resonance of an occupied molecular state at a binding energy of approximately 0.3 eV. A second occupied state causes the resonance at the binding energy 1.35 eV. In order to clarify the origin of these two resonances, momentum space images are taken, yielding the data sets shown in Fig. 4.12a,b. The intensity in the direction of negative k_y in the top half of the image is stronger than in the direction of positive k_y (bottom half of the images) due to forward emission of photoelectrons in the negative k_y direction. The backward emission yields less photoelectron intensity, which here is the case for positive k_y . This asymmetry is a result of the $\vec{A} \cdot \vec{p}$ dependence of the photoemission intensity in the one-step model and the grazing incidence geometry of the experiment [FGN⁺14]. Both experimental

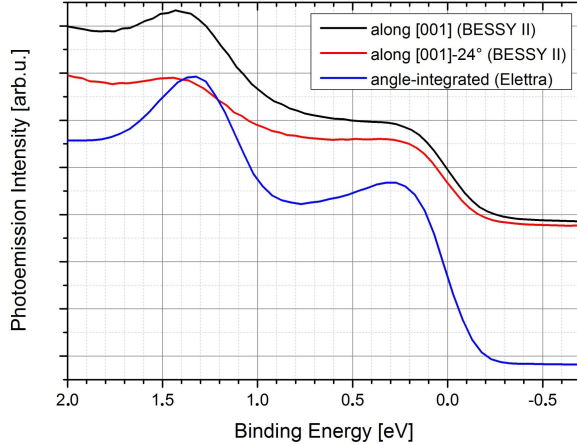


Figure 4.11.: Energy distribution curves along certain silver crystal directions recorded at BESSY II (black and red) and angle-integrated photoemission intensity recorded at Elettra (blue), showing two occupied orbitals at binding energies of 0.3 eV and 1.35 eV

k-space images exhibit weak and sharp parabolic features at about $(k_x, k_y) = (\pm 1, \pm 1.5)$ attributed to the sp-band of the Ag(110) substrate. Molecular features are usually more intense because of the selection of a k-map at a binding energy corresponding to a certain molecular resonance from Fig. 4.11.

In order to reveal the symmetry of the two patterns and facilitate the analysis, intensity profiles for all azimuthal angles are taken by integration over the width of the white empty ring in Fig. 4.12a,b. These profiles, depicted as gray curves in Fig. 4.12c,d, are normalized to a cosine (dashed curve), yielding the black curves, to account for the deviation of intensity between forward (0°) and backward (180°) emission of photoelectrons. The corrected black curve in Fig. 4.12c shows a 4-fold symmetry for the pattern recorded at 1.35 eV binding energy with peaks of highest intensity at 0° , $\pm 90^\circ$ and 180° . Between each of these peaks there are two features of weaker intensity. The corrected pattern recorded at 0.3 eV, given as black curve in Fig. 4.12d, exhibits a 2-fold symmetry with peaks of highest intensity at 0° and 180° . The remarkably strong intensity of the side peaks at about $0^\circ \pm 35^\circ$ compared to the side peaks at $180^\circ \pm 35^\circ$ is due to emission from the substrate sp-band. At azimuthal angles of about $\pm 90^\circ$ there are no intensity maxima but rather minima, which will play a role in the identification of orbitals receiving the charge transferred from the substrate into the molecule.

4. Monolayer formation of CuPc on Ag(110)

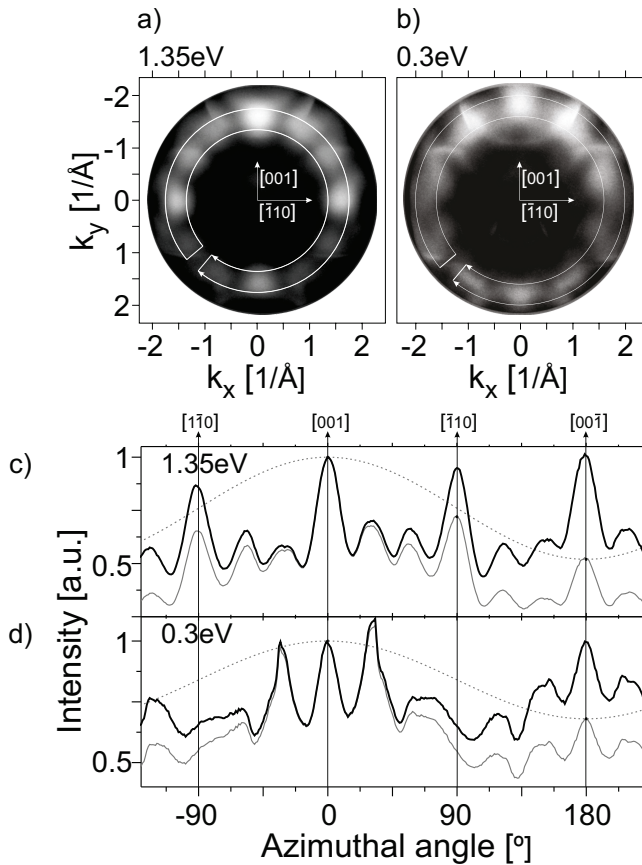


Figure 4.12.: (a,b) Momentum space images recorded with PEEM at Elettra showing the fingerprints of the occupied states at 1.35 eV and 0.3 eV. (c,d) Gray curves: intensity profiles along the white ring marked in the momentum space images, integrated over the width of the ring. Black curves: corrected profiles accounting for the intensity modulation along k_y due to the asymmetry between forward and backward photoemission.

The experimental patterns obtained by k -space imaging in PEEM are compared (cf. Fig. 4.13) to simulated k -space maps calculated as follows: The real space distribution of an orbital across the molecule as given in Fig. 4.13a,b,c is Fourier transformed and projected onto the k_x - k_y -plane to obtain its 2-dimensional reciprocal space image (Fig. 4.13d,e,f). Since in the case presented here the CuPc molecules are rotated on the Ag[110] surface as shown in Fig. 4.13g,h,i, the Fourier transform is applied to the

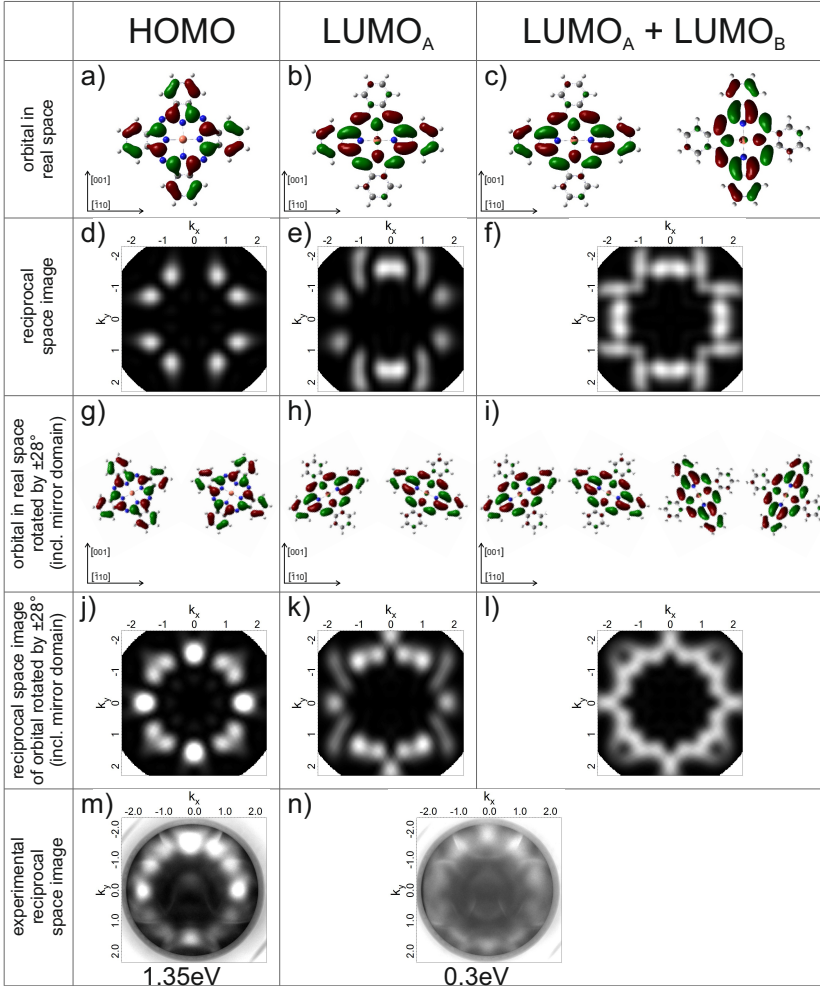


Figure 4.13.: k -space imaging results: HOMO (a,d,g,j), LUMO_A (b,e,h,k), LUMO_A+LUMO_B (c,f,i,l) of CuPc; (a)-(c) orbitals in real space; (d)-(f) corresponding reciprocal space images obtained by Fourier transform of the images above; (g)-(i) real space images of molecular orbitals rotated on the surface including the mirror domain; (j)-(l) corresponding reciprocal space images of the rotated molecules; (m)-(n) experimental reciprocal space patterns. The comparison reveals that the orbital detected at 1.35 eV is the HOMO and the orbital found at 0.3 eV better resembles the 2-fold symmetric LUMO_A simulation pattern than the 4-fold symmetric LUMO_A+LUMO_B simulation pattern.

4. Monolayer formation of CuPc on Ag(110)

molecules in both mirror domains, yielding the reciprocal space images Fig. 4.13j,k,l. The first column of Fig. 4.13 (a,d,g,j,m) presents the simulation data for the HOMO and the experimental image taken at 1.35 eV. The second column (b,e,h,k) gives the simulation data for only the 2-fold symmetric LUMO_A and the third column (c,f,i,l) takes into account the degeneracy of LUMO_A and LUMO_B, depicting a 4-fold symmetric reciprocal space simulation image. Substrate effects and features are neglected in the calculations but this will not affect the data analysis and interpretation.

Comparing the experimental k-space images to the simulated ones (Fig. 4.13j-n) we find that the experimental 4-fold symmetric k-map at 1.35 eV (Fig. 4.13m) strongly resembles the simulated 4-fold symmetric k-map of the HOMO (Fig. 4.13j). The four bright intensity maxima at the positions $(k_x, k_y) = (0, \pm 1.5)$ and $(\pm 1.5, 0)$ as well as the eight weaker features between the bright ones are clearly observable in the experimental as well as the theoretical image. In addition, the rotational orientation of the CuPc molecules on the Ag(110) surface of about 28° is confirmed.

The experimental k-space image recorded at 0.3 eV (Fig. 4.13n) has its features of brightest intensity only at the top and at the bottom of the image for $-1 < k_x < 1$, as mentioned above in the explanation of Fig. 4.12d. Hence, with the accuracy of the method, the experimental pattern exhibits a 2-fold symmetry and, thus, resembles the simulated 2-fold symmetric k-map of the LUMO_A of CuPc given in Fig. 4.13k. In contrast, the simulated 4-fold symmetric k-map of LUMO_A and LUMO_B together in Fig. 4.13l features a ring with a periodically modulated radius but of nearly constant intensity for all azimuthal angles, which is not found in the experimental pattern of the orbital located at 0.3 eV. Hence, in contrast to the case of FePc on the Ag(111) surface as reported by Feyer et al. [FGN⁺14], here the 2-fold symmetric experimental pattern of the LUMO cannot be constructed if both LUMO_A and LUMO_B were equally occupied, providing evidence for an asymmetric charge transfer.

4.3. Summary and Conclusion

In this chapter we presented the analysis of the properties of a complete monolayer CuPc on the Ag(110) surface. By application of STM and LEED we found a long-range ordered structure and could give a model comprising two matrices describing the molecular structure including dislocation lines in the 2-dimensional molecular lattice. These dislo-

cation lines reflect the interplay of intermolecular forces, causing neighboring molecules to arrange in energetic minima according to their pair potential, and molecule-substrate forces, causing the molecules to arrange in a coincident structure (resulting in a commensurate structure if taken four times in a row). Charge transfer from the substrate into the molecules is the origin of a reorganization of electronic levels around the Fermi energy. By comparison of experimental momentum space maps (k-maps) of photoemission to simulated ones, these occupied states can be assigned to certain orbitals. The one part of the formerly unoccupied LUMO becomes filled, is shifted to a binding energy of 0.33 eV, and the degeneracy of the former LUMO_A with the LUMO_B is lifted. The HOMO has a binding energy of 1.35 eV.

Furthermore, we observed a 2-fold symmetric contrast in STM images that can have two reasons: First, the molecules can be geometrically distorted with one pair of opposite benzene rings bent further down towards the surface than the other [CKB⁺08, CCW⁺10, USR13]. This distortion may appear due to a difference in the interaction strength between substrate and overlayer depending on the substrate crystal direction, which in the case of the Ag(110) surface can be the closer packed $[\bar{1}\bar{1}0]$ or the more open and, hence, more reactive [001] direction. In the case discussed here, the molecular wings appearing darker in STM are arranged with a more acute angle than the perpendicular wings to the reactive [001] direction of the Ag(110) surface, suggesting a downward bending. The second proposed reason for the observed contrast may be a difference in the electron density of the two pairs of benzene rings. The LUMO part distributed over the one pair of rings interacting stronger with the substrate receives the charge donated by the silver while the orbital part distributed over the other pair of benzene rings remains unoccupied. The asymmetric charge transfer means the lifting of the formerly degeneracy of LUMO_A and LUMO_B. Naturally, these two reasons may appear either in a related way – the orbital part distributed over the pair of benzene rings interacting stronger with the substrate and therefore bent downwards receives more charge than the other – or independently – bending occurs without a preferential charge transfer, representing a purely topographic effect, or an uneven charge donation occurs without a noticeable distortion, representing a purely electronic effect.

Assuming electronic effects to cause the 2-fold symmetric contrast in STM, we took differential conductance spectra above the benzene rings and the center of a molecule expecting to obtain different features in the corresponding spectra. One same resonance

4. Monolayer formation of CuPc on Ag(110)

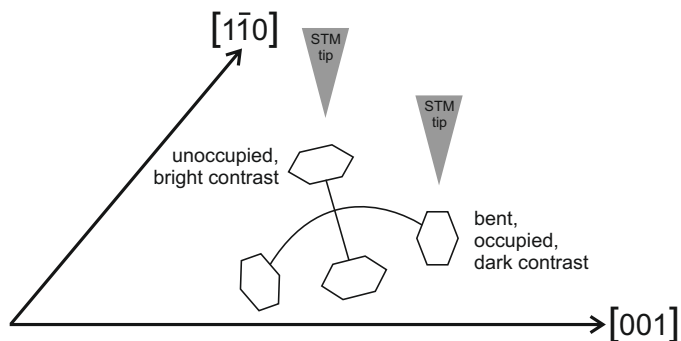


Figure 4.14.: Model of one CuPc molecule in the dense layer on Ag(110): the pair of benzene rings with the more acute angle to the more open Ag[001] direction interacts stronger with the substrate than the perpendicular pair of benzene rings, is slightly bent down towards the substrate, receives the charge donated by the silver, and, due to these related effects, appears with darker contrast in STM.

was found in all spectra suggesting that all tunneling spectra show a density of states averaged over the whole molecule. ARUPS measurements helped to assign the feature found in STS to the corresponding orbital, namely, the 2-fold symmetric LUMO_A. The pair of benzene rings yielding this signal pattern is the one with the more acute angle to the reactive Ag[001] direction, again suggesting a stronger interaction of these rings with the substrate than the other pair of benzene rings. Thus, ARUPS, STS, and STM data are in good agreement with each other concerning the fact that the formerly unoccupied LUMO of CuPc becomes occupied by charge transfer from the silver substrate into the molecule when it adsorbs onto the surface. For this reason the corresponding orbital part is shifted across the Fermi edge to a binding energy of 0.33 eV. ARUPS also confirms that only the LUMO_A becomes occupied and the LUMO_B remains unoccupied. Therefore, the LUMO_B is not observable in STS where it is to be located on the side of positive bias, which is difficult to measure and does not show clear resonances at all.

In summary, we suppose that the observed symmetry reduction from 4-fold to 2-fold for metal phthalocyanines on metal surfaces is a result of geometric and electronic effects interacting with each other, see Fig. 4.14. One pair of molecular benzene rings is bent down towards the surface, with a more acute angle to the more open Ag[001] direction, interacting stronger with the substrate than the other pair of benzene rings, receiving charge from the substrate, filling the LUMO_A, and leaving the perpendicular LUMO_B unoccupied. The geometric distortion also causes the unoccupied pair of benzene rings

to appear with brighter contrast in STM than the other pair, as STM also contains information about the topography of the surface. As a remnant of the electronic structure reordered upon adsorption, the pair of wings bent down becomes v-shaped for negative sampling bias.

5. Hetero-organic layers of CuPc and PTCDA on Ag(110)

In the previous chapter we presented the results of a comprehensive study on the structural and electronic properties of a dense, closed monolayer CuPc on the Ag(110) surface. The next step for a variation of the sample system will now be realized by adsorbing a second species of molecules together with CuPc on this surface.

5.1. Hetero-organic systems involving CuPc and PTCDA

Homo-molecular structures have been widely investigated. Adding a second type of molecules offers a broad variety of possibilities to tune the known adsorbate lattices regarding size and shape by varying the types of molecules and the ratio of molecules of different types on the surface. This way one may become able to specifically modify and even engineer the geometric and electronic structure of the interface between substrate and adsorbed layer. For example, the lateral arrangement of molecules and the charge transfer between all involved components and the corresponding energy level alignment depend on the interplay of molecule-molecule and molecule-substrate interactions. By mixing different molecules in one layer, one can also create new templates for the growth of higher layers.

5.1.1. PTCDA as additional component

For the preparation of hetero-organic layers, we select PTCDA as second organic component to be mixed with CuPc. The adsorption of the prototypical PTCDA molecule on noble metal single crystal surfaces, e.g. on the Ag(110) surface, is very well studied by a variety of experimental and theoretical methods and the structural and electronic properties of the first monolayer are known very well [SAL⁺97, SPF98, BSG⁺98,

5. Hetero-organic layers of CuPc and PTCDA on Ag(110)

GSS⁺⁹⁸, STS⁺⁰⁰, ZKS⁺⁰⁶, KTH⁺⁰⁶, RTT07, KHT⁺⁰⁸, ZFS⁺¹⁰, PRU⁺¹¹, RLZ⁺¹², WHS⁺¹², BMW⁺¹², WSS⁺¹³]. An overview of these features can, for example, be found in the reports of Umbach et al. [USF96, UGS98], Tautz et al. [TES⁺⁰²], and Willenbockel et al. [WLS⁺¹⁵]. In the first monolayer, PTCDA molecules can assemble in two different adsorption geometries depending on the amount of molecules and the area size provided for self-assembly. The less dense ordered phase is the brickwall structure, whose formation is driven by molecule-substrate interaction, forcing the molecules to arrange in a commensurate structure with one molecule per unit cell [SAL⁺⁹⁷, WHS⁺¹²]. The densest phase is the herringbone structure, which is compressed and incommensurate to the substrate with two molecules of different rotational orientation in the unit cell [SPF98, WHS⁺¹²]. Regarding the electronic properties of the PTCDA/Ag(110) interface, it is known that PTCDA molecules are chemisorbed [USF96, GSS⁺⁹⁸, TES⁺⁰²], forming a bond with the π -electron system of their carbon backbone to the silver substrate [EST03, HKC⁺⁰⁵, BMW⁺¹²]. During the adsorption process, charge is transferred from the silver substrate into PTCDA, filling the LUMO, which therefore is shifted across the Fermi level to a binding energy of approximately 0.7 eV [WHS⁺¹²]. The properties of PTCDA adsorbed on Ag(110) differ to some degree from the properties of CuPc. PTCDA molecules form the ordered brickwall structure already at low coverages, since the intrinsic quadrupole moment causes attractive intermolecular forces supporting the formation of hydrogen bonds between adjacent molecules. The charge transfer from the metal substrate into the molecule is great enough for a full occupation of the LUMO, in contrast to the partial occupation of the CuPc LUMO in the homo-molecular phase. These differences make the combination of PTCDA with CuPc an interesting object for experiments on hetero-organic layers.

Laterally mixed layers of CuPc and PTCDA have rarely been investigated, e.g. the adsorption on the compared to Ag(111) more reactive Cu(111) surface has been addressed twice [BWBM03, CSS⁺¹²]. A mixed structure with one CuPc molecule and two PTCDA molecules in the unit cell has been found and described [BWBM03]. Furthermore, the sequence of molecule deposition in the preparation process is found to affect the formation of mixed structures and long-range ordering [BWBM03, CSS⁺¹²]. Stadtmüller et al. prepared mixed layers of CuPc and PTCDA on Ag(111) [Sta13, SLW⁺¹⁴, SSB⁺¹⁴, SHS⁺¹⁵] and found three mixed ordered structures with different molecular ratios, namely, the “mixed brickwall” structure with a CuPc : PTCDA ratio of 1 : 2 in the unit cell, the “mixed zig-zag” structure with a CuPc : PTCDA ratio of 2 : 1 in the unit cell, and the

“mixed 1 to 1” structure with a CuPc : PTCDA ratio of 1 : 1 in the unit cell. Photoemission and STS experiments showed that in the hetero-molecular “mixed brickwall” layer PTCDA receives even more charge than it does in a homo-molecular layer. Meanwhile, the CuPc LUMO, which is also partly occupied in the homo-molecular layer, gets depopulated in the hetero-organic structure. This means that the strong acceptor PTCDA receives even more charge in the hetero-molecular layer and the weak acceptor CuPc is turned into a donor [SLW⁺14].

Mixed ordered structures on Ag(111) have also been reported for variations of the donor and the acceptor molecule, namely CuPc with NTCDA and SnPc with PTCDA, respectively [SSB⁺14]. We assume that ordering may also be possible for the two molecular types CuPc and PTCDA on the Ag(110) surface. Since the (110) surface of crystals with an fcc lattice differs from the (111) surface by higher reactivity and less symmetry, molecules may be less flexible to realize different lateral arrangements and rotational configurations. Our aims are to find recipes for the preparation of different mixed ordered structures, characterize them concerning the geometric arrangement of molecules and the electronic level alignment of the systems, and compare - as far as possible - to the already known hetero-organic structures.

The following chapter consists of two parts for two different mixed ordered structures that will each be investigated by STM and LEED regarding the lateral monolayer structure and by STS for a revelation of the local electronic structure.

5.1.2. Sample preparation

For the preparation of long-range ordered mixed phases of CuPc+PTCDA on Ag(110) we took into account that, as known from literature [SHK⁺09, KLS⁺09, KSS⁺10, SKRK11] and our experience described in the previous chapters, CuPc molecules repel each other and distribute in a dilute phase on the surface when the coverage is not high enough to force them to form an ordered structure. In contrast, PTCDA molecules are known to immediately form islands driven by attractive electrostatic and van-der-Waals intermolecular forces [WHS⁺12, WSS⁺13, SAL⁺97, SPF98, GSS⁺98, UGS98]. Due to these behaviors, we decided to first deposit CuPc with a sub-monolayer coverage followed by annealing to achieve a homogeneous distribution of these molecules on the surface. Secondly, PTCDA molecules are deposited onto the relatively reactive Ag(110) surface, again followed by annealing to facilitate diffusion and desorb molecules from higher layers

than the first monolayer. All experiments are carried out after the last annealing procedure. For these two types of molecules on the Ag(111) surface, it has been shown that the same three reported mixed structures can be obtained in two ways [Sta13, SHS⁺15]: If CuPc is deposited first and then PTCDA molecules are added, they form mixed structures with a ratio only depending on the initial amount of CuPc molecules on the surface. If first PTCDA and then CuPc molecules adsorb onto the surface, subsequent annealing is necessary to add activation energy for the mixing process in which CuPc molecules have to penetrate the PTCDA islands.

5.2. Mixed phases of CuPc and PTCDA on Ag(110)

Similar as described by Stadtmüller [Sta13, SHS⁺15], we find that the molecules do not mix for low coverage but, comparable to pure CuPc on Ag(110), CuPc and PTCDA molecules only form ordered mixed structures when the coverage is high enough to force the molecules to align with respect to each other. When the coverage is less, they mix in disorder as presented in Fig. 5.1 where an only weak tendency for co-orientation and local ordering is observed. If the amount of PTCDA molecules deposited onto the CuPc pre-covered Ag(110) surface is greater than the portion of coverage that the still uncovered surface areas can host until it is completely covered, an interesting exchange is observed after annealing. Additional PTCDA molecules not fitting into the first molecular layer will not adsorb in the second layer. They drive existing CuPc molecules out of the first layer and the PTCDA molecules go to the molecule-metal interface themselves. CuPc molecules driven out to the second layer desorb in the annealing process. This exchange reaction has also been observed by several methods for the same two types of molecules on the Ag(111) surface [Sta13, SGP⁺14].

Depending on the relative amounts of CuPc and PTCDA molecules deposited, we have observed two different mixed ordered structures achieved from two different preparation processes, namely, a structure with a ratio of CuPc : PTCDA = 1 : 4, which we will call the ‘windmill structure’, and a structure with a ratio of CuPc : PTCDA = 4 : 5, which we will call the ‘stripe structure’. Compared to the mixed ordered phases found on Ag(111) as demonstrated in Fig. 5.2, we observe that on Ag(110) there seems to be a tendency towards the formation of larger unit cells with remarkably more molecules and a difficulty to accommodate simple packing motifs of CuPc and PTCDA together.

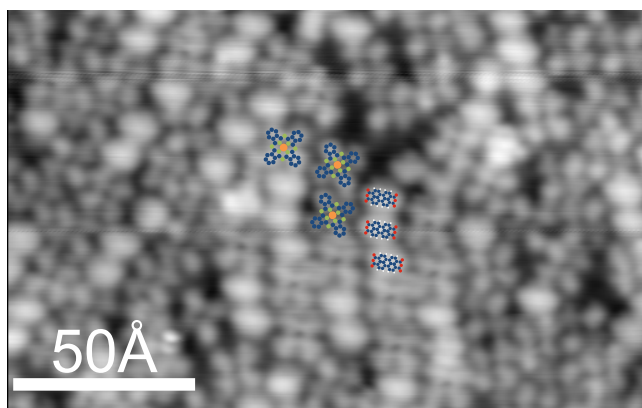


Figure 5.1.: In the low coverage regime, the darker, cross shaped CuPc molecules and the brighter, oval PTCDA molecules form a mixed but disordered phase on the Ag(110) surface, $U_{\text{bias}}=0.126$ V, $I_{\text{setpoint}}=0.35$ nA.

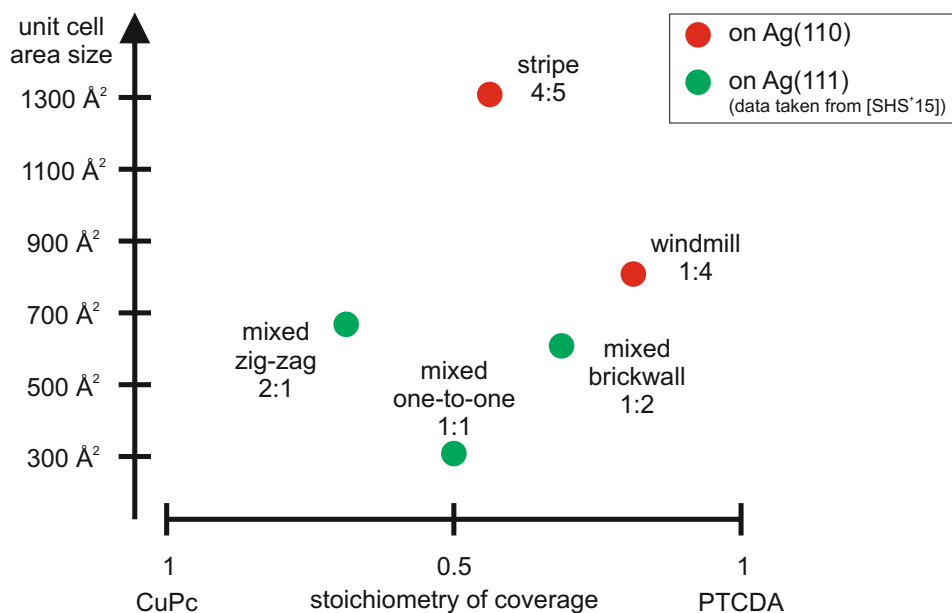


Figure 5.2.: The comparison of laterally mixed ordered structures of CuPc and PTCDA on Ag(111) (green) and on Ag(110) (red) reveals a tendency to form larger unit cells with more molecules on Ag(110).

5.3. Windmill structure (ratio 1:4)

The first phase has been prepared according to the procedure described in Sec. 2.4.2 by first depositing approximately 0.3 ML CuPc followed by soft annealing up to 220 °C for 10 min. Subsequently, approximately 0.8 ML PTCDA have been deposited followed by annealing up to 350 °C for 10 min to desorb molecules from the second and higher layers.

5.3.1. Structural properties: Chiral structure formation

From the preparation description it is likely that the whole surface is covered with molecules and no clean silver surface is available. This fact is verified by STM images that have been recorded of several different areas of the sample. The whole surface is covered with flat lying molecules, mostly in ordered phases, cf. Fig. 5.3. There exist two of these: a mixed phase with CuPc and PTCDA molecules, forming the long-range ordered windmill structure, and another phase containing only PTCDA molecules arranged in the herringbone pattern. Only in some smaller areas at domain boundaries and substrate step edges molecules are not included in the order. The pure PTCDA herringbone phase covers significantly more than 50 % of the surface but the islands of the mixed ordered phase appear frequently and their lateral size of up to 1000 Å is large enough for comprehensive investigations on the structure.

The lateral arrangement of CuPc and PTCDA molecules in the windmill phase is shown in Fig. 5.4. Eight PTCDA molecules form a ring surrounding one CuPc molecule. The PTCDA rings merge into each other and, thus, the ratio of molecules in the unit cell is CuPc : PTCDA = 1 : 4. All CuPc molecules are oriented in the same direction with an angle of $\approx 22^\circ$ with respect to the Ag[001] direction. The four PTCDA molecules of one unit cell exhibit two different rotational orientations that are almost perpendicular to each other, namely, $\approx 0^\circ$ and $\approx 93^\circ$ w.r.t. Ag[001]. Lengths and angles of the unit cell vectors have been measured in 19 different STM images and the evaluation of the data yielded values for the unit cell listed in Tab. 5.1. These values correspond to the matrix

$$M_{1:4} = \begin{pmatrix} 3.9 & 6.5 \\ -4.6 & 5.7 \end{pmatrix} \quad (5.1)$$

describing the molecular structure (uncertainty of ± 0.1 for each matrix element).

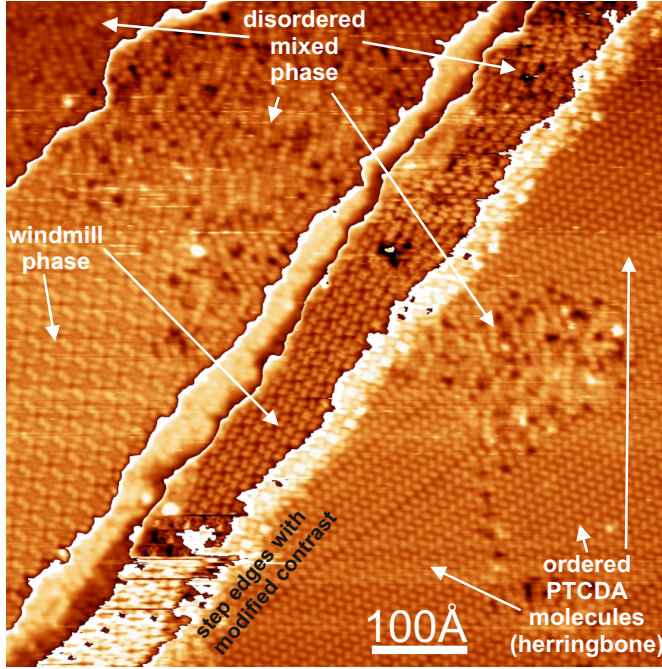


Figure 5.3.: The whole surface is covered with CuPc molecules (approximately 20 %) and PTCDA molecules (approximately 80 %). Three different structures can be observed: the ordered mixed windmill structure (left hand side and center), the ordered PTCDA herringbone structure (right hand side), and a disordered mixed phase (top), $U_{\text{bias}}=0.852 \text{ V}$, $I_{\text{setpoint}}=0.62 \text{ nA}$.

	length	angle to $\text{Ag}[001]$	angle to \vec{b}_2
\vec{b}_1	$24.5 \text{ \AA} \pm 0.5 \text{ \AA}$	$50^\circ \pm 1^\circ$	$89^\circ \pm 1^\circ$
\vec{b}_2	$25.1 \text{ \AA} \pm 0.5 \text{ \AA}$	$139^\circ \pm 1^\circ$	–

Table 5.1.: Values from STM describing the windmill structure of CuPc and PTCDA on Ag(110)

When comparing the mirror domains of the windmill structure in Fig. 5.5, one can see that the structure is chiral. The observed structure is called A and is identical to the structure B, which is obtained by a rotation of A of 180° . Their mirror images A' and B', obtained by a mirror operation at the $[1\bar{1}0]$ surface direction, which are the same as A'' and B'', obtained by a mirror operation at the $[001]$ surface direction, cannot be constructed from the original image A by simple translation and rotation

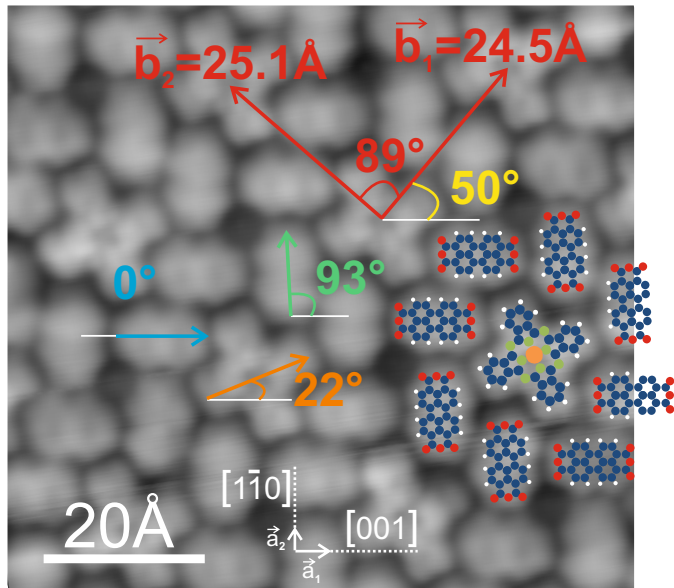


Figure 5.4.: STM image of the windmill structure: PTCDA molecules are oriented in two different rotational directions (0° and 93° w.r.t Ag[001]) and form rings around the CuPc molecules. CuPc molecules are rotated by 22° w.r.t Ag[001]. The unit cell containing one CuPc and four PTCDA molecules is marked with the pair of red vectors (\vec{b}_1 , \vec{b}_2); $U_{\text{bias}}=0.565$ V, $I_{\text{setpoint}}=1.2$ nA.

operations but a mirror operation is required. The reason for the emergence of chirality is not obvious, since neither of the involved types of molecules, CuPc and PTCDA, is chiral. In spite of this fact, recalling the data presented in Ch. 4 about the dense monolayer of CuPc on Ag(110), the homo-molecular phase is chiral taking into account the rotational configuration of the molecule on the surface. The same holds for the homo-molecular PTCDA herringbone phase, which is presented with a model in literature [WHS⁺12, WSS⁺13, WLS⁺15]. Even for achiral molecules, handedness is often created upon adsorption [Rav09, MFR11, Ern13]. In the same way as for the homo-molecular phases, chirality in the hetero-molecular phases is created upon the formation of the ordered structure involving both types of molecules, although the mixed windmill structure is chiral even without taking the substrate into account. The tendency to form large, complex unit cells mentioned before (cf. Fig. 5.2) supports the emergence of chirality.

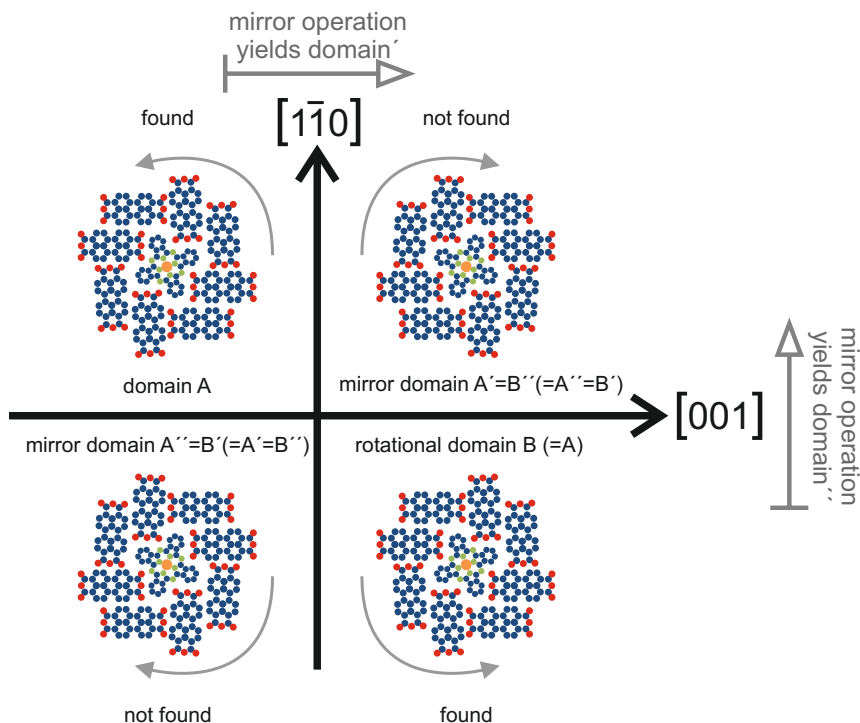


Figure 5.5.: Two rotational domains A and B, rotated by 180° , are not distinguishable from each other and are observed as one domain. Their mirror domains A', B' (mirror axis: $[1\bar{1}0]$ direction), A'', and B'' (mirror axis: $[001]$ direction) also cannot be distinguished from each other forming the expected second domain that is not observed.

Interestingly, only one domain ($A=B$) of the mixed ordered structure has been observed in STM images (e.g. Figs. 5.3 and 5.4), although for the Ag(110) surface we expect two rotational domains and one mirror domain for each rotational domain, i.e. four domains of which two each cannot be distinguished, as explained above, since the molecular structure also exhibits a rotational symmetry that leads to the two expected domains demonstrated in Fig. 5.5. From the symmetry point of view, both the ideal Ag(110) surface crystallography and the CuPc and PTCDA molecular structures, there seems to be no reason for a preferential formation of only one chiral arrangement and the suppression of its mirror domain. Whether the mirror domain does not exist or has simply not been observed by coincidence remains unclear at this point.

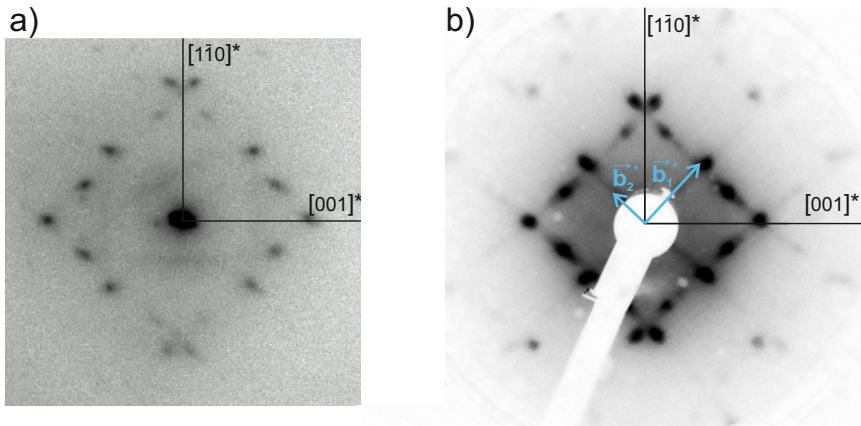


Figure 5.6.: (a) Experimental SPA-LEED image of the sample with patches of the windmill structure and with patches of the PTCDA herringbone structure on Ag(110), 30 eV. (b) Experimental MCP-LEED image of the pure PTCDA herringbone structure on Ag(110), 19 eV.

For further structural investigations, an electron diffraction image is taken with a SPA-LEED and is depicted in Fig. 5.6a. Unfortunately, a more precise analysis is impossible, since due to the preparation conditions required to achieve the windmill phase, the amount of PTCDA molecules provided is dominant and correspondingly the major part of the surface is occupied by the PTCDA herringbone (HB) structure. Accordingly, only diffraction spots of this pattern are observed in LEED. For comparison, an image of the pure PTCDA HB phase is given in Fig. 5.6b and is described by the matrix

$$M_{\text{PTCDA-HB}} = \begin{pmatrix} 1.9 & 3 \\ -3.8 & 5 \end{pmatrix} [\text{WSS}^+13]. \quad (5.2)$$

Comparing $M_{1:4}$ to $M_{\text{PTCDA-HB}}$ it becomes clear that spots of the corresponding diffraction patterns will be close to each other, since the first unit cell vector of the windmill structure is about twice as long and in the same direction as the first unit cell vector of the PTCDA HB phase (upper rows of matrices) and the second vectors of both structures do not differ much in length and direction (bottom rows of matrices). Hence, a separation of the contributions of the two phases, namely PTCDA HB and windmill, will be difficult and requires very clear electron diffraction data.

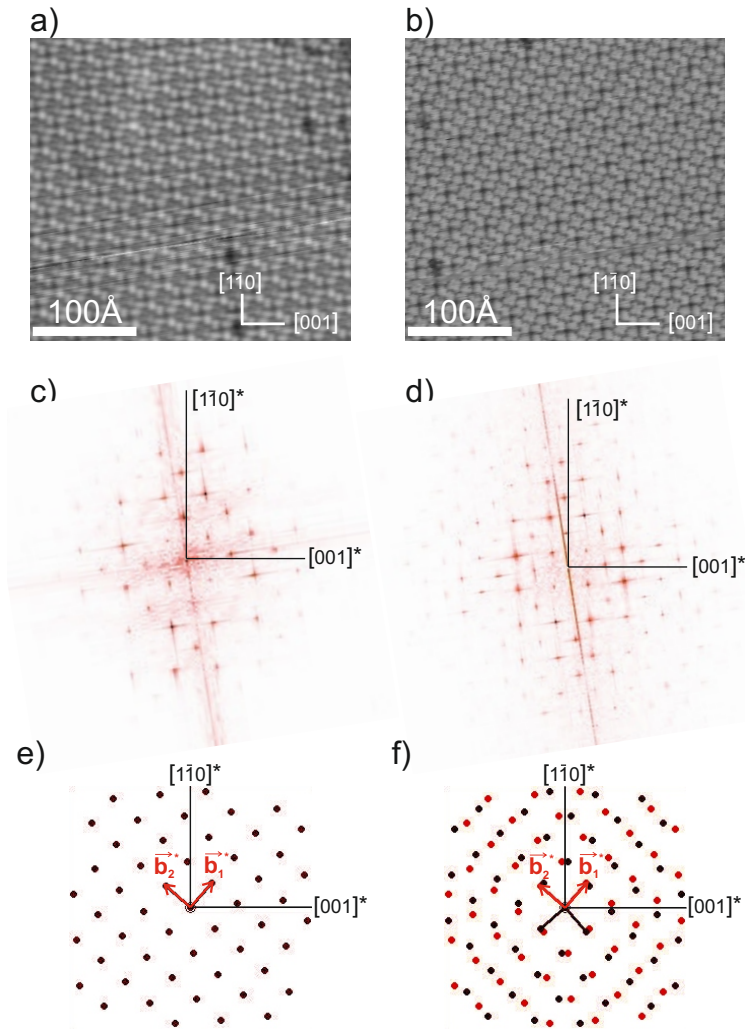


Figure 5.7.: (a,b) STM images and (c,d) their appropriate calculated 2-dimensional Fourier transform, which corresponds to the diffraction image of the displayed molecular structure. (a) $U_{\text{bias}} = 0.814 \text{ V}$, $I_{\text{setpoint}} = 0.6 \text{ nA}$, (b) $U_{\text{bias}} = 2.121 \text{ V}$, $I_{\text{setpoint}} = 1.2 \text{ nA}$. (e,f) The simulated diffraction patterns are constructed with values extracted from the analysis of STM images, reciprocal unit cell vectors are marked (\vec{b}_1^* , \vec{b}_2^*), (e) diffraction pattern of the one domain observed in STM, (f) diffraction pattern of the observed domain (red spots) and its mirror domain (dark spots).

5. Hetero-organic layers of CuPc and PTCDA on Ag(110)

	length	angle to Ag[001]	angle to \vec{b}_2
\vec{b}_1	$24.5 \text{ \AA} \pm 0.3 \text{ \AA}$	$50^\circ \pm 1^\circ$	$89^\circ \pm 1^\circ$
\vec{b}_2	$24.9 \text{ \AA} \pm 0.2 \text{ \AA}$	$139^\circ \pm 1^\circ$	–

Table 5.2.: Values from FFT (of STM images) describing the windmill structure of CuPc and PTCDA on Ag(110)

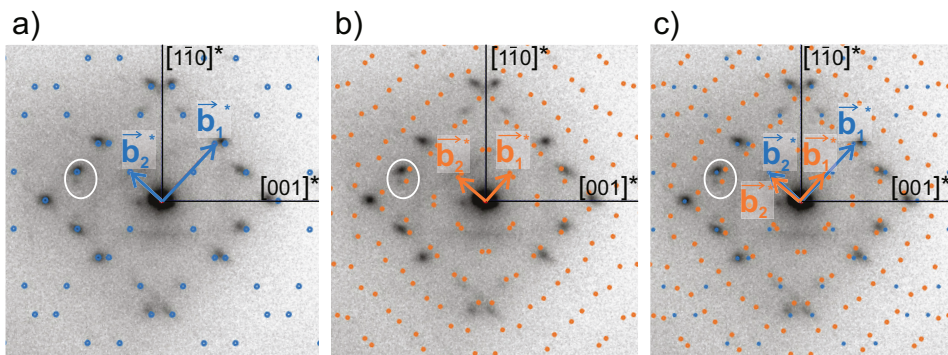


Figure 5.8.: The experimental SPA-LEED image (30 eV) is superimposed with simulated LEED patterns. The corresponding reciprocal unit cell vectors are marked (\vec{b}_1^* , \vec{b}_2^*). (a) Simulation of the PTCDA HB pattern, (b) simulation of the windmill pattern (two domains), (c) both simulations superimposed. The circled area marks a weak diffraction spot contributed by the windmill structure.

In order to obtain indications what the diffraction pattern of the windmill structure would look like, some STM images of the extended windmill structure (Fig. 5.7a,b) are evaluated in WSXM [HFGR⁺07] by a fast Fourier transformation (FFT), which corresponds to the diffraction pattern of the imaged structure. The FFT yields the almost rectangular patterns in Fig. 5.7c,d, which of course represent only the one domain that is present in the corresponding STM images. Additionally, we simulate a diffraction pattern with the unit cell values extracted from STM. Figure 5.7e shows this simulation of only one domain, for direct comparison to the FFT images, and in Fig. 5.7f both domains are taken into account, producing a mirror symmetric pattern. The FFT images and the simulation for the one corresponding domain are in good agreement. For a deeper analysis and more precise values for the unit cell vectors, the reciprocal space vectors are measured in the FFT images yielding the values listed in Tab. 5.2. The matrix elements do not change within the accuracy given in Eq. 5.1.

A comparison of simulated diffraction patterns with the experimental one is depicted in Fig. 5.8 where in (a) the PTCDA HB simulation, in (b) the windmill simulation with both domains, and in (c) the PTCDA HB and the windmill simulation together are superimposed to the experimental pattern. Obviously, the differences are small and we cannot clearly separate the contributions of the pure PTCDA HB and the windmill phase. The contribution of the latter, covering a significantly smaller part of the surface, is too weak to yield a clear signal and the PTCDA HB pattern is in better agreement with the experimental image for large areas in reciprocal space. Only in the circled area one observes a diffraction spot that is assigned to the windmill pattern and is not covered by the PTCDA HB simulation.

5.3.2. Electronic properties

The local electronic properties are investigated recording tunneling spectra above all five different molecules of the unit cell in the range from -1.8 V to 1.8 V . Since, here again, the entire surface is covered with molecules, we cannot present any spectra of areas of clean Ag substrate for comparison with the molecular spectra. Accordingly, the conventional way of preparing a spectroscopically applicable tip by dipping it into the surface, picking up silver atoms, cannot be used.

The molecules are labeled as given in Fig. 5.9e to distinguish their spectra. C denotes spectra corresponding to the CuPc molecule, P_{\parallel} denotes the PTCDA molecules aligned parallel to the Ag[001] direction, and P_{\perp} denotes the PTCDA molecules perpendicular to the Ag[001] direction. The corresponding differential conductance data are shown in Fig. 5.9a in total and in b, c, and d with certain parts enlarged for easier distinction. All spectra are rather smooth without dominating features in different spectra and with similar intensities. Hence, we assume that the tip was clean so that the observed features can be attributed to the sample.

Taking a closer look at the spectra, one can find that for negative bias, i.e. occupied sample states, the spectra of the PTCDA molecules feature a resonance between approximately -0.6 V and -1.0 V that is hardly observable in the spectrum of CuPc (cf. Fig. 5.9b). This peak can probably be assigned to the PTCDA LUMO [ZKS⁺06, ZFS⁺10, PRU⁺11, WSS⁺13]. The slightly enhanced intensity in the PTCDA spectra at about -1.2 V cannot directly be assigned to a molecular orbital since the HOMOs of PTCDA molecules in the herringbone phase are expected to have stronger binding ener-

5. Hetero-organic layers of CuPc and PTCDA on Ag(110)

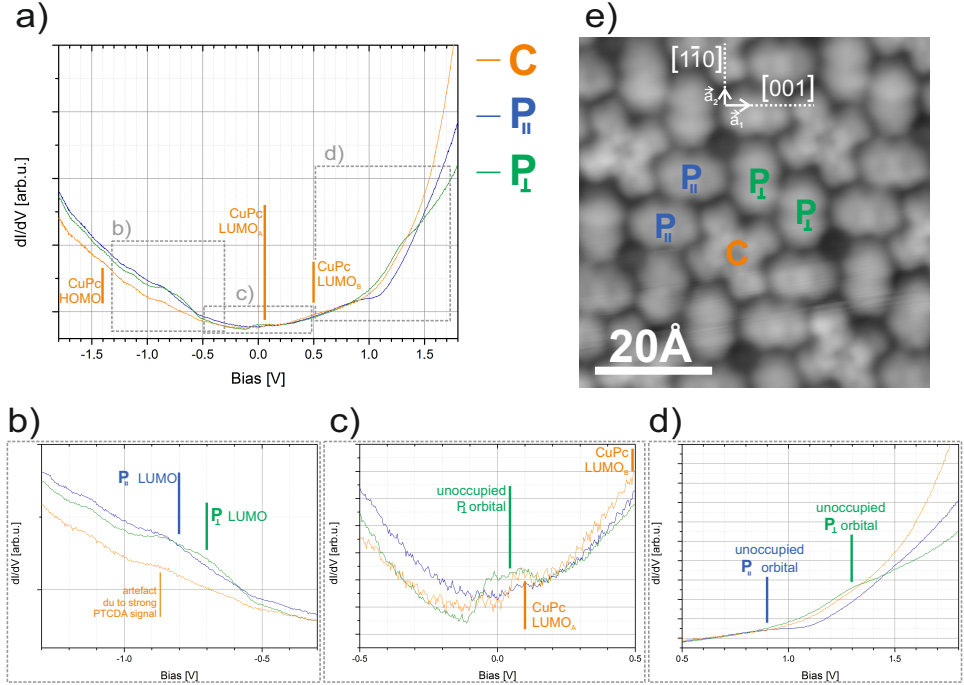


Figure 5.9.: (a) The differential conductance spectra of the two different PTCDA molecules ($P_{||}$ and P_{\perp}) and the CuPc molecule (C) in the unit cell exhibit flat curves with few features, $I_{\text{setpoint}}=1.0$ nA; (b,c,d) zoom images of spectra depicting small differences between the spectra of the different molecules. (e) STM image: The molecules are labeled for distinction of the spectra, $U_{\text{bias}}=0.565$ V, $I_{\text{setpoint}}=1.2$ nA.

gies than 1.5 eV, cf. [ZKS⁺06, ZFS⁺10, PRU⁺11, WSS⁺13]. The weak feature at -1.4 V in the spectrum of CuPc probably appears due to a resonance of the CuPc HOMO, which we found to be located at -1.35 V in Ch. 4. Around the Fermi edge (Fig. 5.9c), the CuPc and the PTCDA_⊥ spectra feature a small dip followed by a small step towards positive bias, which the PTCDA_{||} spectra do not exhibit. This feature might stem from the CuPc LUMO_A which could be depopulated compared to the pure CuPc phase, similar as it is the case in the mixed phase on Ag(111) in [SLW⁺14]. The LUMO_B as second part of the originally degenerate orbital parts (LUMO_A/LUMO_B) might then cause the weak resonance in the CuPc spectrum at 0.5 V. The gap between this latter feature and the assumed HOMO (-1.4 V) corresponds to the band gap of CuPc as mentioned in Ch. 3 and [HH63, Ham67]. On the side of positive bias (Fig. 5.9d), the two PTCDA

molecules again exhibit features that are not observed in the spectrum of CuPc, namely, PTCDA_{||} shows a resonance at about 0.9 V and PTCDA_⊥ at about 1.3 V.

Plotting the data as $\frac{dI_{\text{setpoint}}/dU_{\text{bias}}}{I_{\text{setpoint}}/U_{\text{bias}}}$ for a compensation of the parabolic background intensity does not yield more information. The intensity of individual features increases only very slightly, but the noise level is significantly increased and the data range between -0.1 V and 0.1 V cannot be evaluated anymore due to strongly fluctuating values around $U_{\text{bias}} = 0$, where $I_{\text{setpoint}} \approx 0$, too. Therefore, to make differences between the spectra of the molecules more clear, they are subtracted from each other and the resulting curves are depicted in Fig. 5.10. Here, the features appear with enhanced intensity. Both PTCDA molecules dominate the range of negative bias whereas CuPc dominates the spectra for positive bias. The difference curve between PTCDA_{||} and PTCDA_⊥ reveals that the resonance between -0.6 V and -1.0 V is not equal for the two molecules, but PTCDA_⊥ features this resonance at less negative bias causing the dip at approximately -0.7 V while PTCDA_{||} features this resonance at approximately -0.8 V. Also the energetic distance between the peaks at 0.9 V and 1.3 V becomes more pronounced. Same holds for the dip of PTCDA_⊥ at -0.1 V and the step at the Fermi edge. The step of CuPc at 0.1 V is weakly present in the difference curves of CuPc subtracted from PTCDA_{||} and PTCDA_⊥.

Regarding the spectra of all molecules in the unit cell and the differences between the spectra, we can say that the HOMO of PTCDA mainly contributes to the rising intensity between -1.3 V and -1.8 V while the CuPc HOMO lies at approximately -1.4 V. The PTCDA LUMOs corresponding to the two different molecular rotational configurations are observed at about -0.8 V and -0.7 V with a small difference between the two PTCDA molecules, similar to what has been described for the pure PTCDA HB phase on Ag(110) [WSS⁺13]. The CuPc LUMO_A is probably less occupied than in the homo-molecular phase and may be located at about 0.1 V while the LUMO_B may be located at 0.5 V where CuPc exhibits a slightly stronger intensity compared to PTCDA. Further resonances may originate from higher unoccupied orbitals of PTCDA, again with a small difference between the two PTCDA molecules.

Comparing the values for the orbital binding energies of PTCDA and CuPc in the windmill phase to the values of the pure PTCDA herringbone monolayer in [WSS⁺13] and the pure CuPc monolayer in Ch. 4 as shown in Fig. 5.11, we see that the trend that

5. Hetero-organic layers of CuPc and PTCDA on Ag(110)

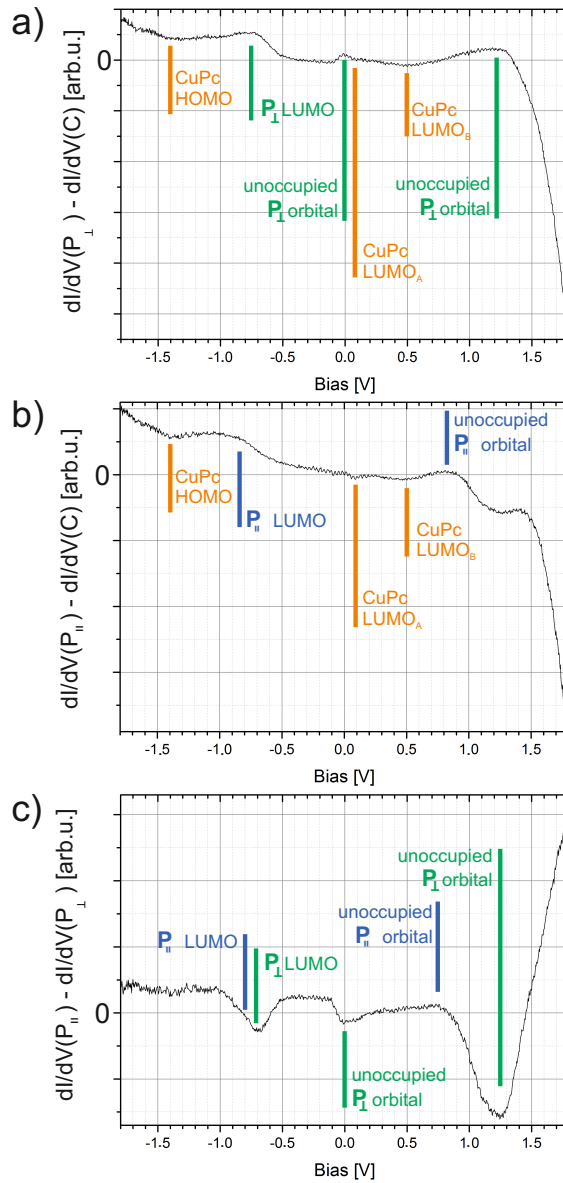


Figure 5.10.: The graphs showing spectra from Fig. 5.9a subtracted from each other enhance the visibility of individual (marked) features. (a) P_{\perp} -C, (b) P_{\parallel} -C, (c) P_{\parallel} - P_{\perp}

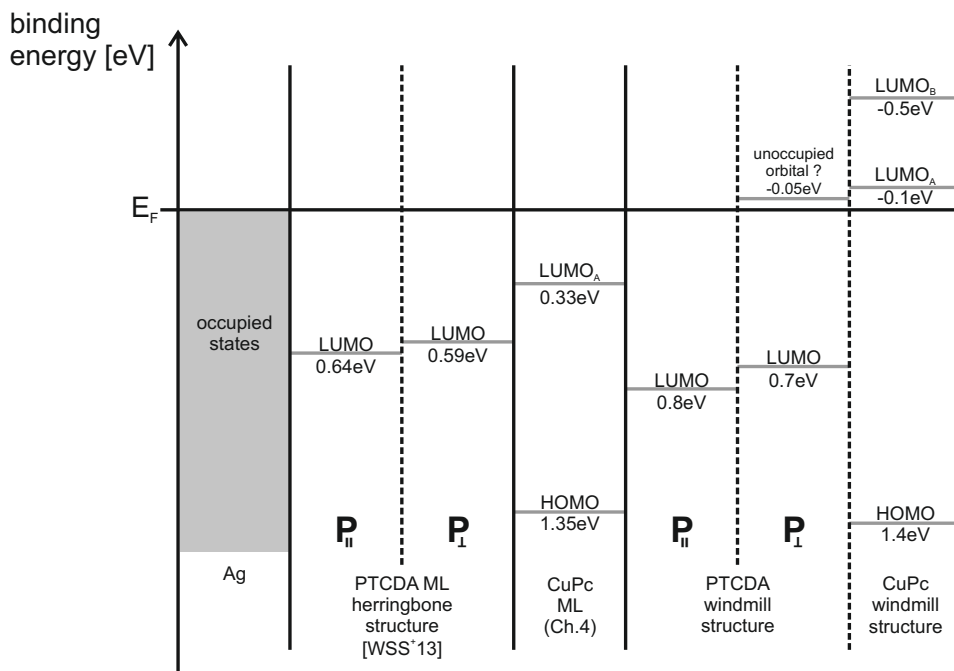


Figure 5.11.: The energy level rearrangement for the windmill structure compared to the energy level rearrangement of the homo-molecular PTCDA herringbone structure on Ag(110) (data taken from [WSS⁺13]) and the dense CuPc monolayer on Ag(110) (data from Ch. 4.)

has been observed for the mixed brickwall structure of CuPc and PTCDA (ratio 1 : 2) on Ag(111) [SLW⁺14] can also be assumed for the windmill structure on Ag(110): PTCDA as the stronger acceptor accumulates even more charge than in its homo-molecular phase, shifting the PTCDA LUMOs to larger binding energies. At the same time, CuPc accepts less charge (almost turning into a donator) with its LUMO_A shifted back across the Fermi level to the side of unoccupied states.

5.4. Stripe structure (ratio 4:5)

For the preparation of the second phase, only the amount of deposited molecules and the subsequent annealing temperature have been changed. First, 0.6 ML CuPc have been deposited followed by soft annealing up to 220 °C for 10 min. Secondly, 0.6 ML PTCDA have been deposited and the sample has been annealed to 400 °C for 10 min. The higher temperature was necessary to desorb molecules that did not fit into the first layer and to provide the molecules in the first layer with enough energy for diffusion and mixing.

5.4.1. Structural properties: Combination of chiral building elements

Similar as described before in Sec. 5.3.1, here again the whole surface is covered with molecules leaving no free silver patches as demonstrated, for example, by STM in Fig. 5.12. The molecules lie flat on the surface and are either arranged in an ordered mixed stripe structure or in disorder but also mixed. The ordered islands cover about 50% of the surface and are large enough for comprehensive investigations on the geometric structure and local electronic properties.

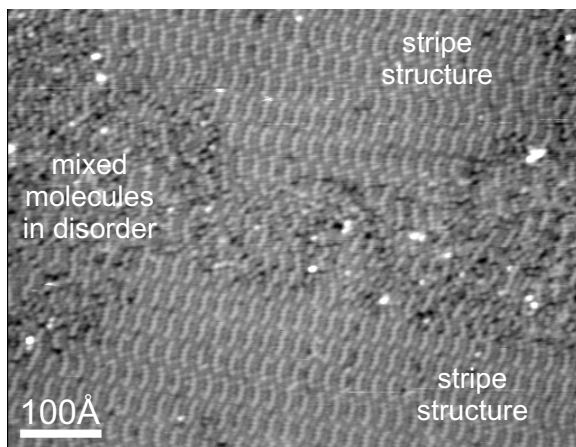


Figure 5.12.: The whole surface is covered with CuPc molecules ($\approx 50\%$) and PTCDA molecules ($\approx 50\%$). Large islands of an ordered mixed structure (top and bottom) can be observed between areas of mixed molecules in disorder, $U_{\text{bias}}=0.565\text{ V}$, $I_{\text{setpoint}}=64\text{ pA}$.

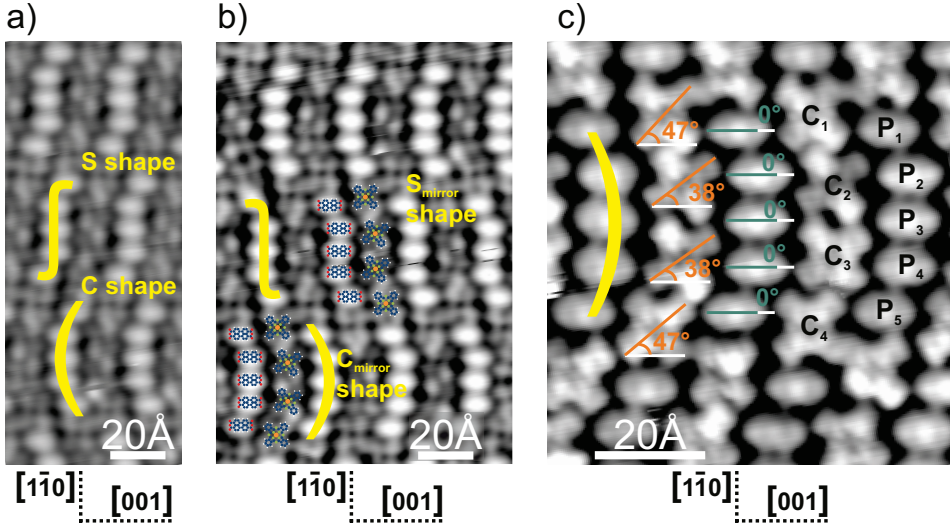


Figure 5.13.: (a) In STM images, stripes of two different molecular arrangements with each five PTCDA and four CuPc molecules are observed: the meandering ‘S’ and the bent ‘C’ configuration, $U_{\text{bias}}=0.493$ V, $I_{\text{setpoint}}=2.1$ nA. (b) The chains of four CuPc molecules exceed the chains of five PTCDA molecules in length along the Ag $[1\bar{1}0]$ direction, forming separating space of darker contrast between the PTCDA chains, which appear with brighter contrast, $U_{\text{bias}}=0.358$ V, $I_{\text{setpoint}}=1.0$ nA. (c) All PTCDA molecules lie parallel to the Ag $[001]$ direction while the CuPc molecules show two different rotational orientations; molecules are labeled for distinction of the nine molecules (P_1 to P_5 for the PTCDA molecules and C_1 to C_4 for the CuPc molecules), $U_{\text{bias}}=0.400$ V, $I_{\text{setpoint}}=1.1$ nA.

Upon a close look, the ordered mixed molecular stripe structure exhibits short chains of five PTCDA and four CuPc molecules, respectively, alternating along the Ag $[001]$ direction. The chains are slightly bent and with their long direction oriented approximately parallel to the Ag $[1\bar{1}0]$ direction. There are two different molecular arrangements of PTCDA and CuPc molecules (plus their mirror domains) observable, an ‘S’-shaped configuration and a ‘C’-shaped configuration, both marked in Fig. 5.13a. In each configuration, comprising nine molecules with a ratio CuPc : PTCDA = 4 : 5 (cf. Fig. 5.13b), the three PTCDA molecules in the middle (P_2 , P_3 , P_4 , cf. Fig. 5.13c) form a straight line along the Ag $[1\bar{1}0]$ direction with their long axis parallel to the Ag $[001]$ direction. The molecules at either end (P_1 and P_5) are rotationally oriented in the same direction but each is shifted parallel to the Ag $[001]$ or Ag $[00\bar{1}]$ direction, yielding the meandering ‘S’ shape or the bent ‘C’ shape. The CuPc molecules are arranged correspondingly in ‘S’

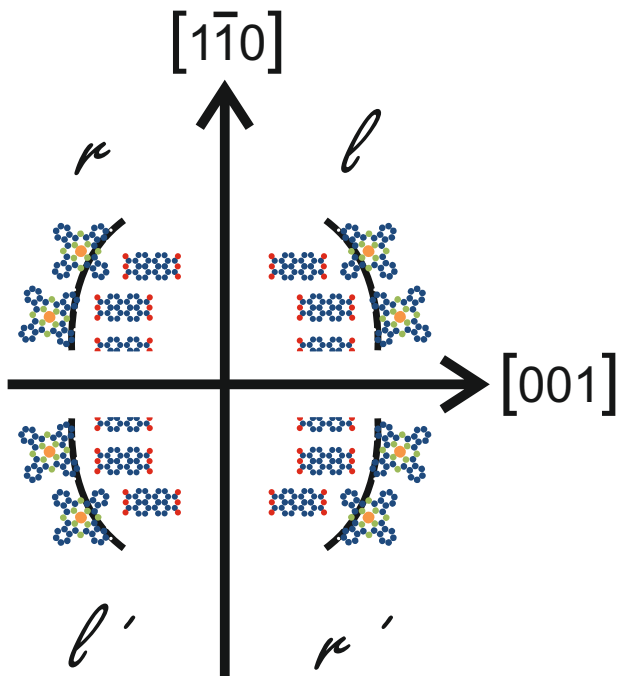


Figure 5.14.: The basic structural unit is chiral and appears with all four rotation and mirror images. r can only be transformed into l by a mirror operation, r' and l' are achieved by application of a rotation by 180° .

or 'C' shape, but the chain of four CuPc molecules is a little bit longer than the chain of five PTCDA molecules. So, benzene rings of the CuPc molecules at the end of the chain reach out and form a short separating space between adjacent PTCDA chains along the $Ag[1\bar{1}0]$ direction, appearing with darker contrast between the brighter PTCDA chains in STM. The four CuPc molecules in one chain exhibit two slightly different rotational orientations of their long axis with respect to $Ag[001]$. The top (C_1) and bottom (C_4) CuPc molecule are rotated by $\approx 47^\circ(\pm 2^\circ)$ and the two CuPc molecules in the middle (C_2 , C_3) are rotated by $\approx 38^\circ(\pm 2^\circ)$.

The two different configurations of the molecular arrangement can be split up into basic structural units comprising two CuPc molecules and two and a half PTCDA molecules as depicted in Fig. 5.14. The involved molecules are arranged along a short bent line and it becomes obvious that this basic structural unit is chiral. The elements r and r' can be

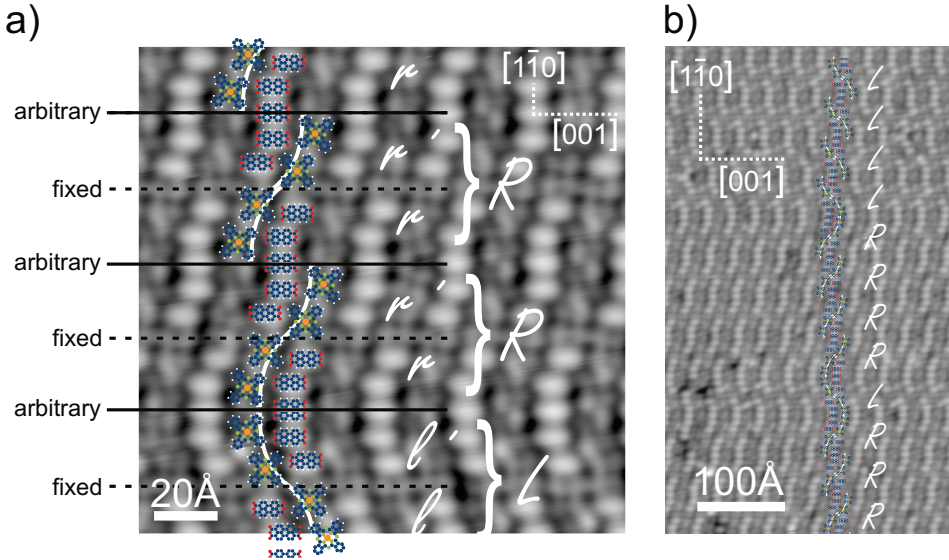


Figure 5.15.: The chiral basic structural units are combined with each other to form the extended stripe structure observed in STM. (a) $U_{\text{bias}}=0.493$ V, $I_{\text{setpoint}}=2.1$ nA, (b) $U_{\text{bias}}=0.619$ V, $I_{\text{setpoint}}=1.1$ nA. The transition between two units next to each other along the Ag[$\bar{1}\bar{1}0$] direction is fixed at the position between two molecular chains, here marked with dashed lines. The transition is arbitrary at the position in the middle of a molecular chain, here marked with solid lines. The two adjacent small units at a fixed transition are combined forming the large units R and L, respectively.

transformed into each other by a rotation operation. Same holds for l and l' , but r and l are connected via a mirror operation and cannot be transformed into each other by a rotation.

From several STM images, e.g. in Fig. 5.15a,b, one can extract rules for the combination of the basic structural units r , r' , l , and l' to form the extended ordered stripe structure. The transition from one unit to the next one in the negative direction of Ag[$\bar{1}\bar{1}0$] between two molecular chains, i.e. between the molecules P5 and P1 and between C4 and C1, is fixed: r' is always followed by r and l' is always followed by l as marked in Fig. 5.15a by dashed lines. In contrast, the transition in the middle of a chain (solid lines in Fig. 5.15a) at the position of the (split) molecule P3 and between the molecules C2 and C3 is arbitrary, such that r can be followed by r' or l' and l can as well

5. Hetero-organic layers of CuPc and PTCDA on Ag(110)

be followed by r' or l' in the negative $[1\bar{1}0]$ direction. Hence, we combine the four basic structural units into two new, larger units R and L, with L being the mirror image of R:

$$R = \begin{Bmatrix} r' \\ r \end{Bmatrix} \quad \text{and} \quad L = \begin{Bmatrix} l' \\ l \end{Bmatrix} . \quad (5.3)$$

Thus, R and L denote the two mirror domains of the ordered stripe structure. The domains extend parallel to the Ag[001] direction and their boundaries occur with an arbitrary probability along the Ag $[1\bar{1}0]$ direction.

Regarding the basic structural units and the possible variations of their order in the stripe structure, this mixed molecular arrangement of CuPc and PTCDA with the ratio 4 : 5 combines periodicity (molecular arrangement within a basic structural unit and along the Ag[001] direction) with stochastics (alternation of the large units along the Ag $[1\bar{1}0]$ direction, i.e. alternation of the two mirror domains).

Taking a careful look at the overview images in Fig. 5.16, basic structural units (circled) can also be found in the areas of the mixed disordered phase of the sample hosting the stripe structure (Fig. 5.16a), demonstrating that the nucleation of the clusters from the gas phase already happens as chiral elements. Thus, here again, the chirality is created upon the formation of the mixed ordered structure. Figure 5.16b, which is the overview image of the windmill structure discussed in Sec. 5.3, even reveals the formation of some basic structural units of the stripe phase in the disordered areas of the layer on the sample mainly hosting the pure PTCDA herringbone phase and the mixed windmill structure. Hence, it seems that these basic structural units consisting of four or five molecules correspond to a stable element of CuPc and PTCDA together on the Ag(110) surface where locally the ratio of CuPc : PTCDA is approximately 4 : 5. In the layer that mainly hosts the PTCDA herringbone and the windmill structure, the overall ratio does not provide enough CuPc for the formation of basic structural units, but locally in the disordered phase there are enough CuPc molecules for combination with PTCDA to yield some of these.

The unit cell for describing the stripe structure is defined by the two vectors \vec{b}_1 and \vec{b}_2 marked in Fig. 5.17. The corresponding lengths and angles have been measured in 33

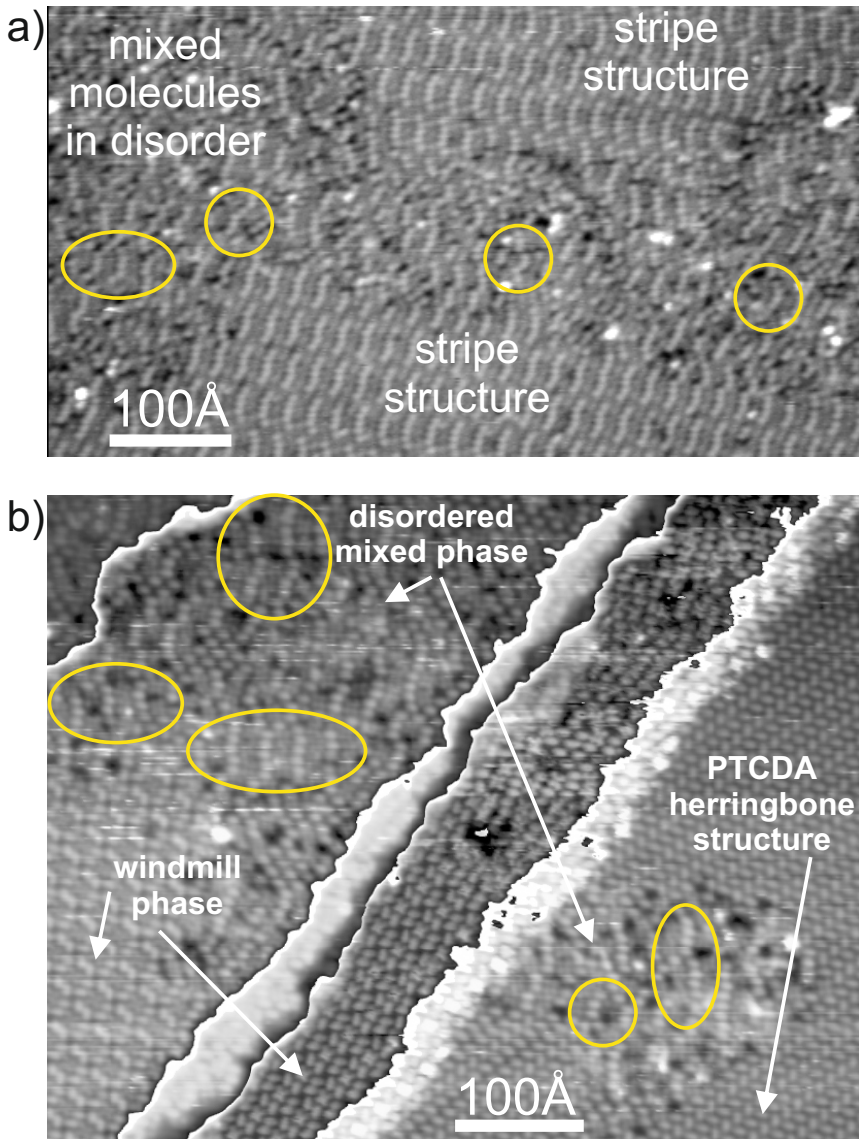


Figure 5.16.: Even in the mixed disordered phase of (a) the sample hosting the stripe structure, $U_{\text{bias}}=0.565\text{ V}$, $I_{\text{setpoint}}=64\text{ pA}$, and (b) the sample hosting the windmill structure (cf. Fig. 5.3), $U_{\text{bias}}=0.852\text{ V}$, $I_{\text{setpoint}}=620\text{ pA}$, some basic structural units (r , l , r' , l') can be found (circled).

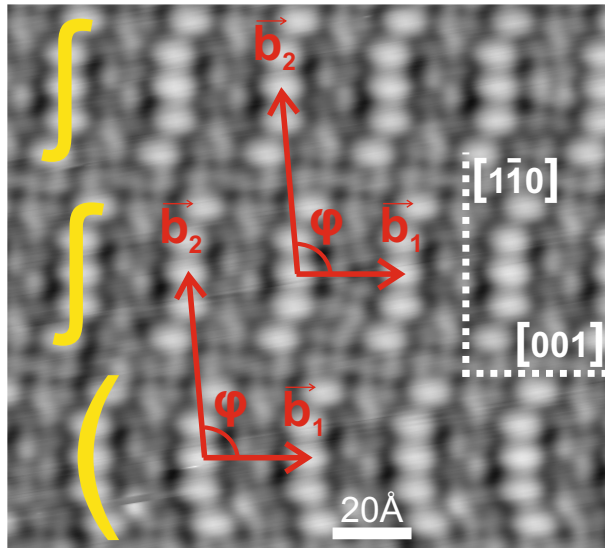


Figure 5.17.: The unit cell is marked with a pair of vectors (\vec{b}_1 , \vec{b}_2) going from the middle of one molecular chain to the next chain, $U_{\text{bias}}=0.493$ V, $I_{\text{setpoint}}=2.1$ nA.

	length	angle to Ag[001]
\vec{b}_1	$27.2 \text{ \AA} \pm 0.3 \text{ \AA}$	0°
\vec{b}_2	$47 \text{ \AA} \pm 1 \text{ \AA}$	$95^\circ \pm 1^\circ$

Table 5.3.: Values of unit cell variables describing the mixed ordered stripe structure of CuPc : PTCDA= 4 : 5 on Ag(110)

STM images and the values describing the whole structure are summarized in Tab. 5.3. The molecular arrangement corresponds to the following matrix:

$$M_{4,5} = \begin{pmatrix} 6.7 \pm 0.1 & 0 \\ -1 \pm 0.5 & 16.3 \pm 0.5 \end{pmatrix}. \quad (5.4)$$

Another remarkable feature of the STM images of the mixed stripe structure is that in most pictures the CuPc molecules C_2 and C_3 (for labeling see Fig. 5.13c) appear with two brighter and two darker molecular wings similar to what has been observed for the homo-molecular layer of CuPc on Ag(110). In the mixed structure it becomes clear

that the 2-fold symmetric contrast probably depends on the rotation of the molecule with respect to the substrate symmetry directions. The molecules C_2 and C_3 have their darker wings oriented with an acute angle to the more open Ag[001] direction, whereas the molecules C_1 and C_4 are rotated by $\approx 45^\circ$, all their benzene rings sense the same substrate directions, and they appear with the same brightness in STM. Furthermore, in some STM images recorded with weakly negative bias, e.g. in Fig. 5.18a,b, it can be observed that the CuPc molecules C_2 and C_3 , instead of showing brighter and darker wings, seem to appear as chiral structures with all wings at the same brightness. There are few reports about similar observations on metal phthalocyanine molecules exhibiting a chiral shape (cf. Fig. 5.18c,d) for certain measurement conditions in STM and corresponding DFT calculations [MLO⁺10, MRK⁺12]. For CuPc on the Ag(100) surface, it is reported that this chirality (in contrast to the structural chirality discussed earlier in this section) is a purely electronic effect originating from the interplay between the rotation of the molecule on the surface by $\approx 30^\circ$ and the charge transfer from the substrate into the molecule, mainly into the LUMO and partially into a singly occupied molecular orbital (SOMO) energetically located between HOMO and LUMO. The chiral contrast being strongest in images measured with negative bias (in [MLO⁺10] as well as here) supports the assumption that it stems from the frontier occupied orbitals.

For an additional structural analysis, we recorded the electron diffraction image of the stripe structure depicted in Fig. 5.19a. According to the structural properties found in STM, this experimental pattern with its broad features corresponds to the pattern described by the matrix $M_{4,5}$ in Eq. 5.4.

In Fig. 5.19b the experimental LEED image is fitted with a simulated pattern constructed of the values extracted from STM images. It is clear that the vector \vec{b}_1 in real space is parallel to the Ag[001] direction and the uncertainty of its length is rather small as the vertical dark lines in LEED are narrow and of precise periodicity. In contrast, the vector \vec{b}_2 cannot be determined more precisely, since the diffraction spots modulating the lines are rather broad and blurry due to the stochastic influence of the frequent alternation between the two domains R and L along the Ag[1 $\bar{1}$ 0] direction, and especially the first order spots are not observable. Similar as reported for PTCDA adsorbed onto the potassium-doped Ag(110) surface in [MBW⁺13], the stochastic distribution of the structural motifs causes the smearing of the diffraction spots along the direction that is less well defined.

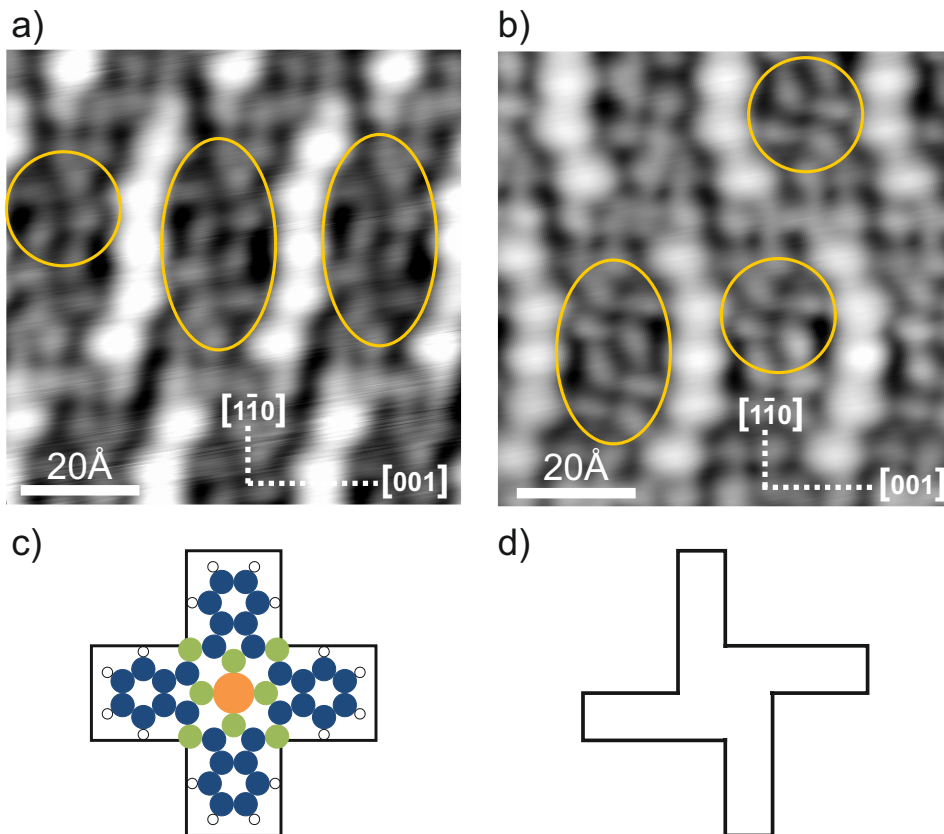


Figure 5.18.: In STM images recorded with small negative bias the CuPc molecules C_2 and C_3 , which are circled here, appear with a chiral contrast shape instead of exhibiting two brighter and two darker molecular wings as they do in STM images with positive bias (cf. Fig. 5.13 and 5.17), (a) $U_{\text{bias}} = -0.2 \text{ V}$, $I_{\text{setpoint}} = 1.0 \text{ nA}$, (b) $U_{\text{bias}} = -0.1 \text{ V}$, $I_{\text{setpoint}} = 0.85 \text{ nA}$. (c) Shape of an originally achiral CuPc molecule, (d) contour of the molecule appearing with electronically chiral contrast.

5.4.2. Electronic properties

For the analysis of the local electronic structure of the molecules involved in the stripe phase we apply differential conductance spectroscopy (STS) to resolve the ordering of the frontier orbitals, hoping to find results comparable to the electronic structure of mixed CuPc+PTCDA layers on Ag(111) [SLW⁺14]. Spectra are recorded between -0.9 V and 0.9 V above all nine molecules of the unit cell with up to 5 spectra per molecule: at

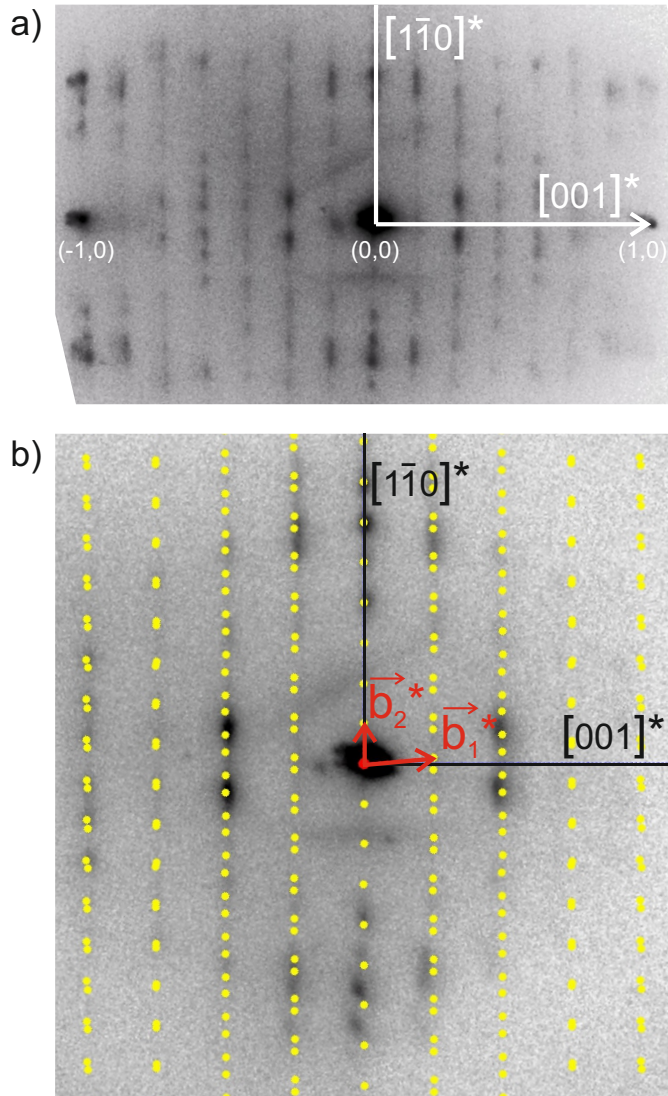


Figure 5.19.: (a) The experimental SPA-LEED image of the sample with the stripe structure is a pattern with stripes of modulated intensity, 50 eV. (b) The SPA-LEED image is superimposed with a pattern simulated corresponding to the unit cell values extracted from the above STM analysis, reciprocal vectors are labeled, 30 V.

5. Hetero-organic layers of CuPc and PTCDA on Ag(110)

the two long sides, the two short ends and the middle of PTCDA molecules, at all four benzene rings and the center of CuPc molecules, as marked in the zoom window of Fig. 5.20a. The spectra of PTCDA molecules do not show any differences neither between the various positions above one molecule nor between the five molecules in the unit cell. Therefore, in Fig. 5.20b the average of all PTCDA spectra is plotted as one (black) line. The spectra of CuPc molecules also do not show any differences between the four molecules in the unit cell and we will not distinguish them. But small differences can be found between spectra taken above the benzene rings appearing with brighter contrast in STM, those with darker contrast, and the center of the molecule. For this reason, the CuPc spectra are plotted separately in Fig. 5.20b.

From negative bias to positive bias, several features are found in all four spectra. The rising background intensity from -0.85 V towards more negative bias is probably due to the HOMOs of PTCDA and CuPc, which are expected to have binding energies larger than 1.0 eV, cf. Ch. 4 and [WSS⁺13]. The shoulder at -0.8 V or the peak at -0.6 V may be assigned to the PTCDA LUMO, which in the pure PTCDA brickwall phase has a binding energy of 0.75 eV [WSS⁺13]. The other one of these two features may originate from a tip state. At -0.23 V, all spectra feature a peak, also probably due to a tip state, which is followed by a second peak at -0.1 V only in the spectra of the CuPc wings with dark contrast and the CuPc center. The latter feature may originate from the CuPc LUMO_A, which is expected to be substantially less populated than the PTCDA LUMO or even depopulated (cf. [SLW⁺14]) and is distributed over two opposite benzene rings (cf. Ch.4). The peak at 0.1 V in all spectra may be a tip state similar to the feature at 0.6 V. At 0.2 V and 0.3 V small features can be observed for the CuPc center and the benzene rings where the intensity of the PTCDA spectrum is lower than that of the three CuPc spectra. Here might be the second part of the degenerate parts of the CuPc LUMO, the LUMO_B, provided that the degeneracy is still lifted in the mixed phase. Since there are no ARPES data for orbital tomography, we cannot make more precise statements about the assignment of peaks in the differential conductance spectra to certain molecular orbitals.

In a comparison of the energy levels in the stripe structure to the corresponding energy levels of the homo-molecular phases of PTCDA, arranged in the brickwall (BW) structure, and CuPc, see Fig. 5.21, it becomes clear that the trend observed for the windmill structure reported in Sec. 5.3.2 and for the mixed brickwall structure of CuPc

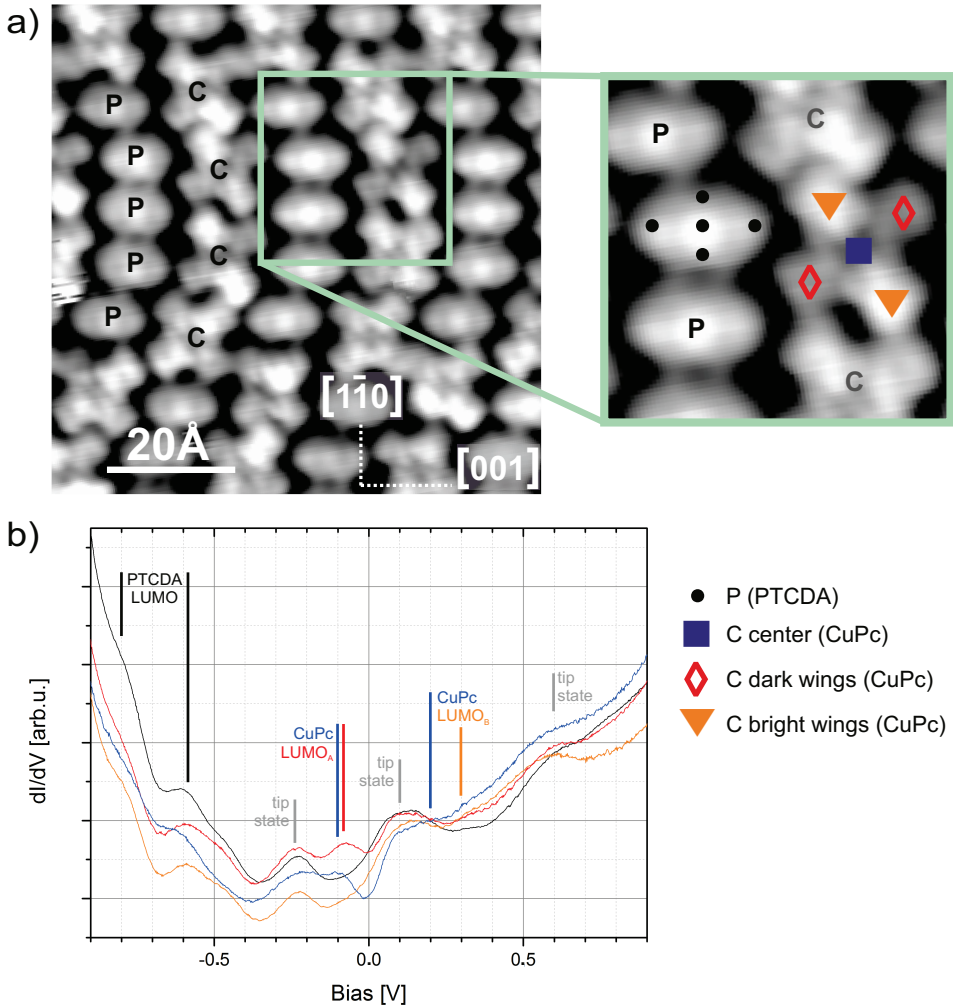


Figure 5.20.: (a) The molecules are labeled (P for PTCDA and C for CuPc) in an STM image and the zoom image gives the positions above the molecules where spectra are taken, $U_{\text{bias}}=0.400$ V, $I_{\text{setpoint}}=1.1$ nA. (b) The differential conductance spectra of all PTCDA molecules in the unit cell and of all positions above them are averaged since they did not exhibit noticeable differences. The spectra of all CuPc molecules in the unit cell also did not differ from each other but so do the spectra recorded at different positions above the CuPc molecules. Thus, spectra taken above dark molecular wings, bright wings, and the molecular center are plotted separately, $I_{\text{setpoint}}=2.1$ nA.

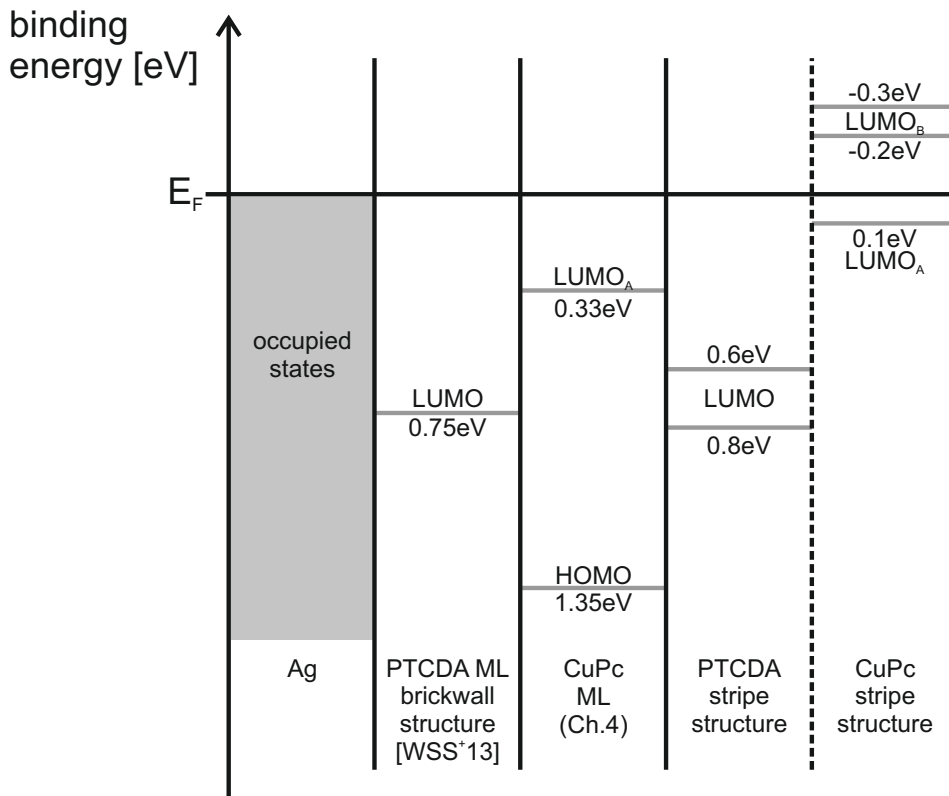


Figure 5.21.: The energy level rearrangement for the stripe structure compared to the energy level rearrangement of the homo-molecular PTCDA brickwall structure on Ag(110) (data taken from [WSS⁺13]) and the dense CuPc monolayer on Ag(110) (data from Ch. 4.)

and PTCDA on Ag(111) [SLW⁺14] is also weakly observable for the stripe structure on Ag(110). Assuming that the PTCDA LUMO in the stripe structure has a binding energy of 0.8 eV and that the feature at a binding energy of 0.6 eV originates from a tip state, which will not be considered further, the PTCDA LUMO is shifted to a slightly larger binding energy. Accordingly, the CuPc LUMO_A shifts from a binding energy of 0.33 eV in the homo-molecular phase to 0.1 eV in the stripe phase. The HOMOs of PTCDA and CuPc cannot be discussed here because the range where differential conductance spectra were measured is too narrow to include these orbitals.

5.5. Summary and Conclusion

In this chapter ordered mixed phases of CuPc and PTCDA molecules on the Ag(110) surface have been presented. Compared to mixed monolayers of these types of molecules on the Ag(111) surface [Sta13, SLW⁺14, SSB⁺14, SHS⁺15], the preparation of mixed ordered structures on the Ag(110) surface yields more complex structures due to the stronger interacting substrate with lower symmetry. We started the preparation of the mixed molecular layers with the deposition of CuPc followed by the deposition of PTCDA. No mixed ordered structure could be obtained for a coverage of less than one monolayer, i.e. when the surface is not completely covered with molecules. Nevertheless, mixed disorder seems to be more favorable than a separation of molecules into two homo-molecular phases and the formation of small basic structural units consisting of about two CuPc and two to three PTCDA molecules can be observed. When enough molecules are on the surface, it requires significantly higher annealing temperatures on Ag(110) than on Ag(111) to form mixed ordered structures and desorb molecules from higher layers.

The two mixed ordered structures here differ remarkably from those with two or three molecules per unit cell found on Ag(111). On Ag(110), we found mixed ordered structures with five and nine molecules per unit cell and corresponding molecular ratios of CuPc : PTCDA = 1 : 4 and 4 : 5, respectively. Hence, the unit cell areas are much larger, similar as observed for mixed ordered structure of CuPc and NTCDA (naphthalene tetracarboxylic dianhydride, C₁₄H₄O₆, similar to PTCDA but shorter carbon backbone) on Ag(111) [Sch15]. In the windmill structure (CuPc : PTCDA = 1 : 4), PTCDA molecules appear with two rotational orientations similar to the herringbone phase on Ag(110) [SPF98, WHS⁺12, WSS⁺13]. This way they form a ring around each CuPc molecule, which does not exhibit any noticeable intramolecular contrast or symmetry change, and create an overall chiral structure. The stripe structure (CuPc : PTCDA = 4 : 5) comprises meandering and bent stripes built of the basic structural unit and the corresponding mirror and rotational images. Here, all PTCDA molecules are oriented parallel to the Ag[001] direction, resembling the homo-molecular brickwall phase [SAL⁺97, BSG⁺98]. The rotation of two out of four CuPc molecules in a unit cell is such that a reduced 2-fold symmetry can be observed similar to what we reported earlier in this work for the homo-molecular phase on Ag(110) (cf. Ch. 4).

5. Hetero-organic layers of CuPc and PTCDA on Ag(110)

Interestingly, for both mixed ordered molecular layers in this chapter, structural chirality is found, even without consideration of the substrate and the orientation of the molecules, although neither CuPc nor PTCDA as single molecules are chiral. In the windmill structure, of which only one mirror domain is observed, the chirality obviously is created by the ring-like arrangement of the 2-fold symmetric PTCDA molecules around the 4-fold symmetric CuPc molecules. In the stripe structure, the basic structural unit is chiral and all rotation and mirror images are observed in STM. For the formation of the extended structure, the basic structural unit is combined with its rotation image creating one domain. The mirror image of the basic structural unit with its own rotation image forms the mirror domain. All domains extend parallel to the Ag[001] direction. The sequence of domains along the Ag[1 $\bar{1}$ 0] direction is arbitrary. The frequently occurring domain boundaries make this ordered structure a combination of periodicity – regarding the basic structural units and the extent of domains in the [001] direction – and stochastics – regarding the alternation of domains perpendicular to their lateral extent direction. In both mixed phases, windmill and stripe, the structural chirality emerges from the molecular arrangement. So, the combination of two different types of achiral molecules on the sample surface imprints this chirality to the jointly formed structures.

STS experiments helped to reveal the electronic structures close to the Fermi energy. The PTCDA LUMO, which in the mixed ordered structures of CuPc+PTCDA on the Ag(111) surface becomes stronger occupied by charge donation from CuPc molecules whose LUMO gets depopulated, could most probably be identified in the spectra. The CuPc LUMO_A and LUMO_B are difficult to assign, especially since we do not know if their degeneracy is lifted as it is the case in the homo-molecular phase. We can speculate that these two orbital parts, which are each distributed across two opposite benzene rings of the molecule, are occupied to different degrees and one is located very close to the Fermi edge, because there one can observe small deviations when comparing differential conductance spectra recorded above different wings of one CuPc molecule. The shift of all LUMO binding energies – to larger binding energies for PTCDA and to smaller or even negative binding energies for CuPc – suggests the same effect occurring in mixed structures on Ag(110) as on Ag(111). The stronger acceptor PTCDA attracts more charge than in its homo-molecular phases and the weak acceptor CuPc receives (almost) no charge anymore from the metal substrate.

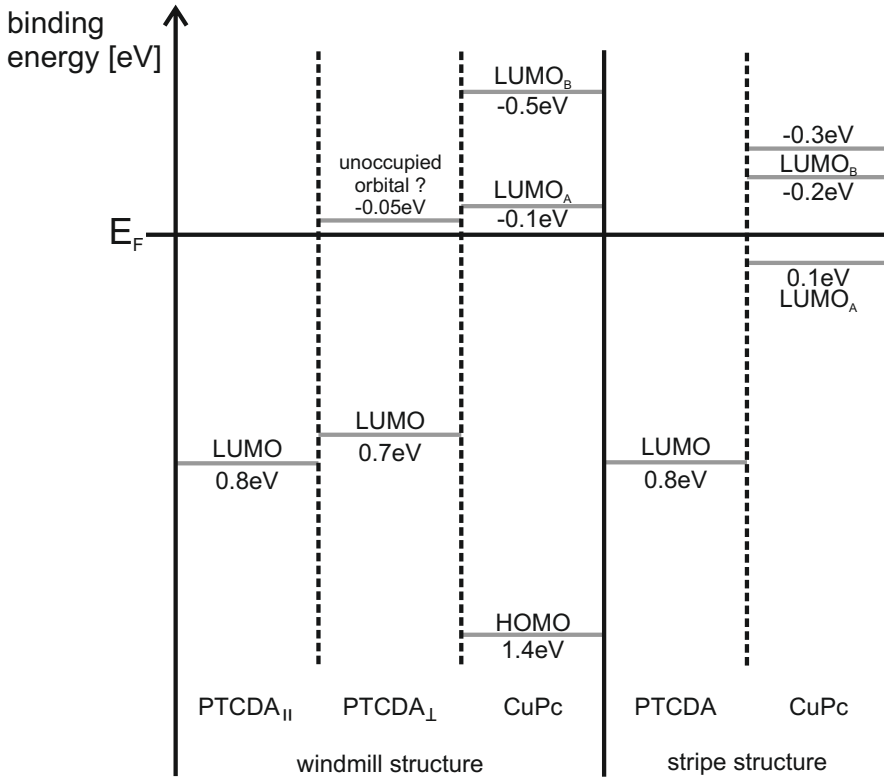


Figure 5.22.: Energy level rearrangements of the two mixed ordered structures investigated here, windmill structure and stripe structure.

Upon a close look at the energy level comparison diagram depicted in Fig.5.22, one can see, that the effect of charge reorganisation between the two types of molecules even seems to depend on the ratio of molecules in the mixed layers. In the windmill structure with one CuPc molecule competing with four PTCDA molecules for the charge transferred from the substrate into the molecular layer, the CuPc receives a very little amount so that its LUMO parts are both located on the side of negative binding energy. In contrast, the four CuPc molecules competing with 'only' five PTCDA molecules in the stripe phase still receive enough charge so that their LUMO_A is shifted across the Fermi edge to the side of positive binding energy. Here it would be interesting to experimentally investigate other molecular ratios and to simulate the charge reorganisation for different molecular ratios, similar as done for CuPc and PTCDA on Ag(111) [SLW⁺14].

6. Summary, Conclusion, and Outlook

In the work of this thesis, homo- and hetero-organic layers comprising the organic molecule CuPc have been investigated on two different silver crystal surfaces. Several sample systems have been developed and studied as variations of the well known system of one monolayer CuPc on Ag(111) by exchange and addition of components.

The first modification discussed in Ch. 3 was realized by depositing a second layer of CuPc on top of the first layer CuPc on Ag(111). Microscopy (STM) and diffraction (LEED) studies demonstrated that the lattice describing the lateral molecular structure of the second layer is the same as for the first layer. While the molecules in the first layer adsorb in a flat geometry on the silver substrate, molecules in the second layer are inclined. The interaction of the first layer with the substrate is much stronger and happens via bonds of the delocalized π -electron system of the molecules to the metal. Molecules in the second layer only sense a weak interaction with the underlying layer and, hence, can take a different configuration. The lateral arrangement of molecules in the first layer still acts as a template for the second layer molecular lattice. The interaction of molecules in the first layer with the Ag(111) substrate is accompanied by a charge transfer from the metal into the molecules filling the former LUMO to a certain degree. This charging of the molecules also causes the intermolecular repulsion observable at low coverage. Molecules in the second layer do probably not receive any charge, which is in agreement with the immediate formation of islands during the growth of the second layer. Our findings about the structural and electronic properties are in agreement with data published before [HHP⁺09, KSS⁺10].

In a second variation step (Ch. 4), the Ag(111) substrate was exchanged by Ag(110), offering stronger interaction of the substrate with adsorbed molecules. In contrast to CuPc on Ag(111) where the densest structure of one monolayer is of point-on-line co-

6. Summary, Conclusion, and Outlook

incidence, the Ag(110) surface dominates the lateral molecular arrangement driving molecules into a coincident structure that becomes commensurate in higher (fourth) order. On the other hand, the intermolecular interaction dominates the lateral arrangement from time to time forming a slightly deviating structure, not admitting the commensurate registry. This interplay of interactions causes the appearance of dislocation lines in the molecular lattice, which are observable in both STM and LEED. Regarding the electronic properties, we applied differential conductance spectroscopy (STS) and angle-resolved PES finding charge transfer from the substrate into the molecule. Here and in combination with a slight downwards bending of two opposite benzene rings that are arranged with a more acute angle to the more open [001] substrate direction, the degeneracy of the two LUMO parts, LUMO_A and LUMO_B, is most probably lifted by filling the orbital part distributed above the pair of opposite benzene rings that interacts stronger with the substrate than the perpendicular pair of benzene rings. The asymmetric charge distribution and the distorted geometry lead to a 2-fold symmetric contrast of the originally 4-fold symmetric molecules in STM.

Comparing homo-organic layers of CuPc on Ag(111) and on Ag(110), we observed the expected increasing influence of the (110) substrate on the layer formation and electronic level alignment at the interfaces, similar to reports about PTCDA on different silver surfaces [TES⁺02, WLS⁺15].

The third part in Ch. 5 dealt with hetero-organic layers. CuPc and PTCDA were found to form mixed ordered structures on Ag(110) characterized by STM and LEED, although mixing on this low-symmetry and reactive substrate shows a higher degree of complexity than mixing on the less reactive Ag(111) substrate [Sta13, SHS⁺15]. Even for a lower coverage when the surface is not completely covered, the mixing in disorder seems to be preferred to a phase separation. The unit cells of the two mixed structure on Ag(110) are remarkably larger than those on Ag(111) and contain more molecules, from this aspect rather resembling the structures that have been found for CuPc and NTCDA on Ag(111) [Sch15]. The windmill structure consists of unit cells with one CuPc and four PTCDA molecules, the unit cell of the stripe structure consists of four CuPc and five PTCDA molecules. Measurements on the local electronic structure of the two mixed phases were dominated by signals assigned to PTCDA molecules. The PTCDA LUMO is most probably filled by charge obtained from the metal substrate. The CuPc molecular orbitals hardly yield any signal so that we cannot say with absolute certainty

whether the CuPc LUMO is filled or not and if the degeneracy of LUMO_A and LUMO_B is lifted or not. The 2-fold symmetric contrast in STM of certain CuPc molecules in the stripe structure suggests a similar asymmetry due to electronic and geometric effects as observed for the homo-molecular phase of CuPc on Ag(110). The same molecules appear with a chiral electronic contrast in STM images recorded with a different bias voltage, which also stems from the asymmetry of the 4-fold symmetric molecule adsorbed onto a 2-fold symmetric substrate with a certain rotational direction.

In general, compared to Ag(111), the stronger interaction with adsorbed molecules and the lower symmetry of the Ag(110) surface strongly affect the lateral molecular arrangement of homo- as well as hetero-organic layers giving rise to considerably different structures. Especially upon the formation of laterally mixed ordered hetero-organic layers on Ag(110) the emergence of structural chirality is observed by the combination of the two achiral molecular types CuPc and PTCDA.

Some additional aspects about one monolayer of CuPc on Ag(110), e.g. the adsorption height and the growth of the monolayer, could be investigated, for example by x-ray standing wave (XSW) experiments and low energy electron microscopy (LEEM). Since many features of this structure are revealed, it would also be interesting to investigate multilayers of CuPc on Ag(110) similar to the experiments performed on Ag(111) in order to find out the influence of the substrate on the second layer and the interaction between the first layer and higher layers. Regarding the hetero-organic systems, adsorption height measurements by XSW and pair-potential calculations could help to clarify the mechanism driving the lateral ordering of the two types of molecules and the emergence of the structural chirality. Together with photoemission spectroscopy and orbital tomography, these methods can give a comprehensive image of the structural and electronic properties and the coupling of geometric and electronic effects as described for, e.g., CuPc and PTCDA on Ag(111) [SLW⁺14, SSB⁺14]. A further aspect is to find out if there exist stable mixed structures containing more CuPc than PTCDA molecules in the unit cell on the Ag(110) surface and if mixing is possible for a variation of the preparation steps when first PTCDA and then CuPc is deposited. The crucial point will probably be the question if by annealing enough energy can be added to enable diffusion before the molecules start to desorb thermally from the surface. Finally, experiments on a stacked hetero-organic system of CuPc on PTCDA on Ag(110) would be interesting to examine regarding the properties of a large area of an organic-organic interface. A system with

6. Summary, Conclusion, and Outlook

PTCDA deposited onto CuPc on Ag(110) will most probably not form stable stacked layers, similar as reported for this stacking series on Ag(111) [Sta13, SGP⁺14], since during the preparation of laterally mixed structure we observed in STM that PTCDA molecules do not stay in the second layer when the first layer is completely filled with CuPc and PTCDA molecules. PTCDA molecules drive CuPc molecules out of the first layer as the interaction of PTCDA with the silver substrate is considerably stronger and preferred.

List of Figures

2.1. (a) Model of a silver crystal showing a face centered cubic (fcc) lattice with a lattice constant of 4.09 Å. The blue and yellow lines mark the (111) and (110) plane. (b) The Ag(111) surface is 3-fold rotational symmetric and the atoms form a hexagonal surface lattice (c) The Ag(110) surface is 2-fold rotational symmetric with a rectangular surface lattice. The uppermost layer of molecules is given in bright gray and the next underlying layer in dark gray.	6
2.2. (a,b) CuPc is a geometrically 4-fold symmetric macrocyclic molecule. The distributions of the electron wave functions of the (c) HOMO and (d) LUMO across a CuPc molecule were calculated by Gaussian [FTS+04].	7
2.3. PTCDA is a geometrically 2-fold symmetric aromatic molecule with negative partial charge located at the oxygen atoms and positive partial charge at the hydrogen atoms. The delocalized π -electron system is distributed over the carbon backbone (perylene core).	9
2.4. In quantum mechanics, a particle, e.g. an electron, with an energy E that is smaller than the height ϕ of a potential barrier of width z between two electrodes can tunnel from one electrode through this barrier into a state of equal energy in the other electrode. Inside the barrier, the particle wave function is exponentially damped.	11
2.5. For STM, a voltage U_{bias} is applied to the sample to be investigated shifting the level of occupied states relatively to the level of the Fermi energy E_{F} . (a) A negative bias voltage raises the sample Fermi level and electrons can tunnel from occupied sample states through the vacuum barrier into the tip. (b) A positive bias voltage lowers the Fermi level in the sample and electrons from the tip can tunnel into unoccupied sample states. . . .	12

- 2.6. In STM measurements a sharp metallic tip is scanned laterally over the (semi)conducting sample surface controlled by piezo elements for the x - and y -direction. The tunneling current is set to be constant. Thus, the distance z between tip and sample is permanently controlled and corrected by a feedback loop and a piezo element adjusting the tip height. The height signal is recorded and processed yielding an image of the sample surface. 13

- 2.7. Constant current mode in STM: The distance z between tip and sample is constant for one material work function ϕ_1 , also across a step of the surface. z changes with changing ϕ adjusting the tip height so that the current between tip and sample is constant. An image of a constant electron LDOS right above the sample surface is obtained by this method. 14

- 2.8. In the Tersoff-Hamann model the tip is assumed to be spherical and represented by an s-wave function. The center of the tip is located at \vec{r}_t and its radius is R . The distance between the tip and the sample is z 16

- 2.9. Setup of a very compact, rigid, easily operable, and thermally stable STM unit: The sample is placed in the middle of three piezo tubes that carry the ramp plate on small insulating spheres. A fourth piezo tube with the probing tip is attached to the center of the ramp plate. Each piezo tube has four contacted segments at its outside for any movements in the x - y -plane parallel to the sample surface. Contacts at the top and at the bottom allow motion along the z -direction. 18

- 2.10. The complete experimental setup comprises the STM unit in a separate vacuum chamber attached to a cryostat system and the preparation chamber with additional elements for sample preparation and investigation. Springs and an eddy current damping system isolate the STM unit from mechanical vibrations. For further explanations on the preparation chamber see Sec. 2.4. 19

- 2.11. In a conventional low-energy electron diffraction experimental setup, electrons hit the crystalline sample surface at normal incidence. The interference pattern of the scattered electrons is detected with angular resolution on a fluorescent screen. 20

- 2.12. The Ewald construction illustrates the creation of an electron diffraction pattern. (a) In a conventional LEED setup the incoming electrons with a wave vector \vec{k}_0 hit the sample at normal incidence and are scattered into the direction of \vec{k}' . Diffraction spots can be observed where the Ewald sphere intersects the reciprocal lattice rods. (b) In a SPA-LEED setup the angle between incident and scattered electrons is fixed and does not change, but the angle of incidence, i.e. the direction of \vec{k}_0 is rotated for a complete scan of the reciprocal space, together with the direction of \vec{k}' 21
- 2.13. In a SPA-LEED the electron detector is mounted at a certain position with a fixed angle relatively to the electron gun. The octopole plates control and vary the path of incident and scattered electrons, thus, scanning the reciprocal space to obtain a 2-dimensional diffraction image. Figure taken from [ZH02]. 22
- 2.14. (a) In an STS measurement the bias voltage is ramped, e.g. from 0 V towards negative U_{bias} . (b) The tunneling current I_{setpoint} increases when going through a resonance. The increase of the current is observable as a peak in the differential conductance $dI_{\text{setpoint}}/dU_{\text{bias}}$, which is directly proportional to the sample LDOS. 24
- 2.15. Photoelectron spectroscopy is based on the photo effect where photons release electrons from a sample. The kinetic energy of the emitted electrons is measured and the binding energy of the state they come from can be calculated as the difference between the photon energy $\hbar\omega$, the work function ϕ_a of the analyzer, and the kinetic energy E_{kin} of the electrons. 26
- 2.16. In angle-resolved photoelectron spectroscopy not only the energy but also the emission angle φ is detected. By a rotation of the sample around the azimuthal angle θ , the full hemisphere above the sample can be imaged. 27
- 3.1. (a) The SPA-LEED image of one monolayer CuPc on Ag(111) shows the experimentally obtained pattern superimposed by a pattern simulated according to the matrix describing the superstructure. The vectors \vec{b}_1^* and \vec{b}_2^* mark the unit cell in reciprocal space. The image is adapted from [KSS⁺10], the abscissa is given in percentage of the Ag(111) Brillouin zone, the matrix relates to the substrate vectors \vec{a}_1 (parallel to $[\bar{1}10]$) and \vec{a}_2 (parallel to $[0\bar{1}1]$) with an angle of 120° between them. (b) STM image of the first layer CuPc on Ag(111) with the unit cell vectors \vec{b}_1 and \vec{b}_2 marked, $U_{\text{bias}} = -1.250$ V, $I_{\text{setpoint}} = 23$ pA. 32

- 3.2. (a) As long as the coverage is in the submonolayer regime, CuPc molecules distribute in a dilute phase all over the surface, $U_{\text{bias}} = -0.200 \text{ V}$, $I_{\text{setpoint}} = 26 \text{ pA}$.
 (b) Flat lying molecules are ordered in the densest possible structure in the first layer. Molecules in the second layer are tilted and form islands even if the second layer is not completed, $U_{\text{bias}} = -1.250 \text{ V}$, $I_{\text{setpoint}} = 59 \text{ pA}$.
 (c) In the zoom image of few molecules in the second layer one can estimate the direction of inclination, $U_{\text{bias}} = -1.250 \text{ V}$, $I_{\text{setpoint}} = 59 \text{ pA}$ 33
- 3.3. Line profiles of STM images (obtained in WSXM [HFGR⁺07]): A sample area with a line is given in the upper row, the corresponding profile is depicted below (from the left end to the right end of the line in the image above). The height (ordinate of profile graph) is not calibrated. (a,b) The roughness of the first layer is that of flat lying molecules, $U_{\text{bias}} = -1.250 \text{ V}$, $I_{\text{setpoint}} = 23 \text{ pA}$. (c,d) The roughness of the second layer shows the inclination of the molecules, $U_{\text{bias}} = -1.250 \text{ V}$, $I_{\text{setpoint}} = 59 \text{ pA}$ 35
- 3.4. Line profiles of STM images (obtained in WSXM [HFGR⁺07]): A sample area with a line is given in the upper row, the corresponding profile is depicted below (from the left end to right end of the line in the image above). The height (ordinate of profile graph) is not calibrated. (a,b) A height profile across a Ag(111) step is shown, i.e. from the second layer with inclined molecules on the lower terrace to the first layer with flat lying molecules on the upper terrace across upright standing molecules at the step edge, $U_{\text{bias}} = -1.250 \text{ V}$, $I_{\text{setpoint}} = 240 \text{ pA}$. (c,d) A height profile across a step from the second layer with inclined molecules to the first layer with flat lying molecules on the same terrace is depicted, $U_{\text{bias}} = -1.250 \text{ V}$, $I_{\text{setpoint}} = 59 \text{ pA}$ 36
- 3.5. STM images of the flat lying molecules in the first and inclined molecules in the second layer on two adjacent terraces, $U_{\text{bias}} = -1.250 \text{ V}$, $I_{\text{setpoint}} = 59 \text{ pA}$.
 (a) The unit cells are the same for the first and the second layer. The pair of vectors (\vec{b}_1, \vec{b}_2) can be shifted laterally and does describe both appearing structures. (b) The adsorption site of the second layer on top of the first layer can be determined by an additional grid. The nodes coincide with the centers of the molecules in the first layer and with the uppermost benzene ring of the molecules in the second layer. 37

- 3.6. LEED images of 1.3 ML CuPc on Ag(110), i.e. the first and the second layer, show 3-fold symmetric diffraction patterns. The experimentally obtained patterns are superimposed with the pattern simulated by Spot-Plotter [Bay08] according to the values describing the molecular lattice of the first layer of adsorbed molecules. (a) Image recorded with a conventional LEED, 12.4 eV. (b) Image recorded with an MCP-LEED, 45 eV. Obviously, the second layer structure can be described by the same values as the first layer structure. 38
- 3.7. (a) Differential conductance spectra of flat lying CuPc molecules in the first layer on Ag(111) feature many resonances, of which several might occur due to tip states. The HOMO can be observed at -1.4 V. The LUMO is expected at approximately -0.15 V and probably disappears in the strong resonance at -0.5 V; $I_{\text{setpoint}}=550$ pA (b) In an STM image of one CuPc molecule the positions are marked where spectra are recorded, $U_{\text{bias}}=-1.250$ V, $I_{\text{setpoint}}=59$ pA. (c) In the difference of the spectrum taken above the molecular center and the spectra taken above the benzene rings the individual contributions can be discriminated more easily. (d) The UPS data of 0.9 ML CuPc on Ag(111) are depicted for comparison with the STS data, figure taken from [KSS⁺10]. 39
- 3.8. Real space distributions of the frontier CuPc orbitals which yield resonances in the differential conductance spectra. 40
- 3.9. (a) Differential conductance spectra of inclined CuPc molecules in the second layer on Ag(111) exhibit many features that partly occur due to tip states, $I_{\text{setpoint}}=59$ pA. The HOMO at -1.7 V is shifted to a larger binding energy compared to spectra of first layer molecules (Fig. 3.7). The LUMO is probably not occupied and may cause the resonances at 0.1 V and 0.3 V taking the degeneracy of LUMO_A and LUMO_B of an isolated molecule into account. (b) The positions where spectra are recorded are marked in STM images, $U_{\text{bias}}=-1.250$ V, $I_{\text{setpoint}}=59$ pA. 41
- 3.10. The energy level rearrangement for the first and second layer of CuPc on Ag(111) found in this work is compared to literature [KSS⁺10]. 44

4.1. STM images of CuPc on Ag(110) at different coverage. (a) At a low coverage of less than one monolayer the molecules distribute in a dilute phase all over the surface. When the coverage is high enough for the molecules to touch, they start to form chains and clusters as marked in the image by a box and an ellipse, $U_{\text{bias}}=0.4\text{ V}$, $I_{\text{setpoint}}=0.75\text{ nA}$. (b) At one monolayer coverage the molecules form an extended ordered structure covering the whole surface, $U_{\text{bias}}=0.6\text{ V}$, $I_{\text{setpoint}}=1.1\text{ nA}$. No clean substrate is visible.	48
4.2. STM image showing the densest structure of one monolayer CuPc on Ag(110), $U_{\text{bias}}=-0.2\text{ V}$, $I_{\text{setpoint}}=30\text{ pA}$. Dislocation lines of the molecular lattice are marked with dashed lines. The unit cell, consisting of \vec{b}_1 and \vec{b}_2 , and the second pair of vectors describing structure with dislocation lines, consisting of \vec{b}_d and \vec{b}_2 , are marked by arrows.	49
4.3. Experimental SPA-LEED image, $E_{\text{kin}}=30\text{ eV}$, with simulated LEED patterns for both sets of vectors (\vec{b}_1 , \vec{b}_2 as small spots and \vec{b}_d , \vec{b}_2 as large rings) showing complete reconstruction.	51
4.4. Model of the unit cell of extended ordered domains of CuPc on Ag(110) described by (\vec{b}_1 , \vec{b}_2) and the second pair of vectors (\vec{b}_d , \vec{b}_2) describing the molecular arrangement at a dislocation line.	52
4.5. Pair potential calculation for CuPc molecules, modified from [KSW ⁺ 11]. The green arrows labeled \vec{b}_1 , \vec{b}_2 , and \vec{b}_d mark the positions of the neighboring molecules in the CuPc monolayer on Ag(110). \vec{b}_2 and \vec{b}_d clearly point towards favorable positions close to energy minima whereas \vec{b}_1 points towards an unfavored position that the molecules are forced to take by interaction with the substrate.	54
4.6. Ag(110) surface lattice (gray) and CuPc lattice (green) with dislocation lines (yellow) depicting how the dislocation lines interrupt the coincident lattice so that commensurism in 4th order is not established.	56
4.7. top: model of the monolayer CuPc on Ag(110) without (black) and with (colored) dislocation lines; bottom: zoom of shift between the structure forced by the molecule-substrate interaction and the structure favored by molecule-molecule interaction	57
4.8. STM images of CuPc on Ag(110) recorded in constant height mode. (a) $U_{\text{bias}}=0.05\text{ V}$, $I_{\text{setpoint}}=0.75\text{ nA}$, (b) $U_{\text{bias}}=-0.05\text{ V}$, $I_{\text{setpoint}}=0.75\text{ nA}$	59

- 4.9. STM images of CuPc on Ag(110) recorded at different bias voltages: (a) $U_{\text{bias}}=0.342\text{ V}$, $I_{\text{setpoint}}=0.5\text{ nA}$, (b) $U_{\text{bias}}=-0.300\text{ V}$, $I_{\text{setpoint}}=0.5\text{ nA}$. A strong contrast difference between the pairs of opposite benzene rings can be observed for positive bias (a). For negative bias (b), the contrast difference is less and v-shaped split wings can be observed. 60
- 4.10. Scanning tunneling spectra, (a) $I_{\text{setpoint}}=1.2\text{ nA}$, (b) $I_{\text{setpoint}}=1.0\text{ nA}$; the resonance at -0.33 V corresponds to an occupied state, namely, of the former LUMO the part LUMO_A , which is filled and shifted to a binding energy of 0.33 eV ; (c) STM image ($U_{\text{bias}}=1.407\text{ V}$, $I_{\text{setpoint}}=1.2\text{ nA}$) and model of a CuPc molecule with positions marked where corresponding spectra are recorded: \blacklozenge at dark molecular wings, $*$ at bright wings, ∇ at the center of the molecule. 61
- 4.11. Energy distribution curves along certain silver crystal directions recorded at BESSY II (black and red) and angle-integrated photoemission intensity recorded at Elettra (blue), showing two occupied orbitals at binding energies of 0.3 eV and 1.35 eV 63
- 4.12. (a,b) Momentum space images recorded with PEEM at Elettra showing the fingerprints of the occupied states at 1.35 eV and 0.3 eV . (c,d) Gray curves: intensity profiles along the white ring marked in the momentum space images, integrated over the width of the ring. Black curves: corrected profiles accounting for the intensity modulation along k_y due to the asymmetry between forward and backward photoemission. 64
- 4.13. k-space imaging results: HOMO (a,d,g,j), LUMO_A (b,e,h,k), $\text{LUMO}_A+\text{LUMO}_B$ (c,f,i,l) of CuPc; (a)-(c) orbitals in real space; (d)-(f) corresponding reciprocal space images obtained by Fourier transform of the images above; (g)-(i) real space images of molecular orbitals rotated on the surface including the mirror domain; (j)-(l) corresponding reciprocal space images of the rotated molecules; (m)-(n) experimental reciprocal space patterns. The comparison reveals that the orbital detected at 1.35 eV is the HOMO and the orbital found at 0.3 eV better resembles the 2-fold symmetric LUMO_A simulation pattern than the 4-fold symmetric $\text{LUMO}_A+\text{LUMO}_B$ simulation pattern. 65

4.14. Model of one CuPc molecule in the dense layer on Ag(110): the pair of benzene rings with the more acute angle to the more open Ag[001] direction interacts stronger with the substrate than the perpendicular pair of benzene rings, is slightly bent down towards the substrate, receives the charge donated by the silver, and, due to these related effects, appears with darker contrast in STM.	68
5.1. In the low coverage regime, the darker, cross shaped CuPc molecules and the brighter, oval PTCDA molecules form a mixed but disordered phase on the Ag(110) surface, $U_{\text{bias}}=0.126\text{ V}$, $I_{\text{setpoint}}=0.35\text{ nA}$	75
5.2. The comparison of laterally mixed ordered structures of CuPc and PTCDA on Ag(111) (green) and on Ag(110) (red) reveals a tendency to form larger unit cells with more molecules on Ag(110).	75
5.3. The whole surface is covered with CuPc molecules (approximately 20%) and PTCDA molecules (approximately 80%). Three different structures can be observed: the ordered mixed windmill structure (left hand side and center), the ordered PTCDA herringbone structure (right hand side), and a disordered mixed phase (top), $U_{\text{bias}}=0.852\text{ V}$, $I_{\text{setpoint}}=0.62\text{ nA}$	77
5.4. STM image of the windmill structure: PTCDA molecules are oriented in two different rotational directions (0° and 93° w.r.t Ag[001]) and form rings around the CuPc molecules. CuPc molecules are rotated by 22° w.r.t Ag[001]. The unit cell containing one CuPc and four PTCDA molecules is marked with the pair of red vectors (\vec{b}_1 , \vec{b}_2); $U_{\text{bias}}=0.565\text{ V}$, $I_{\text{setpoint}}=1.2\text{ nA}$	78
5.5. Two rotational domains A and B, rotated by 180° , are not distinguishable from each other and are observed as one domain. Their mirror domains A', B' (mirror axis: $[1\bar{1}0]$ direction), A'', and B'' (mirror axis: $[001]$ direction) also cannot be distinguished from each other forming the expected second domain that is not observed.	79
5.6. (a) Experimental SPA-LEED image of the sample with patches of the windmill structure and with patches of the PTCDA herringbone structure on Ag(110), 30 eV. (b) Experimental MCP-LEED image of the pure PTCDA herringbone structure on Ag(110), 19 eV.	80

- 5.7. (a,b) STM images and (c,d) their appropriate calculated 2-dimensional Fourier transform, which corresponds to the diffraction image of the displayed molecular structure. (a) $U_{\text{bias}}=0.814\text{ V}$, $I_{\text{setpoint}}=0.6\text{ nA}$, (b) $U_{\text{bias}}=2.121\text{ V}$, $I_{\text{setpoint}}=1.2\text{ nA}$. (e,f) The simulated diffraction patterns are constructed with values extracted from the analysis of STM images, reciprocal unit cell vectors are marked $(\vec{b}_1^*, \vec{b}_2^*)$, (e) diffraction pattern of the one domain observed in STM, (f) diffraction pattern of the observed domain (red spots) and its mirror domain (dark spots). 81
- 5.8. The experimental SPA-LEED image (30 eV) is superimposed with simulated LEED patterns. The corresponding reciprocal unit cell vectors are marked $(\vec{b}_1^*, \vec{b}_2^*)$. (a) Simulation of the PTCDA HB pattern, (b) simulation of the windmill pattern (two domains), (c) both simulations superimposed. The circled area marks a weak diffraction spot contributed by the windmill structure. 82
- 5.9. (a) The differential conductance spectra of the two different PTCDA molecules (P_{\parallel} and P_{\perp}) and the CuPc molecule (C) in the unit cell exhibit flat curves with few features, $I_{\text{setpoint}}=1.0\text{ nA}$; (b,c,d) zoom images of spectra depicting small differences between the spectra of the different molecules. (e) STM image: The molecules are labeled for distinction of the spectra, $U_{\text{bias}}=0.565\text{ V}$, $I_{\text{setpoint}}=1.2\text{ nA}$ 84
- 5.10. The graphs showing spectra from Fig. 5.9a subtracted from each other enhance the visibility of individual (marked) features. (a) P_{\perp} -C, (b) P_{\parallel} -C, (c) P_{\parallel} - P_{\perp} 86
- 5.11. The energy level rearrangement for the windmill structure compared to the energy level rearrangement of the homo-molecular PTCDA herringbone structure on Ag(110) (data taken from [WSS+13]) and the dense CuPc monolayer on Ag(110) (data from Ch. 4.) 87
- 5.12. The whole surface is covered with CuPc molecules ($\approx 50\%$) and PTCDA molecules ($\approx 50\%$). Large islands of an ordered mixed structure (top and bottom) can be observed between areas of mixed molecules in disorder, $U_{\text{bias}}=0.565\text{ V}$, $I_{\text{setpoint}}=64\text{ pA}$ 88

- 5.13. (a) In STM images, stripes of two different molecular arrangements with each five PTCDA and four CuPc molecules are observed: the meandering ‘S’ and the bent ‘C’ configuration, $U_{\text{bias}}=0.493\text{ V}$, $I_{\text{setpoint}}=2.1\text{ nA}$. (b) The chains of four CuPc molecules exceed the chains of five PTCDA molecules in length along the $\text{Ag}[1\bar{1}0]$ direction, forming separating space of darker contrast between the PTCDA chains, which appear with brighter contrast, $U_{\text{bias}}=0.358\text{ V}$, $I_{\text{setpoint}}=1.0\text{ nA}$. (c) All PTCDA molecules lie parallel to the $\text{Ag}[001]$ direction while the CuPc molecules show two different rotational orientations; molecules are labeled for distinction of the nine molecules (P_1 to P_5 for the PTCDA molecules and C_1 to C_4 for the CuPc molecules), $U_{\text{bias}}=0.400\text{ V}$, $I_{\text{setpoint}}=1.1\text{ nA}$ 89
- 5.14. The basic structural unit is chiral and appears with all four rotation and mirror images. r can only be transformed into l by a mirror operation, r' and l' are achieved by application of a rotation by 180° 90
- 5.15. The chiral basic structural units are combined with each other to form the extended stripe structure observed in STM. (a) $U_{\text{bias}}=0.493\text{ V}$, $I_{\text{setpoint}}=2.1\text{ nA}$, (b) $U_{\text{bias}}=0.619\text{ V}$, $I_{\text{setpoint}}=1.1\text{ nA}$. The transition between two units next to each other along the $\text{Ag}[1\bar{1}0]$ direction is fixed at the position between two molecular chains, here marked with dashed lines. The transition is arbitrary at the position in the middle of a molecular chain, here marked with solid lines. The two adjacent small units at a fixed transition are combined forming the large units R and L, respectively. 91
- 5.16. Even in the mixed disordered phase of (a) the sample hosting the stripe structure, $U_{\text{bias}}=0.565\text{ V}$, $I_{\text{setpoint}}=64\text{ pA}$, and (b) the sample hosting the windmill structure (cf. Fig. 5.3), $U_{\text{bias}}=0.852\text{ V}$, $I_{\text{setpoint}}=620\text{ pA}$, some basic structural units (r , l , r' , l') can be found (circled). 93
- 5.17. The unit cell is marked with a pair of vectors (\vec{b}_1 , \vec{b}_2) going from the middle of one molecular chain to the next chain, $U_{\text{bias}}=0.493\text{ V}$, $I_{\text{setpoint}}=2.1\text{ nA}$. 94
- 5.18. In STM images recorded with small negative bias the CuPc molecules C_2 and C_3 , which are circled here, appear with a chiral contrast shape instead of exhibiting two brighter and two darker molecular wings as they do in STM images with positive bias (cf. Fig. 5.13 and 5.17), (a) $U_{\text{bias}}=-0.2\text{ V}$, $I_{\text{setpoint}}=1.0\text{ nA}$, (b) $U_{\text{bias}}=-0.1\text{ V}$, $I_{\text{setpoint}}=0.85\text{ nA}$. (c) Shape of an originally achiral CuPc molecule, (d) contour of the molecule appearing with electronically chiral contrast. 96

5.19. (a) The experimental SPA-LEED image of the sample with the stripe structure is a pattern with stripes of modulated intensity, 50 eV. (b) The SPA-LEED image is superimposed with a pattern simulated corresponding to the unit cell values extracted from the above STM analysis, reciprocal vectors are labeled, 30 V.	97
5.20. (a) The molecules are labeled (P for PTCDA and C for CuPc) in an STM image and the zoom image gives the positions above the molecules where spectra are taken, $U_{\text{bias}}=0.400$ V, $I_{\text{setpoint}}=1.1$ nA. (b) The differential conductance spectra of all PTCDA molecules in the unit cell and of all positions above them are averaged since they did not exhibit noticeable differences. The spectra of all CuPc molecules in the unit cell also did not differ from each other but so do the spectra recorded at different positions above the CuPc molecules. Thus, spectra taken above dark molecular wings, bright wings, and the molecular center are plotted separately, $I_{\text{setpoint}}=2.1$ nA.	99
5.21. The energy level rearrangement for the stripe structure compared to the energy level rearrangement of the homo-molecular PTCDA brickwall structure on Ag(110) (data taken from [WSS ⁺ 13]) and the dense CuPc monolayer on Ag(110) (data from Ch. 4.)	100
5.22. Energy level rearrangements of the two mixed ordered structures investigated here, windmill structure and stripe structure.	103

List of Tables

4.1. Values describing the molecular structure of a closed monolayer CuPc on Ag(110)	52
5.1. Values from STM describing the windmill structure of CuPc and PTCDA on Ag(110)	77
5.2. Values from FFT (of STM images) describing the windmill structure of CuPc and PTCDA on Ag(110)	82
5.3. Values of unit cell variables describing the mixed ordered stripe structure of CuPc : PTCDA= 4 : 5 on Ag(110)	94

Bibliography

- [AGTA09] AMSALEM, P. ; GIOVANELLI, L. ; THEMLIN, J. M. ; ANGOT, T.: Electronic and vibrational properties at the ZnPc/Ag(110) interface. In: *Phys. Rev. B* 79 (2009), Jun, 235426. <http://dx.doi.org/10.1103/PhysRevB.79.235426>. – DOI 10.1103/PhysRevB.79.235426
- [ATG91] ANTOHE, S. ; TOMOZEIU, N. ; GOGONEA, S.: Properties of the Organic-Inorganic Semiconductor Barrier Contact Diodes In/PTCDI/p-Si and Ag/CuPc/p-Si. In: *physica status solidi (a)* 125 (1991), Nr. 1, 397-408. <http://dx.doi.org/10.1002/pssa.2211250138>. – DOI 10.1002/pssa.2211250138. – ISSN 1521-396X
- [Bar61] BARDEEN, J.: Tunnelling from a Many-Particle Point of View. In: *Phys. Rev. Lett.* 6 (1961), Jan, 57-59. <http://dx.doi.org/10.1103/PhysRevLett.6.57>. – DOI 10.1103/PhysRevLett.6.57
- [Bay08] BAYERSDORFER, Patrick: *SPA-LEED-Studie zur Adsorption von metallfreien Phthalocyaninen auf Ag(111) Bereich kleiner Bedeckungen*, Universität Würzburg, Diplomarbeit, 2008
- [BBR83] BARATOFF, A. ; BINNIG, G. ; ROHRER, H.: Summary Abstract: Scanning tunneling microscopy of semiconductor surfaces. In: *Journal of Vacuum Science & Technology B* 1 (1983), Nr. 3, 703-704. <http://dx.doi.org/http://dx.doi.org/10.1116/1.582583>. – DOI <http://dx.doi.org/10.1116/1.582583>
- [BBS97] BÖHRINGER, Matthias ; BERNDT, Richard ; SCHNEIDER, Wolf-Dieter: Transition from three-dimensional to two-dimensional faceting of Ag(110) induced by Cu-phthalocyanine. In: *Phys. Rev. B* 55 (1997), Jan, 1384-1387. <http://dx.doi.org/10.1103/PhysRevB.55.1384>. – DOI 10.1103/PhysRevB.55.1384

Bibliography

- [BCK05] BARTH, Johannes V. ; COSTANTINI, Giovanni ; KERN, Klaus: Engineering atomic and molecular nanostructures at surfaces. In: *Nature* 437 (2005), Sep, 671-679. <http://dx.doi.org/10.1038/nature04166>
- [BCN56] BABA, H. ; CHITOKU, K. ; NITTA, K.: Photoelectric Phenomena with Copper Phthalocyanine. In: *Nature* 177 (1956), Nr. 4510, S. 672 – 672. <http://dx.doi.org/http://dx.doi.org/10.1038/177672a0>. – DOI <http://dx.doi.org/10.1038/177672a0>
- [BDL36] BARRETT, P. A. ; DENT, C. E. ; LINSTEAD, R. P.: 382. Phthalocyanines. Part VII. Phthalocyanine as a co-ordinating group. A general investigation of the metallic derivatives. In: *J. Chem. Soc.* (1936), 1719-1736. <http://dx.doi.org/10.1039/JR9360001719>. – DOI 10.1039/JR9360001719
- [Bes87] BESOCKE, K.: An easily operable scanning tunneling microscope. In: *Surface Science* 181 (1987), Nr. 1-2, 145 - 153. [http://dx.doi.org/http://dx.doi.org/10.1016/0039-6028\(87\)90151-8](http://dx.doi.org/http://dx.doi.org/10.1016/0039-6028(87)90151-8). – DOI [http://dx.doi.org/10.1016/0039-6028\(87\)90151-8](http://dx.doi.org/10.1016/0039-6028(87)90151-8). – ISSN 0039-6028
- [BL13] BARAN, Jakub D. ; LARSSON, J. A.: Theoretical Insights into Adsorption of Cobalt Phthalocyanine on Ag(111): A Combination of Chemical and van der Waals Bonding. In: *The Journal of Physical Chemistry C* 117 (2013), Nr. 45, 23887-23898. <http://dx.doi.org/10.1021/jp409127e>. – DOI 10.1021/jp409127e
- [BMW⁺12] BAUER, Oliver ; MERCURIO, Giuseppe ; WILLENBOCKEL, Martin ; RECKIEN, Werner ; HEINRICH SCHMITZ, Christoph ; FIEDLER, Benjamin ; SOUBATCH, Serguei ; BREDOW, Thomas ; TAUTZ, Frank S. ; SOKOLOWSKI, Moritz: Role of functional groups in surface bonding of planar π -conjugated molecules. In: *Phys. Rev. B* 86 (2012), Dec, 235431. <http://dx.doi.org/10.1103/PhysRevB.86.235431>. – DOI 10.1103/PhysRevB.86.235431
- [BR82] BINNIG, G. ; ROHRER, H.: Scanning tunneling microscopy. In: *Helvetica Physica Acta* 55 (1982), S. 726-735. <http://dx.doi.org/http://dx.doi.org/10.5169/seals-115309>. – DOI <http://dx.doi.org/10.5169/seals-115309>
- [BR83a] BINNIG, G. ; ROHRER, H.: Scanning tunneling microscopy. In: *Surface Science* 126 (1983), Nr. 1-3, 236 - 244. [http://dx.doi.org/10.1016/0021-4901\(83\)90127-7](http://dx.doi.org/10.1016/0021-4901(83)90127-7)

- doi.org/http://dx.doi.org/10.1016/0039-6028(83)90716-1. – DOI
http://dx.doi.org/10.1016/0039-6028(83)90716-1. – ISSN 0039-6028
- [BR83b] BINNIG, G. ; ROHRER, H.: Scanning tunneling microscopy, an atomic probe. In: *Scanning Electron Microscopy* 3 (1983), S. 1079–1082
- [BR83c] BINNIG, G. ; ROHRER, H.: Scanning tunneling microscopy on crystal surfaces. In: *Journal of Crystal Growth* 65 (1983), Nr. 1-3, 679 - 680. [http://dx.doi.org/http://dx.doi.org/10.1016/0022-0248\(83\)90118-5](http://dx.doi.org/http://dx.doi.org/10.1016/0022-0248(83)90118-5). – DOI [http://dx.doi.org/10.1016/0022-0248\(83\)90118-5](http://dx.doi.org/10.1016/0022-0248(83)90118-5). – ISSN 0022-0248
- [BRGW82a] BINNIG, G. ; ROHRER, H. ; GERBER, Ch. ; WEIBEL, E.: Surface Studies by Scanning Tunneling Microscopy. In: *Phys. Rev. Lett.* 49 (1982), Jul, 57–61. <http://dx.doi.org/10.1103/PhysRevLett.49.57>. – DOI 10.1103/PhysRevLett.49.57
- [BRGW82b] BINNIG, G. ; ROHRER, H. ; GERBER, Ch. ; WEIBEL, E.: Tunneling through a controllable vacuum gap. In: *Applied Physics Letters* 40 (1982), Nr. 2, 178-180. <http://dx.doi.org/10.1063/1.92999>. – DOI 10.1063/1.92999
- [BSG+98] BÖHRINGER, M. ; SCHNEIDER, W.-D. ; GLÖCKLER, K. ; UMBACH, E. ; BERNDT, R.: Adsorption site determination of PTCDA on Ag(110) by manipulation of adatoms. In: *Surface Science* 419 (1998), Nr. 1, L95 - L99. [http://dx.doi.org/10.1016/S0039-6028\(98\)00733-X](http://dx.doi.org/10.1016/S0039-6028(98)00733-X). – DOI 10.1016/S0039-6028(98)00733-X. – ISSN 0039-6028
- [BWBM03] BOBISCH, C. ; WAGNER, Th. ; BANNANI, A. ; MÖLLER, R.: Ordered binary monolayer composed of two organic molecules: Copper-phthalocyanine and 3,4,9,10-perylene-tetra-carboxylic-dianhydride on Cu(111). In: *The Journal of Chemical Physics* 119 (2003), Nr. 18, 9804-9808. <http://dx.doi.org/10.1063/1.1615492>. – DOI 10.1063/1.1615492
- [CCW+10] CUADRADO, Ramon ; CERDA, Jorge I. ; WANG, Yongfeng ; XIN, Ge ; BERNDT, Richard ; TANG, Hao: CoPc adsorption on Cu(111): Origin of the C4 to C2 symmetry reduction. In: *The Journal of Chemical Physics* 133 (2010), Nr. 15, -. <http://dx.doi.org/http://dx.doi.org/10.1063/1.3502682>. – DOI <http://dx.doi.org/10.1063/1.3502682>

Bibliography

- [CGD⁺07] CHENG, Z. H. ; GAO, L. ; DENG, Z. T. ; LIU, Q. ; JIANG, N. ; LIN, X. ; HE, X. B. ; DU, S. X. ; GAO, H.-J.: Epitaxial Growth of Iron Phthalocyanine at the Initial Stage on Au(111) Surface. In: *The Journal of Physical Chemistry C* 111 (2007), Nr. 6, 2656-2660. <http://dx.doi.org/10.1021/jp0660738>. – DOI 10.1021/jp0660738
- [CHC⁺08] CHEN, Wei ; HUANG, Han ; CHEN, Shi ; GAO, Xing Y. ; WEE, Andrew Thye S.: Low-Temperature Scanning Tunneling Microscopy and Near-Edge X-ray Absorption Fine Structure Investigations of Molecular Orientation of Copper(II) Phthalocyanine Thin Films at Organic Heterojunction Interfaces. In: *The Journal of Physical Chemistry C* 112 (2008), Nr. 13, 5036-5042. <http://dx.doi.org/10.1021/jp710722s>. – DOI 10.1021/jp710722s
- [Che08] CHEN, C. J.: *Introduction to Scanning Tunneling Microscopy*. 2nd. Oxford University Press, 2008
- [Chr72] CHRISTENSEN, N. E.: The Band Structure of Silver and Optical Interband Transitions. In: *physica status solidi (b)* 54 (1972), Nr. 2, 551–563. <http://dx.doi.org/10.1002/pssb.2220540219>. – DOI 10.1002/pssb.2220540219. – ISSN 1521–3951
- [CKB⁺08] CHANG, Shih-Hsin ; KUCK, Stefan ; BREDE, Jens ; LICHTENSTEIN, Leonid ; HOFFMANN, Germar ; WIESENDANGER, Roland: Symmetry reduction of metal phthalocyanines on metals. In: *Phys. Rev. B* 78 (2008), Dec, 233409. <http://dx.doi.org/10.1103/PhysRevB.78.233409>. – DOI 10.1103/PhysRevB.78.233409
- [CQH⁺11] CHEN, Wei ; QI, Dong-Chen ; HUANG, Han ; GAO, Xingyu ; WEE, Andrew T. S.: Organic-Organic Heterojunction Interfaces: Effect of Molecular Orientation. In: *Advanced Functional Materials* 21 (2011), Nr. 3, 410–424. <http://dx.doi.org/10.1002/adfm.201000902>. – DOI 10.1002/adfm.201000902. – ISSN 1616–3028
- [CSS⁺12] COTTIN, M.C. ; SCHAFFERT, J. ; SONNTAG, A. ; KARACUBAN, H. ; MÖLLER, R. ; BOBISCH, C.A.: Supramolecular architecture of organic molecules: PTCDA and CuPc on a Cu(111) substrate. In: *Applied Surface Science* 258 (2012), Nr. 6, 2196 - 2200. <http://dx.doi.org/10.1016/j.>

apsusc.2011.02.038. – DOI 10.1016/j.apsusc.2011.02.038. – ISSN 0169–4332. – <ce:title>International Vacuum Congress (IVC-18)</ce:title>

- [CWH⁺84] COURTHS, R ; WERN, H ; HAU, U ; CORD, B ; BACHELIER, V ; HUFNER, S: Band structure of Cu, Ag and Au: location of direct transitions on the Λ line using angle-resolved photoelectron spectroscopy (ARUPS). In: *Journal of Physics F: Metal Physics* 14 (1984), Nr. 6, 1559. <http://stacks.iop.org/0305-4608/14/i=6/a=023>
- [DL34] DENT, C. E. ; LINSTEAD, R. P.: 215. Phthalocyanines. Part IV. Copper phthalocyanines. In: *J. Chem. Soc.* (1934), 1027-1031. <http://dx.doi.org/10.1039/JR9340001027>. – DOI 10.1039/JR9340001027
- [ECS⁺07] EVANGELISTA, Fabrizio ; CARRAVETTA, Vincenzo ; STEFANI, Giovanni ; JANSIK, Branislav ; ALAGIA, Michele ; STRANGES, Stefano ; RUOCCO, Alessandro: Electronic structure of copper phthalocyanine: An experimental and theoretical study of occupied and unoccupied levels. In: *The Journal of Chemical Physics* 126 (2007), Nr. 12, 124709. <http://dx.doi.org/10.1063/1.2712435>. – DOI 10.1063/1.2712435
- [Ein05] EINSTEIN, A.: Über einen die Erzeugung und Verwandlung des Lichtes betreffenden heuristischen Gesichtspunkt. In: *Annalen der Physik* 322 (1905), Nr. 6, 132–148. <http://dx.doi.org/10.1002/andp.19053220607>. – DOI 10.1002/andp.19053220607. – ISSN 1521–3889
- [EK85] ERTL, G. ; KÜPPERS, J.: *Low Energy Electrons and Surface Chemistry*. 2nd. VCH, 1985
- [Ern13] ERNST, Karl-Heinz: Molecular chirality in surface science. In: *Surface Science* 613 (2013), Nr. 0, 1 - 5. <http://dx.doi.org/http://dx.doi.org/10.1016/j.susc.2013.03.014>. – DOI <http://dx.doi.org/10.1016/j.susc.2013.03.014>. – ISSN 0039–6028
- [ERS⁺13] EGGER, David A. ; RUIZ, Victor G. ; SAIDI, Wissam A. ; BUCKO, Tomas ; TKATCHENKO, Alexandre ; ZOJER, Egbert: Understanding Structure and Bonding of Multilayered Metal-Organic Nanostructures. In: *The Journal of Physical Chemistry C* 117 (2013), Nr. 6, 3055-3061. <http://dx.doi.org/10.1021/jp309943k>. – DOI 10.1021/jp309943k. – PMID: 23447750

Bibliography

- [EST03] EREMTCHENKO, M. ; SCHAEFER, J. A. ; TAUTZ, F. S.: Understanding and tuning the epitaxy of large aromatic adsorbates by molecular design. In: *Nature* 425 (2003), Oct, 602-605. <http://dx.doi.org/10.1038/nature01901>
- [FGN⁺14] FEYER, V. ; GRAUS, M. ; NIGGE, P. ; WIESSNER, M. ; ACRES, R.G. ; WIEMANN, C. ; SCHNEIDER, C.M. ; SCHÖLL, A. ; REINERT, F.: Adsorption geometry and electronic structure of iron phthalocyanine on Ag surfaces: A LEED and photoelectron momentum mapping study. In: *Surface Science* 621 (2014), Nr. 0, 64 - 68. <http://dx.doi.org/http://dx.doi.org/10.1016/j.susc.2013.10.020>. – DOI <http://dx.doi.org/10.1016/j.susc.2013.10.020>. – ISSN 0039-6028
- [FLSY89] FORREST, S. R. ; LEU, L. Y. ; So, F. F. ; YOON, W. Y.: Optical and electrical properties of isotype crystalline molecular organic heterojunctions. In: *Journal of Applied Physics* 66 (1989), Nr. 12, 5908-5914. <http://dx.doi.org/10.1063/1.343616>. – DOI 10.1063/1.343616
- [FTB⁺90] FUSTER, G. ; TYLER, J. M. ; BRENER, N. E. ; CALLAWAY, J. ; BAGAYOKO, D.: Electronic structure and related properties of silver. In: *Phys. Rev. B* 42 (1990), Oct, 7322-7329. <http://dx.doi.org/10.1103/PhysRevB.42.7322>. – DOI 10.1103/PhysRevB.42.7322
- [FTS⁺04] FRISCH, M. J. ; TRUCKS, G. W. ; SCHLEGEL, H. B. ; SCUSERIA, G. E. ; ROBB, M. A. ; CHEESEMAN, J. R. ; MONTGOMERY, J. A. Jr. ; VREVEN, T. ; KUDIN, K. N. ; BURANT, J. C. ; MILLAM, J. M. ; IYENGAR, S. S. ; TOMASI, J. ; BARONE, V. ; MENNUCCI, B. ; COSSI, M. ; SCALMANI, G. ; REGA, N. ; PETERSSON, G. A. ; NAKATSUJI, H. ; HADA, M. ; EHARA, M. ; TOYOTA, K. ; FUKUDA, R. ; HASEGAWA, J. ; ISHIDA, M. ; NAKAJIMA, T. ; HONDA, Y. ; KITAO, O. ; NAKAI, H. ; KLENE, M. ; LI, X. ; KNOX, J. E. ; HRATCHIAN, H. P. ; CROSS, J. B. ; BAKKEN, V. ; ADAMO, C. ; JARAMILLO, J. ; GOMPERTS, R. ; STRATMANN, R. E. ; YAZYEV, O. ; AUSTIN, A. J. ; CAMMI, R. ; POMELLI, C. ; OCHTERSKI, J. W. ; AYALA, P. Y. ; MOROKUMA, K. ; VOTH, G. A. ; SALVADOR, P. ; DANNENBERG, J. J. ; ZAKRZEWSKI, V. G. ; DAPPRICH, S. ; DANIELS, A. D. ; STRAIN, M. C. ; FARKAS, O. ; MALICK, D. K. ; RABUCK, A. D. ; RAGHAVACHARI, K. ; FORESMAN, J. B. ; ORTIZ, J. V. ; CUI, Q. ; BABOUL, A. G. ; CLIF-

- FORD, S. ; CIOSLOWSKI, J. ; STEFANOV, B. B. ; LIU, G. ; LIASHENKO, A. ; PISKORZ, P. ; KOMAROMI, I. ; MARTIN, R. L. ; FOX, D. J. ; KEITH, T. ; AL-LAHAM, M. A. ; PENG, C. Y. ; NANAYAKKARA, A. ; CHALLACOMBE, M. ; GILL, P. M. W. ; JOHNSON, B. ; CHEN, W. ; WONG, M. W. ; GONZALEZ, C. ; POPLER, J. A.: Gaussian 03, Revision C.02. In: *Gaussian, Inc., Wallingford, CT, 2004* (2004). – Gaussian, Inc., Wallingford, CT, 2004
- [GAA⁺10] GIOVANELLI, L. ; AMSALEM, P. ; ANGOT, T. ; PETACCIA, L. ; GOROVIKOV, S. ; PORTE, L. ; GOLDONI, A. ; THEMLIN, J. M.: Valence band photoemission from the Zn-phthalocyanine/Ag(110) interface: Charge transfer and scattering of substrate photoelectrons. In: *Physical Review B* 82 (2010), S. 125431
- [GBK⁺11] GOPAKUMAR, T. G. ; BRUMME, T. ; KROGER, J. ; TOHER, C. ; CUNIBERTI, G. ; BERNDT, R.: Coverage-Driven Electronic Decoupling of Fe-Phthalocyanine from a Ag(111) Substrate. In: *The Journal of Physical Chemistry C* 115 (2011), Nr. 24, 12173-12179. <http://dx.doi.org/10.1021/jp2038619>. – DOI 10.1021/jp2038619
- [GG10] GAO, H.-J. ; GAO, Li: Scanning tunneling microscopy of functional nanostructures on solid surfaces: Manipulation, self-assembly, and applications. In: *Progress in Surface Science* 85 (2010), Nr. 1-4, 28 - 91. <http://dx.doi.org/10.1016/j.progsurf.2009.10.001>. – DOI 10.1016/j.progsurf.2009.10.001. – ISSN 0079-6816
- [GGR⁺92] GAISCH, R. ; GIMZEWSKI, J.K. ; REIHL, B. ; SCHLITTLER, R.R. ; TSCHUDY, M. ; SCHNEIDER, W.D.: Low-temperature ultra-high-vacuum scanning tunneling microscope. In: *Ultramicroscopy* 42-44, Part 2 (1992), Nr. 0, 1621 - 1626. [http://dx.doi.org/http://dx.doi.org/10.1016/0304-3991\(92\)90495-6](http://dx.doi.org/http://dx.doi.org/10.1016/0304-3991(92)90495-6). – DOI [http://dx.doi.org/10.1016/0304-3991\(92\)90495-6](http://dx.doi.org/10.1016/0304-3991(92)90495-6). – ISSN 0304-3991
- [GKH⁺96] GRAND, J.-Y. ; KUNSTMANN, T. ; HOFFMANN, D. ; HAAS, A. ; DIETSCH, M. ; SEIFRITZ, J. ; MOELLER, R.: Epitaxial growth of copper phthalocyanine monolayers on Ag(111). In: *Surface Science* 366 (1996), Nr. 3, 403 - 414. [http://dx.doi.org/http://dx.doi.org/10.1016/0039-6028\(96\)00838-2](http://dx.doi.org/http://dx.doi.org/10.1016/0039-6028(96)00838-2). – DOI [http://dx.doi.org/10.1016/0039-6028\(96\)00838-2](http://dx.doi.org/10.1016/0039-6028(96)00838-2). – ISSN 0039-6028

Bibliography

- [GSS+98] GLÖCKLER, K ; SEIDEL, C ; SOUKOPP, A ; SOKOLOWSKI, M ; UMBACH, E ; BÖHRINGER, M ; BERNDT, R ; SCHNEIDER, W.-D: Highly ordered structures and submolecular scanning tunnelling microscopy contrast of PTCDA and DM-PBDCI monolayers on Ag(111) and Ag(110). In: *Surface Science* 405 (1998), Nr. 1, 1 - 20. [http://dx.doi.org/10.1016/S0039-6028\(97\)00888-1](http://dx.doi.org/10.1016/S0039-6028(97)00888-1). – DOI 10.1016/S0039-6028(97)00888-1. – ISSN 0039-6028
- [GSS+07] GERLACH, A. ; SELLNER, S. ; SCHREIBER, F. ; KOCH, N. ; ZEGENHAGEN, J.: Substrate-dependent bonding distances of PTCDA: A comparative x-ray standing-wave study on Cu(111) and Ag(111). In: *Phys. Rev. B* 75 (2007), Jan, Nr. 4, S. 045401. <http://dx.doi.org/10.1103/PhysRevB.75.045401>. – DOI 10.1103/PhysRevB.75.045401
- [Hö3] HÜFNER, Stefan: *Photoelectron Spectroscopy, Principles and Applications*. Third Edition. Springer, 2003
- [HA64] HARRISON, S. E. ; ASSOUR, J. M.: Relationship of Electron Spin Resonance and Semiconduction in Phthalocyanines. In: *The Journal of Chemical Physics* 40 (1964), Nr. 2, 365-370. <http://dx.doi.org/http://dx.doi.org/10.1063/1.1725120>. – DOI <http://dx.doi.org/10.1063/1.1725120>
- [Hal88] HALLWACHS, Wilhelm: Ueber den Einfluss des Lichtes auf electrostatisch geladene Körper. In: *Annalen der Physik* 269 (1888), Nr. 2, 301-312. <http://dx.doi.org/10.1002/andp.18882690206>. – DOI 10.1002/andp.18882690206. – ISSN 1521-3889
- [Ham67] HAMANN, C.: On the Electric and Thermoelectric Properties of Copper Phthalocyanine Single Crystals. In: *physica status solidi (b)* 20 (1967), Nr. 2, 481-491. <http://dx.doi.org/10.1002/pssb.19670200209>. – DOI 10.1002/pssb.19670200209. – ISSN 1521-3951
- [Hee98] HEEGER, Alan J.: Light emission from semiconducting polymers: Light-emitting diodes, light-emitting electrochemical cells, lasers and white light for the future. In: *Solid State Communications* 107 (1998), Nr. 11, 673 - 679. [http://dx.doi.org/http://dx.doi.org/10.1016/S0038-1098\(98\)00215-4](http://dx.doi.org/http://dx.doi.org/10.1016/S0038-1098(98)00215-4). – DOI [http://dx.doi.org/10.1016/S0038-1098\(98\)00215-4](http://dx.doi.org/10.1016/S0038-1098(98)00215-4). – ISSN 0038-1098
- [Hen15] HENNEKE, C., RWTH Aachen University / FZ Jülich, Diss., 2015

- [Her87] HERTZ, H.: Ueber einen Einfluss des ultravioletten Lichtes auf die electrische Entladung. In: *Annalen der Physik* 267 (1887), Nr. 8, 983–1000. <http://dx.doi.org/10.1002/andp.18872670827>. – DOI 10.1002/andp.18872670827. – ISSN 1521–3889
- [HFGR⁺07] HORCAS, I. ; FERNANDEZ, R. ; GOMEZ-RODRIGUEZ, J. M. ; COLCHERO, J. ; GOMEZ-HERRERO, J. ; BARO, A. M.: WSXM: A software for scanning probe microscopy and a tool for nanotechnology. In: *Review of Scientific Instruments* 78 (2007), Nr. 1, -. <http://dx.doi.org/http://dx.doi.org/10.1063/1.2432410>. – DOI <http://dx.doi.org/10.1063/1.2432410>
- [HFW01] HOOKS, D. E. ; FRITZ, T. ; WARD, M. D.: Epitaxy and Molecular Organization on Solid Substrates. In: *Advanced Materials* 13 (2001), Nr. 4, 227–241. [http://dx.doi.org/10.1002/1521-4095\(200102\)13:4<227::AID-ADMA227>3.0.CO;2-P](http://dx.doi.org/10.1002/1521-4095(200102)13:4<227::AID-ADMA227>3.0.CO;2-P). – DOI 10.1002/1521-4095(200102)13:4<227::AID-ADMA227>3.0.CO;2-P. – ISSN 1521–4095
- [HGS⁺10] HÄMING, M. ; GREIF, M. ; SAUER, C. ; SCHÖLL, A. ; REINERT, F.: Electronic structure of ultrathin heteromolecular organic-metal interfaces: SnPc/PTCDA/Ag(111) and SnPc/Ag(111). In: *Phys. Rev. B* 82 (2010), Dec, 235432. <http://dx.doi.org/10.1103/PhysRevB.82.235432>. – DOI 10.1103/PhysRevB.82.235432
- [HGW⁺10] HÄMING, M. ; GREIF, M. ; WIESSNER, M. ; SCHÖLL, A. ; REINERT, F.: Characterization of ultra-thin organic hetero-interfaces - SnPc/PTCDA/Ag(111). In: *Surface Science* 604 (2010), Nr. 19-20, 1619 - 1622. <http://dx.doi.org/10.1016/j.susc.2010.06.004>. – DOI 10.1016/j.susc.2010.06.004. – ISSN 0039–6028
- [HH63] HEILMEIER, George H. ; HARRISON, Sol E.: Charge Transport in Copper Phthalocyanine Single Crystals. In: *Phys. Rev.* 132 (1963), Dec, 2010–2016. <http://dx.doi.org/10.1103/PhysRev.132.2010>. – DOI 10.1103/PhysRev.132.2010
- [HHP⁺09] HUANG, Han ; HUANG, Yuli ; PFLAUM, Jens ; WEE, Andrew Thye S. ; CHEN, Wei: Nanoscale phase separation of a binary molecular system of copper phthalocyanine and di-indenoperylene on Ag(111). In: *Applied*

- Physics Letters* 95 (2009), Nr. 26, 263309. <http://dx.doi.org/10.1063/1.3280858>. – DOI 10.1063/1.3280858
- [HKC⁺05] HAUSCHILD, A. ; KARKI, K. ; COWIE, B. C. C. ; ROHLFING, M. ; TAUTZ, F. S. ; SOKOLOWSKI, M.: Molecular Distortions and Chemical Bonding of a Large π -Conjugated Molecule on a Metal Surface. In: *Phys. Rev. Lett.* 94 (2005), Jan, 036106. <http://dx.doi.org/10.1103/PhysRevLett.94.036106>. – DOI 10.1103/PhysRevLett.94.036106
- [HMSK00] HILL, I.G. ; MILLIRON, D. ; SCHWARTZ, J. ; KAHN, A.: Organic semiconductor interfaces: electronic structure and transport properties. In: *Applied Surface Science* 166 (2000), Nr. 1-4, 354 - 362. [http://dx.doi.org/10.1016/S0169-4332\(00\)00449-9](http://dx.doi.org/10.1016/S0169-4332(00)00449-9). – DOI 10.1016/S0169-4332(00)00449-9. – ISSN 0169-4332
- [Hoe99] HOEGEN, M. Horn-von: Growth of semiconductor layers studied by spot profile analysing low energy electron diffraction - Part I. In: *Zeitschrift für Kristallographie* 214 (1999), S. 591-629
- [HT87] HANSMA, Paul K. ; TERSOFF, Jerry: Scanning tunneling microscopy. In: *Journal of Applied Physics* 61 (1987), Nr. 2, R1-R24. <http://dx.doi.org/10.1063/1.338189>. – DOI 10.1063/1.338189
- [HWC86] HOVE, M.A. V. ; WEINBERG, W.H. ; CHAN, C.-M.: *Low-Energy Electron Diffraction*. Springer-Verlag Berlin Heidelberg, 1986
- [HWST72] HÜFNER, S. ; WERTHEIM, G.K. ; SMITH, N.V. ; TRAUM, M.M.: XPS density of states of copper, silver, and nickel. In: *Solid State Communications* 11 (1972), Nr. 2, 323 - 326. [http://dx.doi.org/http://dx.doi.org/10.1016/0038-1098\(72\)90242-6](http://dx.doi.org/http://dx.doi.org/10.1016/0038-1098(72)90242-6). – DOI [http://dx.doi.org/10.1016/0038-1098\(72\)90242-6](http://dx.doi.org/10.1016/0038-1098(72)90242-6). – ISSN 0038-1098
- [IRH⁺08] IACOVITA, C. ; RASTEI, M. V. ; HEINRICH, B. W. ; BRUMME, T. ; KORTUS, J. ; LIMOT, L. ; BUCHER, J. P.: Visualizing the Spin of Individual Cobalt-Phthalocyanine Molecules. In: *Phys. Rev. Lett.* 101 (2008), Sep, 116602. <http://dx.doi.org/10.1103/PhysRevLett.101.116602>. – DOI 10.1103/PhysRevLett.101.116602

- [JBS⁺93] JUNG, M. ; BASTON, U. ; SCHNITZLER, G. ; KAISER, M. ; PAPST, J. ; PORWOL, T. ; FREUND, H.J. ; UMBACH, E.: The electronic structure of adsorbed aromatic molecules: Perylene and PTCDA on Si(111) and Ag(111). In: *Journal of Molecular Structure* 293 (1993), Nr. 0, 239 - 244. [http://dx.doi.org/10.1016/0022-2860\(93\)80058-4](http://dx.doi.org/10.1016/0022-2860(93)80058-4). – DOI 10.1016/0022-2860(93)80058-4. – ISSN 0022-2860
- [KAM⁺06] KOUDIA, Mathieu ; ABEL, Mathieu ; MAUREL, Christian ; BLIEK, Ariane ; CATALIN, Daniel ; MOSSOYAN, Mireille ; MOSSOYAN, Jean-Charles ; PORTE, Louis: Influence of Chlorine Substitution on the Self-Assembly of Zinc Phthalocyanine. In: *The Journal of Physical Chemistry B* 110 (2006), Nr. 20, 10058-10062. <http://dx.doi.org/10.1021/jp0571980>. – DOI 10.1021/jp0571980
- [KHT⁺08] KILIAN, L. ; HAUSCHILD, A. ; TEMIROV, R. ; SOUBATCH, S. ; SCHÖLL, A. ; BENDOUNAN, A. ; REINERT, F. ; LEE, T.-L. ; TAUTZ, F. S. ; SOKOLOWSKI, M. ; UMBACH, E.: Role of Intermolecular Interactions on the Electronic and Geometric Structure of a Large π -Conjugated Molecule Adsorbed on a Metal Surface. In: *Phys. Rev. Lett.* 100 (2008), Apr, 136103. <http://dx.doi.org/10.1103/PhysRevLett.100.136103>. – DOI 10.1103/PhysRevLett.100.136103
- [KKL⁺11] KIM, Sunkook ; KWON, Hyuk-Jun ; LEE, Sunghun ; SHIM, Hongshik ; CHUN, Youngtea ; CHOI, Woong ; KWACK, Jinho ; HAN, Dongwon ; SONG, MyoungSeop ; KIM, Sungchul ; MOHAMMADI, Saeed ; KEE, InSeo ; LEE, Sang Y.: Low-Power Flexible Organic Light-Emitting Diode Display Device. In: *Advanced Materials* 23 (2011), Nr. 31, 3511-3516. <http://dx.doi.org/10.1002/adma.201101066>. – DOI 10.1002/adma.201101066. – ISSN 1521-4095
- [KLS⁺09] KARACUBAN, H. ; LANGE, M. ; SCHAFFERT, J. ; WEINGART, O. ; WAGNER, Th. ; MÖLLER, R.: Substrate-induced symmetry reduction of CuPc on Cu(111): An LT-STM study. In: *Surface Science* 603 (2009), Nr. 5, L39 - L43. <http://dx.doi.org/http://dx.doi.org/10.1016/j.susc.2009.01.029>. – DOI <http://dx.doi.org/10.1016/j.susc.2009.01.029>. – ISSN 0039-6028

- [KRMG13] KRULL, Cornelius ; ROBLES, Roberto ; MUGARZA, Aitor ; GAMBARELLA, Pietro: Site- and orbital-dependent charge donation and spin manipulation in electron-doped metal phthalocyanines. In: *NATURE MATERIALS* 12 (2013), APR, Nr. 4, S. 337–343. <http://dx.doi.org/10.1038/NMAT3547>. – DOI 10.1038/NMAT3547. – ISSN 1476–1122
- [Kro10] KROEGER, Ingo: *Adsorption von Phthalocyaninen auf Edelmetalloberflächen*, Uni Würzburg / FZ Jülich, Diss., 2010
- [KSS+10] KRÖGER, Ingo ; STADTMÜLLER, Benjamin ; STADLER, Christoph ; ZIROFF, Johannes ; KOCHLER, Mario ; STAHL, Andreas ; POLLINGER, Florian ; LEE, Tien-Lin ; ZEGENHAGEN, Jörg ; REINERT, Friedrich ; KUMPF, Christian: Submonolayer growth of copper-phthalocyanine on Ag(111). In: *New Journal of Physics* 12 (2010), Nr. 8, 083038. <http://stacks.iop.org/1367-2630/12/i=8/a=083038>
- [KSW+11] KRÖGER, Ingo ; STADTMÜLLER, Benjamin ; WAGNER, Christian ; WEISS, Christian ; TEMIROV, Ruslan ; TAUTZ, F. S. ; KUMPF, Christian: Modeling intermolecular interactions of physisorbed organic molecules using pair potential calculations. In: *The Journal of Chemical Physics* 135 (2011), Nr. 23, -. <http://dx.doi.org/http://dx.doi.org/10.1063/1.3665923>. – DOI <http://dx.doi.org/10.1063/1.3665923>
- [KTH+06] KRAFT, A. ; TEMIROV, R. ; HENZE, S. K. M. ; SOUBATCH, S. ; ROHLFING, M. ; TAUTZ, F. S.: Lateral adsorption geometry and site-specific electronic structure of a large organic chemisorbate on a metal surface. In: *Phys. Rev. B* 74 (2006), Jul, 041402. <http://dx.doi.org/10.1103/PhysRevB.74.041402>. – DOI 10.1103/PhysRevB.74.041402
- [LBF07] LUNT, R.R. ; BENZIGER, J.B. ; FORREST, S.R.: Growth of an Ordered Crystalline Organic Heterojunction. In: *Advanced Materials* 19 (2007), Nr. 23, 4229–4233. <http://dx.doi.org/10.1002/adma.200701572>. – DOI 10.1002/adma.200701572. – ISSN 1521–4095
- [Lec87] LECKEY, R.C.G.: Recent developments in electron energy analysers. In: *Journal of Electron Spectroscopy and Related Phenomena* 43 (1987), Nr. 3, 183 - 214. [http://dx.doi.org/10.1016/0368-2048\(87\)80001-4](http://dx.doi.org/10.1016/0368-2048(87)80001-4). – DOI 10.1016/0368–2048(87)80001–4. – ISSN 0368–2048

- [LH02] LACKINGER, Markus ; HIETSCHOLD, Michael: Determining adsorption geometry of individual tin-phthalocyanine molecules on Ag(111) - a STM study at submonolayer coverage. In: *Surface Science* 520 (2002), Nr. 1-2, L619 - L624. [http://dx.doi.org/http://dx.doi.org/10.1016/S0039-6028\(02\)02269-0](http://dx.doi.org/http://dx.doi.org/10.1016/S0039-6028(02)02269-0). – DOI [http://dx.doi.org/10.1016/S0039-6028\(02\)02269-0](http://dx.doi.org/10.1016/S0039-6028(02)02269-0). – ISSN 0039-6028
- [LMH⁺14] LÜFTNER, Daniel ; MILKO, Matus ; HUPPMANN, Sophia ; SCHOLZ, Markus ; NGYUEN, Nam ; WIESSNER, Michael ; SCHÖLL, Achim ; REINERT, Friedrich ; PUSCHNIG, Peter: CuPc/Au(110): Determination of the azimuthal alignment by a combination of angle-resolved photoemission and density functional theory. In: *Journal of Electron Spectroscopy and Related Phenomena* 195 (2014), Nr. 0, 293 - 300. <http://dx.doi.org/http://dx.doi.org/10.1016/j.elspec.2014.06.002>. – DOI <http://dx.doi.org/10.1016/j.elspec.2014.06.002>. – ISSN 0368-2048
- [LR85] LECKEY, R.C.G. ; RILEY, J.D.: A toroidal angle-resolving electron spectrometer for surface studies. In: *Applications of Surface Science* 22-23, Part 1 (1985), Nr. 0, 196 - 205. [http://dx.doi.org/http://dx.doi.org/10.1016/0378-5963\(85\)90052-2](http://dx.doi.org/http://dx.doi.org/10.1016/0378-5963(85)90052-2). – DOI [http://dx.doi.org/10.1016/0378-5963\(85\)90052-2](http://dx.doi.org/10.1016/0378-5963(85)90052-2). – ISSN 0378-5963
- [LUR⁺14] LÜFTNER, Daniel ; ULES, Thomas ; REINISCH, Eva M. ; KOLLER, Georg ; SOUBATCH, Serguei ; TAUTZ, F. S. ; RAMSEY, Michael G. ; PUSCHNIG, Peter: Imaging the wave functions of adsorbed molecules. In: *Proceedings of the National Academy of Sciences* 111 (2014), 605-610. <http://dx.doi.org/10.1073/pnas.1315716110>. – DOI 10.1073/pnas.1315716110
- [LWM⁺89] LIPPEL, P. H. ; WILSON, R. J. ; MILLER, M. D. ; WÖLL, Ch. ; CHIANG, S.: High-Resolution Imaging of Copper-Phthalocyanine by Scanning-Tunneling Microscopy. In: *Phys. Rev. Lett.* 62 (1989), Jan, 171-174. <http://dx.doi.org/10.1103/PhysRevLett.62.171>. – DOI 10.1103/PhysRevLett.62.171
- [MBW⁺13] MERCURIO, G. ; BAUER, O. ; WILLENBOCKEL, M. ; FIEDLER, B. ; SUEYOSHI, T. ; WEISS, C. ; TEMIROV, R. ; SOUBATCH, S. ; SOKOLOWSKI, M. ; TAUTZ, F. S.: Tuning and probing interfacial bonding channels for a functionalized organic molecule by surface modification. In: *Phys. Rev.*

- B* 87 (2013), Mar, 121409. <http://dx.doi.org/10.1103/PhysRevB.87.121409>. – DOI 10.1103/PhysRevB.87.121409
- [MEP⁺07] MANANDHAR, K. ; ELLIS, T. ; PARK, K.T. ; CAI, T. ; SONG, Z. ; HRBEK, J.: A scanning tunneling microscopy study on the effect of post-deposition annealing of copper phthalocyanine thin films. In: *Surface Science* 601 (2007), Nr. 17, 3623 - 3631. <http://dx.doi.org/10.1016/j.susc.2007.07.007>. – DOI 10.1016/j.susc.2007.07.007. – ISSN 0039-6028
- [MFR11] MARK, Andrew G. ; FORSTER, Matthew ; RAVAL, Rasmita: Recognition and Ordering at Surfaces: The Importance of Handedness and Footedness. In: *ChemPhysChem* 12 (2011), Nr. 8, 1474–1480. <http://dx.doi.org/10.1002/cphc.201001034>. – DOI 10.1002/cphc.201001034. – ISSN 1439-7641
- [MHKS08] MAROM, Noa ; HOD, Oded ; SCUSERIA, Gustavo E. ; KRONIK, Leor: Electronic structure of copper phthalocyanine: A comparative density functional theory study. In: *The Journal of Chemical Physics* 128 (2008), Nr. 16, -. <http://dx.doi.org/http://dx.doi.org/10.1063/1.2898540>. – DOI <http://dx.doi.org/10.1063/1.2898540>
- [MLO⁺10] MUGARZA, A. ; LORENTE, N. ; ORDEJÓN, P. ; KRULL, C. ; STEPANOW, S. ; BOCQUET, M.-L. ; FRAXEDAS, J. ; CEBALLOS, G. ; GAMBARDELLA, P.: Orbital Specific Chirality and Homochiral Self-Assembly of Achiral Molecules Induced by Charge Transfer and Spontaneous Symmetry Breaking. In: *Phys. Rev. Lett.* 105 (2010), Sep, 115702. <http://dx.doi.org/10.1103/PhysRevLett.105.115702>. – DOI 10.1103/PhysRevLett.105.115702
- [MRK⁺12] MUGARZA, A. ; ROBLES, R. ; KRULL, C. ; KORYTÁR, R. ; LORENTE, N. ; GAMBARDELLA, P.: Electronic and magnetic properties of molecule-metal interfaces: Transition-metal phthalocyanines adsorbed on Ag(100). In: *Phys. Rev. B* 85 (2012), Apr, 155437. <http://dx.doi.org/10.1103/PhysRevB.85.155437>. – DOI 10.1103/PhysRevB.85.155437
- [PAN⁺08] PALMGREN, P. ; ANGOT, T. ; NLEBEDIM, C. I. ; LAYET, J.-M. ; LAY, G. L. ; GOTHELID, M.: Ordered phthalocyanine superstructures on Ag(110). In: *The Journal of Chemical Physics* 128 (2008), Nr. 6, 064702. <http://dx.doi.org/10.1063/1.2827864>. – DOI 10.1063/1.2827864

- [PF01] PEUMANS, P. ; FORREST, S. R.: Very-high-efficiency double-heterostructure copper phthalocyanine/C₆₀ photovoltaic cells. In: *Applied Physics Letters* 79 (2001), Nr. 1, 126-128. <http://dx.doi.org/10.1063/1.1384001>. – DOI 10.1063/1.1384001
- [Pio57] PIOCH, Winfried: Über die Darstellung saurer Mucopolysaccharide mit dem Kupferphthalocyaninfarbstoff Astrablau. In: *Virchows Archiv für pathologische Anatomie und Physiologie und für klinische Medizin* 330 (1957), Nr. 3, 337-346. <http://dx.doi.org/10.1007/BF00954964>. – DOI 10.1007/BF00954964. – ISSN 0376-0081
- [PRU+11] PUSCHNIG, P. ; REINISCH, E.-M. ; ULES, T. ; KOLLER, G. ; SOUBATCH, S. ; OSTLER, M. ; ROMANER, L. ; TAUTZ, F. S. ; AMBROSCH-DRAXL, C. ; RAMSEY, M. G.: Orbital tomography: Deconvoluting photoemission spectra of organic molecules. In: *Phys. Rev. B* 84 (2011), Dec, 235427. <http://dx.doi.org/10.1103/PhysRevB.84.235427>. – DOI 10.1103/PhysRevB.84.235427
- [Rav09] RAVAL, R.: Nanoscale insights into the creation of chiral surfaces. In: *Journal of Molecular Catalysis A: Chemical* 305 (2009), Nr. 1-2, 112 - 116. <http://dx.doi.org/http://dx.doi.org/10.1016/j.molcata.2008.11.032>. – DOI <http://dx.doi.org/10.1016/j.molcata.2008.11.032>. – ISSN 1381-1169. – In memory of Eric Derouane
- [RB92] ROSA, A. ; BAERENDS, E. J.: Origin and relevance of the staggering in one-dimensional molecular metals. A density functional study of metallophthalocyanine model dimers. In: *Inorganic Chemistry* 31 (1992), Nr. 23, 4717-4726. <http://dx.doi.org/10.1021/ic00049a002>. – DOI 10.1021/ic00049a002
- [REG+08] RUOCCO, A. ; EVANGELISTA, F. ; GOTTER, R. ; ATILI, A. ; STEFANI, G.: Evidence of charge transfer at the Cu-phthalocyanine/AI(100) interface (Reprinted from *J. Phys. Chem A*, vol 111, 2007). In: *JOURNAL OF PHYSICAL CHEMISTRY C* 112 (2008), FEB 14, Nr. 6, S. 2016-2025. <http://dx.doi.org/10.1021/jp076299q>. – DOI 10.1021/jp076299q. – ISSN 1932-7447

- [RLZ⁺12] RUIZ, Victor G. ; LIU, Wei ; ZOJER, Egbert ; SCHEFFLER, Matthias ; TKATCHENKO, Alexandre: Density-Functional Theory with Screened van der Waals Interactions for the Modeling of Hybrid Inorganic-Organic Systems. In: *Phys. Rev. Lett.* 108 (2012), Apr, 146103. <http://dx.doi.org/10.1103/PhysRevLett.108.146103>. – DOI 10.1103/PhysRevLett.108.146103
- [Rob35] ROBERTSON, J. M.: 136. An X-ray study of the structure of the phthalocyanines. Part I. The metal-free, nickel, copper, and platinum compounds. In: *J. Chem. Soc.* (1935), 615-621. <http://dx.doi.org/10.1039/JR9350000615>. – DOI 10.1039/JR9350000615
- [RTT07] ROHLFING, Michael ; TEMIROV, Ruslan ; TAUTZ, Frank S.: Adsorption structure and scanning tunneling data of a prototype organic-inorganic interface: PTCDA on Ag(111). In: *Phys. Rev. B* 76 (2007), Sep, 115421. <http://dx.doi.org/10.1103/PhysRevB.76.115421>. – DOI 10.1103/PhysRevB.76.115421
- [SA94] SCHUERLEIN, T. J. ; ARMSTRONG, N. R.: Formation and characterization of epitaxial phthalocyanine and perylene monolayers and bilayers on Cu(100): Low energy electron diffraction and thermal desorption mass spectrometry studies. In: *Journal of Vacuum Science & Technology A* 12 (1994), Nr. 4, 1992-1997. <http://dx.doi.org/http://dx.doi.org/10.1116/1.578995>. – DOI <http://dx.doi.org/10.1116/1.578995>
- [SAL⁺97] SEIDEL, C. ; AWATER, C. ; LIU, X. D. ; ELLERBRAKE, R. ; FUCHS, H.: A combined STM, LEED and molecular modelling study of PTCDA grown on Ag(110). In: *Surface Science* 371 (1997), Nr. 1, 123 - 130. [http://dx.doi.org/DOI:10.1016/S0039-6028\(96\)00981-8](http://dx.doi.org/DOI:10.1016/S0039-6028(96)00981-8). – DOI DOI: 10.1016/S0039-6028(96)00981-8. – ISSN 0039-6028
- [Sch15] SCHRÖDER, S.: *Structural and electronic characterization of hetero-organic NTCDA-CuPc adsorbate systems on Ag(111)*, RWTH Aachen University / FZ Jülich, Diss., 2015
- [SCK⁺08] SCARFATO, Alessandro ; CHANG, Shih-Hsin ; KUCK, Stefan ; BREDE, Jens ; HOFFMANN, Germar ; WIESENDANGER, Roland: Scanning tunneling microscope study of iron(II) phthalocyanine growth on metals and insulat-

- ing surfaces. In: *Surface Science* 602 (2008), Nr. 3, 677 - 683. <http://dx.doi.org/http://dx.doi.org/10.1016/j.susc.2007.11.011>. – DOI <http://dx.doi.org/10.1016/j.susc.2007.11.011>. – ISSN 0039-6028
- [SGP⁺14] STADTMÜLLER, Benjamin ; GRUENEWALD, Marco ; PEUKER, Julia ; FORKER, Roman ; FRITZ, Torsten ; KUMPF, Christian: Molecular Exchange in a Heteromolecular PTCDA/CuPc Bilayer Film on Ag(111). In: *The Journal of Physical Chemistry C* 118 (2014), Nr. 49, 28592-28602. <http://dx.doi.org/10.1021/jp5078104>. – DOI 10.1021/jp5078104
- [SH06] SYLVESTER-HVID, Kristian O.: Two-Dimensional Simulations of CuPc-PCTDA Solar Cells: The Importance of Mobility and Molecular π Stacking. In: *The Journal of Physical Chemistry B* 110 (2006), Nr. 6, 2618-2627. <http://dx.doi.org/10.1021/jp055321h>. – DOI 10.1021/jp055321h. – PMID: 16471863
- [SHD⁺07] SONG, Fei ; HUANG, Han ; DOU, Weidong ; ZHANG, Hanjie ; HU, Yunwan ; QIAN, Huiqin ; LI, Haiyang ; HE, Pimo ; BAO, Shining ; CHEN, Qiao ; ZHOU, Wuzong: Electronic structures of CuPc on a Ag(110) surface. In: *Journal of Physics: Condensed Matter* 19 (2007), Nr. 13, 136002. <http://stacks.iop.org/0953-8984/19/i=13/a=136002>
- [SHFS⁺97] SCHMITZ-HÜBSCH, T. ; FRITZ, T. ; SELLAM, F. ; STAUB, R. ; LEO, K.: Epitaxial growth of 3,4,9,10-perylene-tetracarboxylic-dianhydride on Au(111): A STM and RHEED study. In: *Phys. Rev. B* 55 (1997), Mar, 7972-7976. <http://dx.doi.org/10.1103/PhysRevB.55.7972>. – DOI 10.1103/PhysRevB.55.7972
- [SHFS⁺99] SCHMITZ-HUEBSCH, T. ; FRITZ, T. ; STAUB, R. ; BACK, A. ; ARMSTRONG, N.R. ; LEO, K.: Structure of 3,4,9,10-perylene-tetracarboxylic-dianhydride grown on reconstructed and unreconstructed Au(100). In: *Surface Science* 437 (1999), Nr. 1-2, 163 - 172. [http://dx.doi.org/http://dx.doi.org/10.1016/S0039-6028\(99\)00711-6](http://dx.doi.org/http://dx.doi.org/10.1016/S0039-6028(99)00711-6). – DOI [http://dx.doi.org/10.1016/S0039-6028\(99\)00711-6](http://dx.doi.org/10.1016/S0039-6028(99)00711-6). – ISSN 0039-6028
- [SHK⁺09] STADLER, Christoph ; HANSEN, Sören ; KRÖGER, Ingo ; KUMPF, Christian ; UMBACH, Eberhard: Tuning intermolecular interaction in long-range-

- ordered submonolayer organic films. In: *Nat Phys* 5 (2009), Februar, Nr. 2, 153-158. <http://dx.doi.org/10.1038/nphys1176>. – ISSN 1745-2473
- [SHS⁺15] STADTMÜLLER, Benjamin ; HENNEKE, Caroline ; SOUBATCH, Serguei ; TAUTZ, F S. ; KUMPF, Christian: Tailoring metal-organic hybrid interfaces: heteromolecular structures with varying stoichiometry on Ag(111). In: *New Journal of Physics* 17 (2015), Nr. 2, 023046. <http://stacks.iop.org/1367-2630/17/i=2/a=023046>
- [SKRK11] STADTMÜLLER, Benjamin ; KRÖGER, Ingo ; REINERT, Friedrich ; KUMPF, Christian: Submonolayer growth of CuPc on noble metal surfaces. In: *Phys. Rev. B* 83 (2011), Feb, 085416. <http://dx.doi.org/10.1103/PhysRevB.83.085416>. – DOI 10.1103/PhysRevB.83.085416
- [SLW⁺14] STADTMÜLLER, Benjamin ; LÜFTNER, Daniel ; WILLENBOCKEL, Martin ; REINISCH, Eva M. ; SUEYOSHI, Tomoki ; KOLLER, Georg ; SOUBATCH, Serguei ; RAMSEY, Michael G. ; PUSCHNIG, Peter ; TAUTZ, F. S. ; KUMPF, Christian: Unexpected interplay of bonding height and energy level alignment at heteromolecular hybrid interfaces. In: *Nat Commun* 5 (2014), April, 3685. <http://dx.doi.org/10.1038/ncomms4685>
- [SMH86] SCHEITHAUER, U. ; MEYER, G. ; HENZLER, M.: A new LEED instrument for quantitative spot profile analysis. In: *Surface Science* 178 (1986), Nr. 1-3, 441 - 451. [http://dx.doi.org/http://dx.doi.org/10.1016/0039-6028\(86\)90321-3](http://dx.doi.org/http://dx.doi.org/10.1016/0039-6028(86)90321-3). – DOI [http://dx.doi.org/10.1016/0039-6028\(86\)90321-3](http://dx.doi.org/10.1016/0039-6028(86)90321-3). – ISSN 0039-6028
- [SPF98] SEIDEL, C. ; POPPENSIEKER, J. ; FUCHS, H.: Real-time monitoring of phase transitions of vacuum deposited organic films by molecular beam deposition LEED. In: *Surface Science* 408 (1998), Nr. 1-3, 223 - 231. [http://dx.doi.org/DOI:10.1016/S0039-6028\(98\)00231-3](http://dx.doi.org/DOI:10.1016/S0039-6028(98)00231-3). – DOI DOI: 10.1016/S0039-6028(98)00231-3. – ISSN 0039-6028
- [SR94] SCHULZ, R.R. ; ROSSEL, C.: A beetle-like low-temperature scanning tunneling microscope in ultra-high vacuum. In: *Physica B: Condensed Matter* 194-196, Part 1 (1994), Nr. 0, 389 - 390. [http://dx.doi.org/http://dx.doi.org/10.1016/0921-4526\(94\)90524-X](http://dx.doi.org/http://dx.doi.org/10.1016/0921-4526(94)90524-X). – DOI [http://dx.doi.org/10.1016/0921-4526\(94\)90524-X](http://dx.doi.org/10.1016/0921-4526(94)90524-X). – ISSN 0921-4526

- [SSB⁺14] STADTMÜLLER, Benjamin ; SCHRÖDER, Sonja ; BOCQUET, François C. ; HENNEKE, Caroline ; KLEIMANN, Christoph ; SOUBATCH, Serguei ; WILLENBOCKEL, Martin ; DETLEFS, Blanka ; ZEGENHAGEN, Jörg ; LEE, Tien-Lin ; TAUTZ, F. S. ; KUMPF, Christian: Adsorption height alignment at heteromolecular hybrid interfaces. In: *Phys. Rev. B* 89 (2014), Apr, 161407. <http://dx.doi.org/10.1103/PhysRevB.89.161407>. – DOI 10.1103/PhysRevB.89.161407
- [SSF01] SCHAEFER, A. H. ; SEIDEL, C. ; FUCHS, H.: LEED and Optical Spectroscopy Study of an Organic Epitaxial Multilayer Film. In: *Advanced Functional Materials* 11 (2001), Nr. 3, 193–197. [http://dx.doi.org/10.1002/1616-3028\(200106\)11:3<193::AID-ADFM193>3.0.CO;2-L](http://dx.doi.org/10.1002/1616-3028(200106)11:3<193::AID-ADFM193>3.0.CO;2-L). – DOI 10.1002/1616-3028(200106)11:3<193::AID-ADFM193>3.0.CO;2-L. – ISSN 1616-3028
- [SSK⁺12] STADTMÜLLER, Benjamin ; SUEYOSHI, Tomoki ; KICHIN, Georgy ; KRÖGER, Ingo ; SOUBATCH, Sergey ; TEMIROV, Ruslan ; TAUTZ, F. S. ; KUMPF, Christian: Commensurate Registry and Chemisorption at a Hetero-organic Interface. In: *Phys. Rev. Lett.* 108 (2012), Mar, 106103. <http://dx.doi.org/10.1103/PhysRevLett.108.106103>. – DOI 10.1103/PhysRevLett.108.106103
- [Sta13] STADTMÜLLER, B: *Study of intermolecular interactions in hetero-organic thin films*, RWTH Aachen University / FZ Jülich, Diss., 2013
- [STS⁺00] SHKLOVER, V ; TAUTZ, F.S ; SCHOLZ, R ; SLOBOSHANIN, S ; SOKOLOWSKI, M ; SCHAEFER, J.A ; UMBACH, E: Differences in vibronic and electronic excitations of PTCDA on Ag(111) and Ag(110). In: *Surface Science* 454-456 (2000), Nr. 0, 60 - 66. [http://dx.doi.org/http://dx.doi.org/10.1016/S0039-6028\(00\)00136-9](http://dx.doi.org/http://dx.doi.org/10.1016/S0039-6028(00)00136-9). – DOI [http://dx.doi.org/10.1016/S0039-6028\(00\)00136-9](http://dx.doi.org/10.1016/S0039-6028(00)00136-9). – ISSN 0039-6028
- [SWP⁺12] SCHNEIDER, C.M. ; WIEMANN, C. ; PATT, M. ; FEYER, V. ; PLUCINSKI, L. ; KRUG, I.P. ; ESCHER, M. ; WEBER, N. ; MERKEL, M. ; RENAULT, O. ; BARRETT, N.: Expanding the view into complex material systems: From micro-ARPES to nanoscale HAXPES. In: *Journal of Electron Spectroscopy and Related Phenomena* 185 (2012), Nr. 10, 330 - 339. <http://dx.doi.org/http://dx.doi.org/10.1016/j.elspec.2012.08.003>. –

- DOI <http://dx.doi.org/10.1016/j.elspec.2012.08.003>. – ISSN 0368–2048.
– Photoelectron microscopy, Time resolved pump-probe {PES}
- [Tan86] TANG, C. W.: Two-layer organic photovoltaic cell. In: *Applied Physics Letters* 48 (1986), Nr. 2, 183-185. <http://dx.doi.org/http://dx.doi.org/10.1063/1.96937>. – DOI <http://dx.doi.org/10.1063/1.96937>
- [Tau07] TAUTZ, F.S.: Structure and bonding of large aromatic molecules on noble metal surfaces: The example of PTCDA. In: *Progress in Surface Science* 82 (2007), Nr. 9-12, 479 - 520. <http://dx.doi.org/10.1016/j.progsurf.2007.09.001>. – DOI 10.1016/j.progsurf.2007.09.001. – ISSN 0079–6816
- [TES+02] TAUTZ, F.S. ; EREMTCHENKO, M. ; SCHAEFER, J.A. ; SOKOLOWSKI, M. ; SHKLOVER, V. ; GLÖCKLER, K. ; UMBACH, E.: A comparison of the chemisorption behaviour of PTCDA on different Ag surfaces. In: *Surface Science* 502-503 (2002), Nr. 0, 176 - 184. [http://dx.doi.org/http://dx.doi.org/10.1016/S0039-6028\(01\)01930-6](http://dx.doi.org/http://dx.doi.org/10.1016/S0039-6028(01)01930-6). – DOI [http://dx.doi.org/10.1016/S0039-6028\(01\)01930-6](http://dx.doi.org/10.1016/S0039-6028(01)01930-6). – ISSN 0039–6028
- [TGAHH10] TOADER, Marius ; GOPAKUMAR, Thiruvancheril G. ; ABDEL-HAFIEZ, Mahmoud ; HIETSCHOLD, Michael: Exploring the F16CoPc/Ag(110) Interface Using Scanning Tunneling Microscopy and Spectroscopy. Part 1: Template-Guided Adlayer Structure Formation. In: *The Journal of Physical Chemistry C* 114 (2010), Nr. 8, 3537-3543. <http://dx.doi.org/10.1021/jp9078019>. – DOI 10.1021/jp9078019
- [TGSH10] TOADER, Marius ; GOPAKUMAR, Thiruvancheril G. ; SHUKRYNAU, Pavel ; HIETSCHOLD, Michael: Exploring the F16CoPc/Ag(110) Interface Using Scanning Tunneling Microscopy and Spectroscopy. 2. Adsorption-Induced Charge Transfer Effect. In: *The Journal of Physical Chemistry C* 114 (2010), Nr. 49, 21548-21554. <http://dx.doi.org/10.1021/jp1078295>. – DOI 10.1021/jp1078295
- [TH83] TERSOFF, J. ; HAMANN, D. R.: Theory and Application for the Scanning Tunneling Microscope. In: *Phys. Rev. Lett.* 50 (1983), Jun, 1998–2001. <http://dx.doi.org/10.1103/PhysRevLett.50.1998>. – DOI 10.1103/PhysRevLett.50.1998

- [TH85] TERSOFF, J. ; HAMANN, D. R.: Theory of the scanning tunneling microscope. In: *Phys. Rev. B* 31 (1985), Jan, 805–813. <http://dx.doi.org/10.1103/PhysRevB.31.805>. – DOI 10.1103/PhysRevB.31.805
- [TRH⁺10] TADICH, A. ; RILEY, J. ; HUWALD, E. ; LECKEY, R. ; SEYLLER, T. ; LEY, L.: Full Hemisphere Fermi Surface Mapping Using A Novel Toroidal Electron Spectrometer. In: *AIP Conference Proceedings* 1234 (2010), Nr. 1, 943 - 946. <http://search.ebscohost.com/login.aspx?direct=true&db=aph&AN=51975333&site=ehost-live>. – ISSN 0094243X
- [TVD⁺95] TABORSKI, J. ; VÄTERLEIN, P. ; DIETZ, H. ; ZIMMERMANN, U. ; UMBACH, E.: NEXAFS investigations on ordered adsorbate layers of large aromatic molecules. In: *Journal of Electron Spectroscopy and Related Phenomena* 75 (1995), Nr. 0, 129 - 147. [http://dx.doi.org/http://dx.doi.org/10.1016/0368-2048\(95\)02397-6](http://dx.doi.org/http://dx.doi.org/10.1016/0368-2048(95)02397-6). – DOI [http://dx.doi.org/10.1016/0368-2048\(95\)02397-6](http://dx.doi.org/10.1016/0368-2048(95)02397-6). – ISSN 0368-2048. – Future Perspectives for Electron Spectroscopy with Synchrotron Radiation
- [UGS98] UMBACH, E ; GLÖCKLER, K ; SOKOLOWSKI, M: Surface architecture with large organic molecules: interface order and epitaxy. In: *Surface Science* 402-404 (1998), Nr. 0, 20 - 31. [http://dx.doi.org/10.1016/S0039-6028\(98\)00014-4](http://dx.doi.org/10.1016/S0039-6028(98)00014-4). – DOI 10.1016/S0039-6028(98)00014-4. – ISSN 0039-6028
- [Umb90] UMBACH, E.: Characterization of organic overlayers on well-defined substrates. In: *Progress in Surface Science* 35 (1990), Nr. 1-4, 113 - 127. [http://dx.doi.org/http://dx.doi.org/10.1016/0079-6816\(90\)90030-N](http://dx.doi.org/http://dx.doi.org/10.1016/0079-6816(90)90030-N). – DOI [http://dx.doi.org/10.1016/0079-6816\(90\)90030-N](http://dx.doi.org/10.1016/0079-6816(90)90030-N). – ISSN 0079-6816
- [USF96] UMBACH, E. ; SOKOLOWSKI, M. ; FINK, R.: Substrate-interaction, long-range order, and epitaxy of large organic adsorbates. In: *Applied Physics A* 63 (1996), Nr. 6, 565-576. <http://dx.doi.org/10.1007/BF01567212>. – DOI 10.1007/BF01567212. – ISSN 0947-8396
- [USR13] UHLMANN, C. ; SWART, I. ; REPP, J.: Controlling the Orbital Sequence in Individual Cu-Phthalocyanine Molecules. In: *Nano Letters* 13 (2013), Nr. 2, 777-780. <http://dx.doi.org/10.1021/nl304483h>. – DOI 10.1021/nl304483h

Bibliography

- [VGFK05] VÁZQUEZ, H. ; GAO, W. ; FLORES, F. ; KAHN, A.: Energy level alignment at organic heterojunctions: Role of the charge neutrality level. In: *Phys. Rev. B* 71 (2005), Jan, 041306. <http://dx.doi.org/10.1103/PhysRevB.71.041306>. – DOI 10.1103/PhysRevB.71.041306
- [WGM⁺09] WANG, Yongfeng ; GE, Xin ; MANZANO, Carlos ; KRÖGER, Jörg ; BERNDT, Richard ; HOFER, Werner A. ; TANG, Hao ; CERDA, Jorge: Supramolecular Patterns Controlled by Electron Interference and Direct Intermolecular Interactions. In: *Journal of the American Chemical Society* 131 (2009), Nr. 30, 10400-10402. <http://dx.doi.org/10.1021/ja903506s>. – DOI 10.1021/ja903506s. – PMID: 19594153
- [WH01] WALZER, K ; HIETSCHOLD, M: STM and STS investigation of ultrathin tin phthalocyanine layers adsorbed on HOPG(0001) and Au(111). In: *Surface Science* 471 (2001), Nr. 1-3, 1 - 10. [http://dx.doi.org/http://dx.doi.org/10.1016/S0039-6028\(00\)00909-2](http://dx.doi.org/http://dx.doi.org/10.1016/S0039-6028(00)00909-2). – DOI [http://dx.doi.org/10.1016/S0039-6028\(00\)00909-2](http://dx.doi.org/10.1016/S0039-6028(00)00909-2). – ISSN 0039-6028
- [WHS⁺12] WIESSNER, M. ; HAUSCHILD, D. ; SCHÖLL, A. ; REINERT, F. ; FEYER, V. ; WINKLER, K. ; KRÖMKER, B.: Electronic and geometric structure of the PTCDA/Ag(110) interface probed by angle-resolved photoemission. In: *Phys. Rev. B* 86 (2012), Jul, 045417. <http://dx.doi.org/10.1103/PhysRevB.86.045417>. – DOI 10.1103/PhysRevB.86.045417
- [Wie94] WIESENDANGER, Roland: *Scanning Probe Microscopy and Spectroscopy*. Cambridge University Press, 1994
- [WLS⁺15] WILLENBOCKEL, M. ; LUFTNER, D. ; STADTMULLER, B. ; KOLLER, G. ; KUMPF, C. ; SOUBATCH, S. ; PUSCHNIG, P. ; RAMSEY, M. G. ; TAUTZ, F. S.: The interplay between interface structure, energy level alignment and chemical bonding strength at organic-metal interfaces. In: *Phys. Chem. Chem. Phys.* 17 (2015), 1530-1548. <http://dx.doi.org/10.1039/C4CP04595E>. – DOI 10.1039/C4CP04595E
- [WMPL07] WALZER, K. ; MAENNIG, B. ; PFEIFFER, M. ; LEO, K.: Highly Efficient Organic Devices Based on Electrically Doped Transport Layers. In: *Chemical Reviews* 107 (2007), Nr. 4, 1233-1271. <http://dx.doi.org/10.1021/cr050156n>. – DOI 10.1021/cr050156n. – PMID: 17385929

- [WSS⁺13] WILLENBOCKEL, M ; STADTMÜLLER, B ; SCHÖNAUER, K ; BOCQUET, F C. ; LÜFTNER, D ; REINISCH, E M. ; ULES, T ; KOLLER, G ; KUMPF, C ; SOUBATCH, S ; PUSCHNIG, P ; RAMSEY, M G. ; TAUTZ, F S.: Energy offsets within a molecular monolayer: the influence of the molecular environment. In: *New Journal of Physics* 15 (2013), Nr. 3, 033017. <http://stacks.iop.org/1367-2630/15/i=3/a=033017>
- [WW04] WITTE, Gregor ; WÖLL, Christof: Growth of aromatic molecules on solid substrates for applications in organic electronics. In: *Journal of Materials Research* 19 (2004), 7, 1889–1916. <http://dx.doi.org/10.1557/JMR.2004.0251>. – DOI 10.1557/JMR.2004.0251. – ISSN 2044–5326
- [WWKB12] WANG, Yongfeng ; WU, Kai ; KROEGER, Joerg ; BERNDT, Richard: Structures of phthalocyanine molecules on surfaces studied by STM. In: *AIP ADVANCES* 2 (2012), DEC, Nr. 4. <http://dx.doi.org/10.1063/1.4773458>. – DOI 10.1063/1.4773458. – ISSN 2158–3226
- [ZFS⁺10] ZIROFF, J. ; FORSTER, F. ; SCHÖLL, A. ; PUSCHNIG, P. ; REINERT, F.: Hybridization of Organic Molecular Orbitals with Substrate States at Interfaces: PTCDA on Silver. In: *Phys. Rev. Lett.* 104 (2010), Jun, 233004. <http://dx.doi.org/10.1103/PhysRevLett.104.233004>. – DOI 10.1103/PhysRevLett.104.233004
- [ZH02] ZAHL, P. ; HOEGEN, M. Horn-von: Third-generation conical spot profile analyzing low-energy electron diffraction. In: *Review of Scientific Instruments* 73 (2002), Nr. 8, 2958-2962. <http://dx.doi.org/http://dx.doi.org/10.1063/1.1489074>. – DOI <http://dx.doi.org/10.1063/1.1489074>
- [ZKS⁺06] ZOU, Y. ; KILIAN, L. ; SCHÖLL, A. ; SCHMIDT, Th. ; FINK, R. ; UMBACH, E.: Chemical bonding of PTCDA on Ag surfaces and the formation of interface states. In: *Surface Science* 600 (2006), Nr. 6, 1240 - 1251. <http://dx.doi.org/http://dx.doi.org/10.1016/j.susc.2005.12.050>. – DOI <http://dx.doi.org/10.1016/j.susc.2005.12.050>. – ISSN 0039–6028

Acknowledgements

My time as a PhD student at the PGI-3 in Jülich has been a great experience and this work would not have been possible without the assistance and contributions of many people. Here I would like to give my thanks to

- first of all my PhD mentor Prof. Stefan Tautz for giving me the opportunity to work in his group and institute. I am grateful for discussions and ideas helping to develop my research topics and this thesis.
- Prof. Peter Jakob from Philipps-University Marburg for his interest in our work and accepting to co-referee this thesis.
- Dr. Sergey Subach for being my supervisor. I am very grateful for a lot of help in the lab and at synchrotrons, with the STM and the data evaluation, for discussions and ideas about interpretations, comments and help with all aspects for scientific work.
- Dr. Benjamin Stadtmüller and Dr. Martin Willenbockel for introducing me to the experimental work in surface science, for many helpful advices and discussions, and for measurements and assistance during beamtimes at Elettra and BESSY II.
- the research group of Dr. Ruslan Temirov for help with the STM and taking turns refilling the cryostats during holidays.
- the research group of Dr. Christian Kumpf, besides Christian K. especially Caroline and Sonja, for helping hands (in the lab and during synchrotron beamtimes) and ideas, fruitful discussions, pleasant visits to conferences, and three great years together in Jülich.
- Simon Weiß for measurements at Elettra in 2013 when I was on holidays and for help with the data processing.
- additionally Dr. Daniel Schwarz and Dr. Tomoki Sueyoshi for measurements at Elettra.

Bibliography

- Jessica Sforzini for help with the Gaussian program.
- Prof. Michael Ramsey, Prof. Georg Koller, Eva Reinisch, and Thomas Ules from the University of Graz for their assistance during beamtimes at BESSY II.
- Prof. Peter Puschnig and Daniel Lüftner from the University of Graz for supporting theoretical calculations of momentum space maps and wave function distributions.
- my colleagues at the PGI-3 for their help and assistance and for the friendly and warm atmosphere in the institute.
- my family, especially my parents Klaus and Ingrid, for supporting me at any time.
- my friends and especially Bernhard for support and understanding.

Band / Volume 103

Metabolic engineering of *Escherichia coli* for the production of plant phenylpropanoid derived compounds

P. V. van Summeren-Wesenhagen (2015), V, 92 pp

ISBN: 978-3-95806-039-5

Band / Volume 104

Spin-reorientation transition in epitaxial Ni_xPd_{1-x} films on Cu(001): a microscopic analysis

D. Gottlob (2015), x, 134 pp

ISBN: 978-3-95806-049-4

Band / Volume 105

Resonant Magnetic Scattering Studies using Synchrotron Radiation and Laser-Generated Extreme Ultraviolet Light

C. M. Weier (2015), vii, 143 pp

ISBN: 978-3-95806-052-4

Band / Volume 106

Neutron Scattering

Lectures of the JCNS Laboratory Course held at Forschungszentrum Jülich and at the Heinz-Maier-Leibnitz Zentrum Garching

edited by Th. Brückel, D. Richter, G. Roth, A. Wischnewski and R. Zorn (2015), ca 300 pp

ISBN: 978-3-95806-055-5

Band / Volume 107

Neutron Scattering

Experimental Manuals of the JCNS Laboratory Course held at

Forschungszentrum Jülich and at the Heinz-Maier-Leibnitz Zentrum Garching

edited by Th. Brückel, D. Richter, G. Roth, A. Wischnewski and R. Zorn (2015), ca 150 pp

ISBN: 978-3-95806-056-2

Band / Volume 108

STM-based quantum transport through molecular wires

N. Fournier (2015), ix, 295 pp

ISBN: 978-3-95806-059-3

Band / Volume 109

Study on the electroforming and resistive switching behaviour of nickel oxide thin films for non-volatile memory applications

R. Weng (2015), xxi, 159 pp

ISBN: 978-3-95806-062-3

Band / Volume 110

Microswimmers – From Single Particle Motion to Collective Behaviour

Lecture Notes of the DFG SPP Summer School 2015

edited by G. Gompper, C. Bechinger, S. Herminghaus, R. E. Isele-Holder,
U.B. Kaupp, H. Löwen, H. Stark, R. G. Winkler (2015)

ISBN: 978-3-95806-083-8

Band / Volume 111

Long range order in 3D nanoparticle assemblies

E. Josten (2015), 238 pp

ISBN: 978-3-95806-087-6

Band / Volume 112

Silicon nanowire structures for neuronal cell interfacing

S. Pud (2015), 153 pp

ISBN: 978-3-95806-089-0

Band / Volume 113

Memristive Phenomena -

From Fundamental Physics to Neuromorphic Computing

Lecture Notes of the 47th IFF Spring School 2016

22 February – 04 March 2016, Jülich, Germany

ed. by R. Waser and M. Wuttig (2016), ca 1000 pp

ISBN: 978-3-95806-091-3

Band / Volume 114

**Single-Cell Analysis of Microbial Production Strains
in Microfluidic Bioreactors**

A. M. Grünberger (2015), XIX, 225 pp

ISBN: 978-3-95806-092-0

Band / Volume 115

**Magnetic order and spin dynamics in the
extended kagome system $\text{CaBaCo}_2\text{Fe}_2\text{O}_7$**

J. Reim (2015), viii, 144 pp

ISBN: 978-3-95806-097-5

Band / Volume 116

**Structural and electronic investigations on homo- and hetero-organic
layers involving CuPc on silver single crystal surfaces**

K. M. Schönauer (2015), x, 148 pp

ISBN: 978-3-95806-112-5

**Schlüsseltechnologien /
Key Technologies
Band / Volume 116
ISBN 978-3-95806-112-5**

